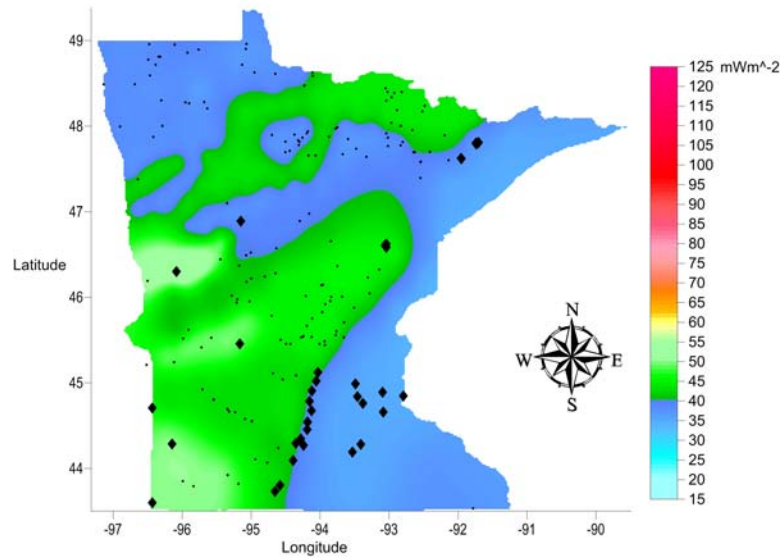


**NEW HEAT FLOW MAP OF MINNESOTA
CORRECTED FOR THE EFFECTS OF
CLIMATE CHANGE AND AN ASSESSMENT OF
ENHANCED GEOTHERMAL SYSTEM RESOURCES**

by

Robert Klenner¹, William Gosnold¹, John J. Heine, Mark J. Severson,
Steven A. Hauck, George Hudak, and Donald R. Fosnacht



**January 2012
TECHNICAL REPORT
NRRI/TR-2012/01**

**Funded by Minnesota Department of Commerce, Permanent University
Trust Fund, NRRI, Association of American State Geologists/U.S.
Department of Energy, and Initiative for Renewable Energy and the
Environment**

**Project Nos. 3005-10416-00013310
1750-10416-20090-1000012922
1801-10416-20900
3014-10416-00020610
3005-11130-00012443**

**Natural Resources Research Institute
University of Minnesota, Duluth
5013 Miller Trunk Highway
Duluth, MN 55811-1442**

¹ Dept. of Engineering, University of North Dakota, Grand Forks, ND 58202

This publication is accessible from the home page of the Economic Geology Group of the Center for Applied Research and Technology Development at the Natural Resources Research Institute, University of Minnesota, Duluth (<http://www.nrri.umn.edu/egg>) as a PDF file readable with Adobe Acrobat 6.0.

Date of release: January 2012

Cover Photo Caption

New Heat flow map of Minnesota using both traditional heat flow measurements (diamonds) and calculated heat flow measurements (dots) based on the Q-A relationship. The colored vertical scale is heat flow in mW m^{-2} . Horizontal and vertical axes on the map are in degrees latitude and longitude.

Recommended Citation

Klenner, R., Gosnold, W., Heine, J.J., Severson, M.J., Hauck, S.A., Hudak, G., and Fosnacht, D.R., 2012, New Heat Flow Map of Minnesota Corrected for the Effects of Climate Change and an Assessment of Enhanced Geothermal System Resources: University of Minnesota Duluth, Natural Resources Research Institute, Technical Report NRRI/TR-2012/01, 109 p.

Natural Resources Research Institute
University of Minnesota, Duluth
5013 Miller Trunk Highway
Duluth, MN 55811-1442
Telephone: 218-720-4272
Fax: 218-720-4329
e-mail: shauck@nrri.umn.edu

Web site: <http://www.nrri.umn.edu/egg>

©2012 by the Regents of the University of Minnesota

All rights reserved.

The University of Minnesota is committed to the policy that all persons shall have equal access to its programs, facilities, and employment without regard to race, color, creed, religion, national origin, sex, age, marital status, disability, public assistance status, veteran status, or sexual orientation.

EXECUTIVE SUMMARY

This investigation greatly improves the original heat flow map of Minnesota (Blackwell and Richards, 2004) that was based upon four points within the landmass of Minnesota and 162 samples collected 2.5m below Lake Superior (Fig. 1a-b). The new map incorporates:

- 1) new heat flow data from exploration drill holes and water wells throughout Minnesota;
 - 795 wells inspected, and over 100 boreholes were measured;
 - about half of these 100 wells had noise disturbances creating isothermal or perturbed gradients and could not be used in heat flow calculations; and
 - 57 new temperature measurements were made and compiled into 31 new heat flow sites.
- 2) removal of the paleoclimate signal from previous data of Roy et al. (1968), Roy et al. (1972), and Hart et al. (1994) that caused the heat flow to be underestimated. These climatic changes have affected temperature gradients up to 30% in the upper two kilometers (km) of the crust; and
- 3) collection of granitic samples from across MN from outcrops and mineral exploration drill holes for:
 - whole rock and trace element chemistry, including uranium and thorium;
 - thermal conductivity; and
 - radionuclide analyses (^{238}U , ^{232}Th , and ^{40}K) to supplement and infill heat flow data between and around water well and drill hole temperature data.

The newly constructed downhole temperature maps (Fig. 2 and Appendix A) indicate:

- 1) the available heat and electrical power potential is three times greater than previous estimates, i.e., 96,794 exajoules (EJ) or 18,409 MW more are available at depths >7-10 km (Fig. 3) compared to the previous MIT-DOE 2006 assessments of 6,161 MW;
- 2) this vast amount of energy found in this study could essentially power Minnesota through a clean base load power;
- 3) together, the new heat flow measurements, thermal conductivity measurements, and correction of heat flow data has raised the mean heat flow from 40 mW m^{-2} to 44.1 mW m^{-2} , an increase of 10%;
- 4) the 10% increase in heat flow positively affects the enhanced geothermal resources for power production (Fig. 3), e.g., in Otter Tail-Wilkin counties at 7 km depth, and also potentially in Murray-Nobles-Pipestone-Rock and Pope counties at 8.8 to 9 km depth;
- 5) the new map shows that certain counties, e.g., in Wilkin and Otter Tail counties, have the best currently-estimated environments for enhanced geothermal heat extraction and that the depth for extraction of heat from these counties is just over 7 km in depth. This depth is over 3 km shallower than the previous measurements would indicate for extracting this potential resource. This depth will dramatically reduce drilling costs associated with this type of technology implementation;
- 6) to have to drill to 150°C heat on the original map would have been about 10 km. These new data have reduced the drilling depth by 3 km, a definite savings in drilling and related costs; and

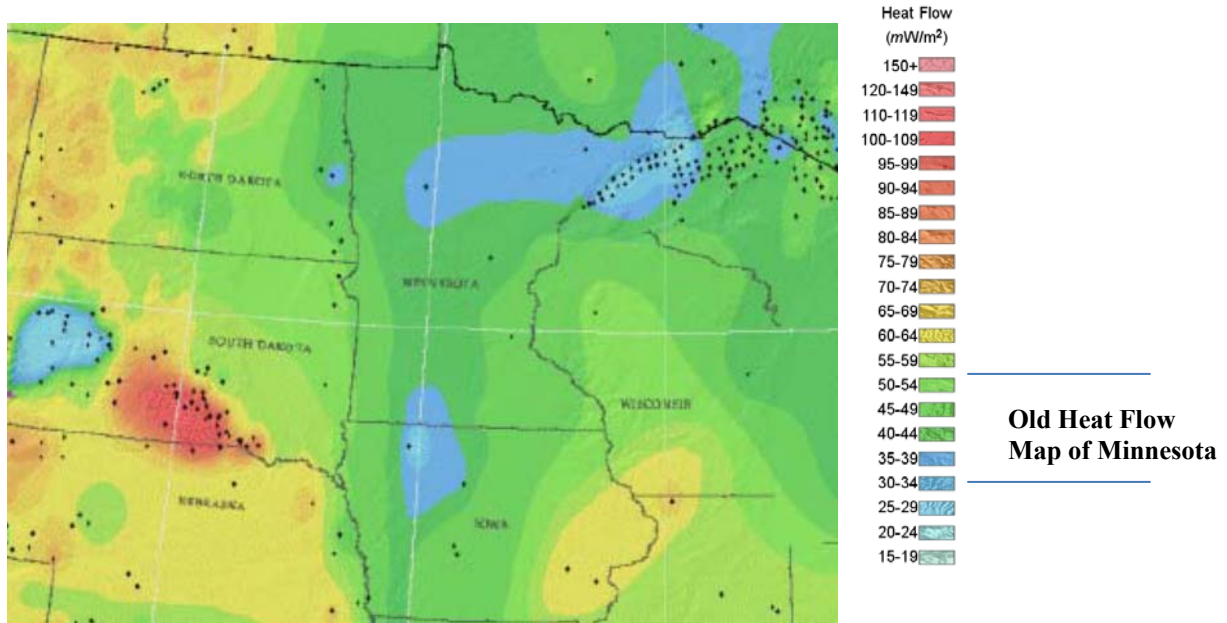
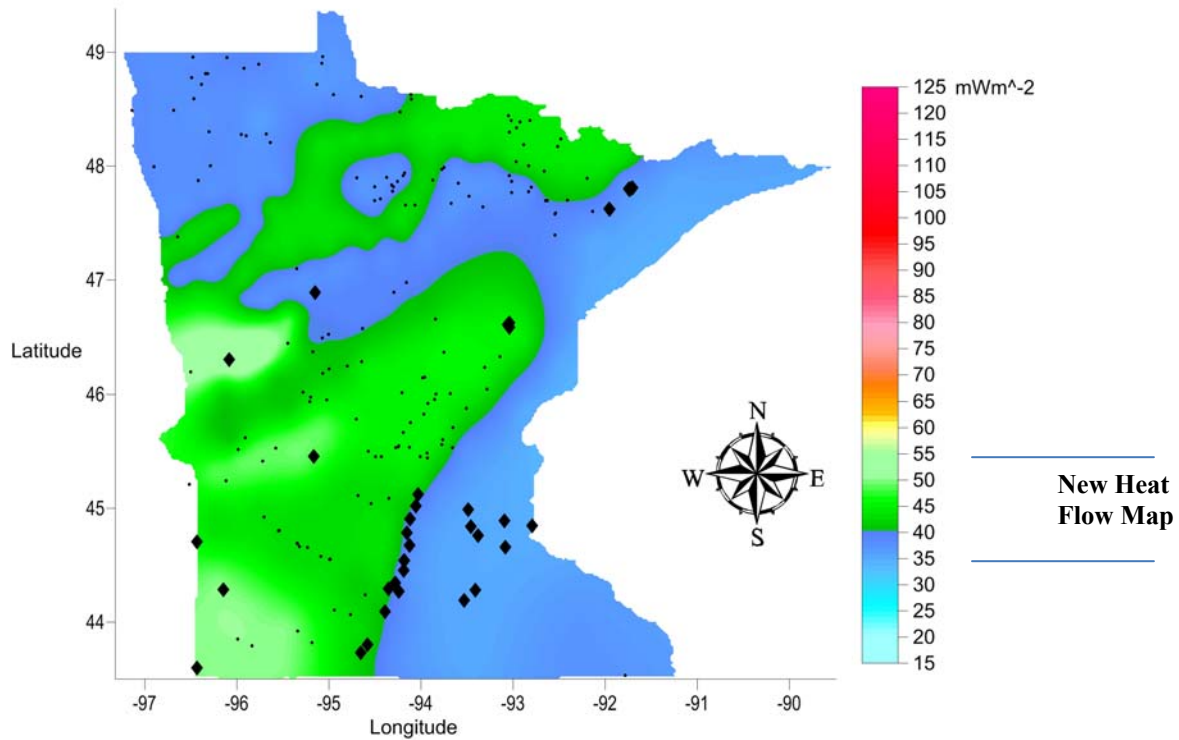


Figure 1a. The Blackwell and Richards map of 2004 (below) was developed to show heat flow ranges for the continent and uses a range of 15-150+ mW m⁻². MN has a range 25-55 mW m⁻². Applying the same range employed for the national study to Minnesota shows the difference in results for maps using the same scale (above). Changing scale to take advantage of the additional data collected for this project allows for finer granularity. These improved data use a heat flow range of 20-115 mW m⁻².

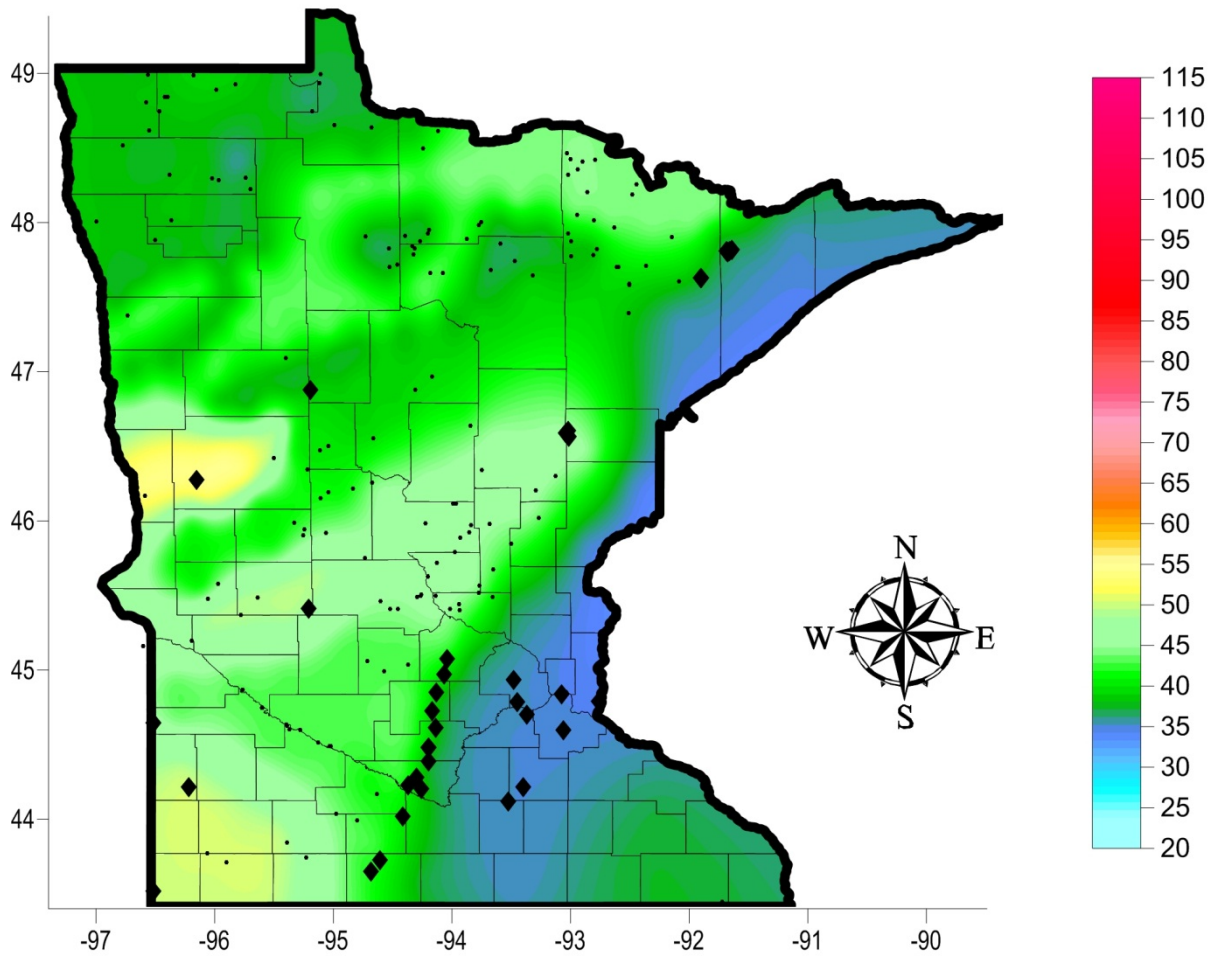
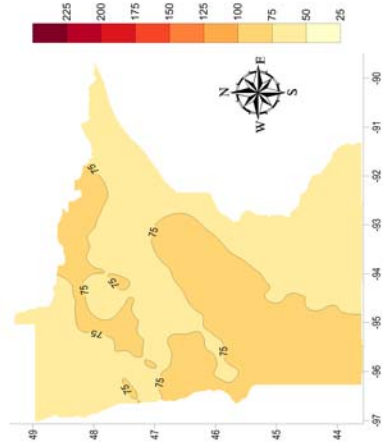
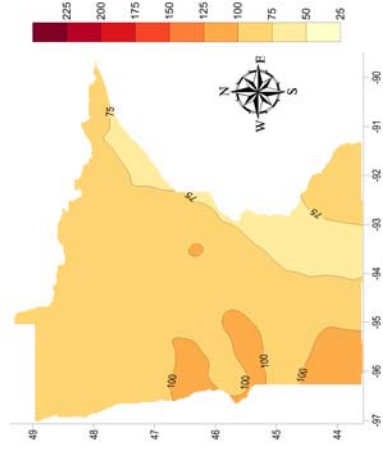


Figure 1b. Final heat flow map of Minnesota using a different-colored temperature scale to illustrate the greater heat flow detail in the new map. Note the presence of the Mid-Continent Rift (blue color) and high heat flow areas in west-central Minnesota in Otter Tail-Wilkin counties, in southwest Minnesota in Murray-Nobles-Pipestone-Rock counties, and in central Minnesota in Pope County. (Vertical colored scale in mW m^{-2} and vertical and horizontal scales on the map represent latitude and longitude.)

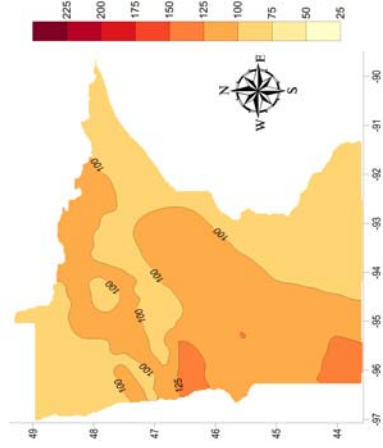
Figure 2. New depth (5-10km) versus temperature (°C) maps based on the new heat flow map of Minnesota
 (Vertical colored scale in °C and horizontal scales are degrees latitude and longitude)
 (See Appendix A)



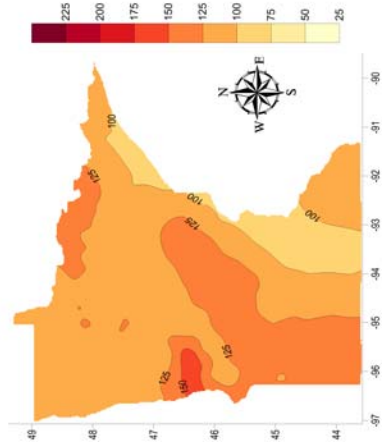
Depth at 5 Kilometers



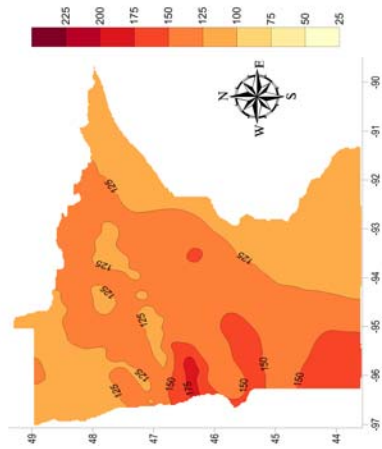
Depth at 6 Kilometers



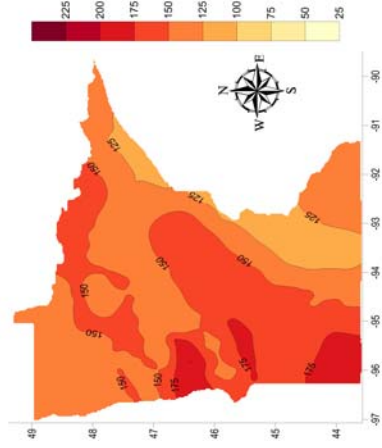
Depth at 7 Kilometers



Depth at 8 Kilometers



Depth at 9 Kilometers



Depth at 10 Kilometers

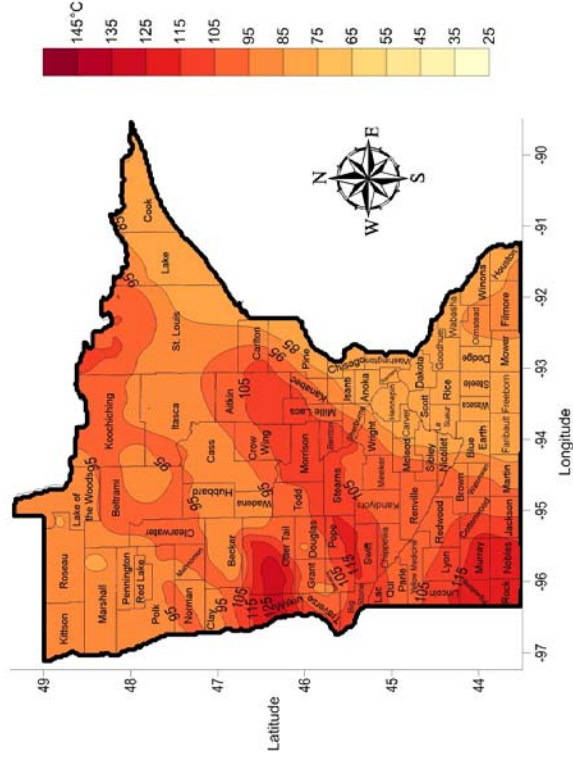
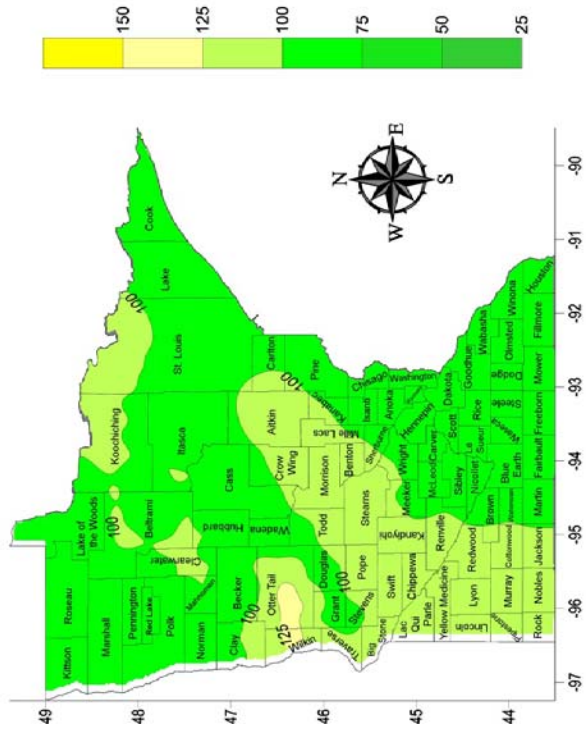
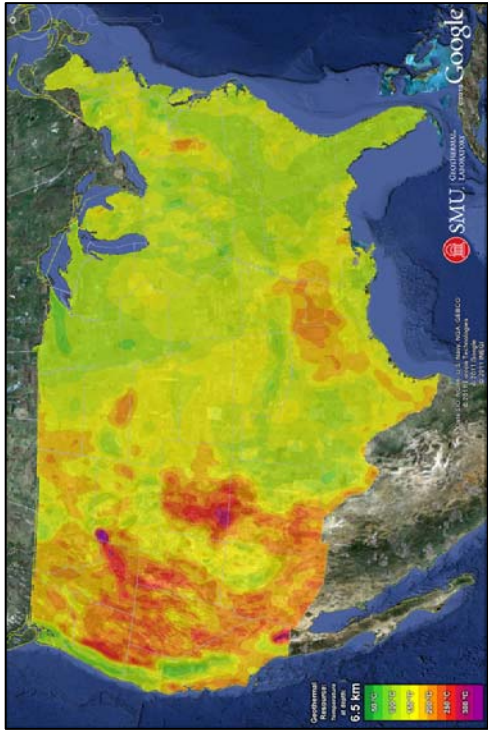


Figure 3. Comparison of temperature data ($^{\circ}\text{C}$) at 6.5 km from Tester et al. (2006 – at the top left and right) and this study. Note the local increases in temperature and detail at the same depth with the new data. The colored vertical scale is temperature in degrees Celsius. Horizontal and vertical axes on the map are in degrees latitude and longitude.

- 7) To drill to 100°C temperature rocks, many more areas of the state (Fig. 2), e.g., at 8 km, Murray-Nobles-Pipestone-Rock and Pope counties have availability for enhanced geothermal electrical power generating systems using organic Rankine or Kalina cycle heat transfer technology (see Fig. 7 bottom).

In addition to recording the downhole temperature data from wells and mineral exploration drill holes (Fig. 4), various granitic rock samples were also collected and processed (Fig. 5) to determine:

- 1) the chemistry and mineral composition of 100 granitic rock samples from throughout Minnesota;
- 2) the thermal conductivity (Fig. 6) of the granitic rocks (rate at which heat flows through the rock);
- 3) the general whole rock and trace element chemistry of the rock to determine how granitic the rock is and what other elements it contains, especially uranium and thorium; and
- 4) the radioactivity of the sample to determine the heat production ability of the rock.

Combining these data together with the downhole temperature data allowed us to construct the new heat flow map of Minnesota.

Results of this study are further validated by heat flow measurements in the other geological terrains of the stable Superior Craton in Canada (Quetico (46.5 mW m⁻²), Wawa-Abitibi (45.1 mW m⁻²), and Wabigoon (40.3 mW m⁻²) Subprovinces). The finding that the average heat flow in Minnesota is 44.1 plus or minus 6.6 milliWatts per meter squared is similar to that of comparable rock types in Canada.

The MIT-DOE report (Tester et al., 2006) indicates Minnesota has a “low” geothermal resource for developing geothermal electrical power in the upper 10 km and rates the enhanced geothermal system potential as highly unlikely. This study refutes this observation based on new data that indicates acceptable geothermal heat occurs at 7 km in at least one location (Figs. 1a-b, 3).

With heat flow higher in the gneissic rocks of the Minnesota River Valley (MRV) subprovince and in the granites of the Giants Range Batholith and Vermilion Massif, these areas have potential for geothermal development in Minnesota. Further investigations of the MRV using traditional heat flow observations will further quantify this resource and determine if heat flow may be higher in some areas of the MRV. Also, the rock chemistry in Appendix F indicates elevated rare earth element (REE) concentration compared to the other granitic rocks. Elevated REE concentrations generally accompany higher uranium and thorium values. Additional follow-up sampling, chemical and radionuclide, and thermal conductivity analyses are recommended to add additional detail to this study.

Technological advancements in drilling, reservoir stimulation, and binary power plant efficiency must be met in order to economically extract this heat for geothermal electrical power. However, several organizations, e.g., DOE, Google, are currently funding some of this research.



Figure 4. Hand crank used to lower temperature probe into the wellbore.



Figure 5. Various sample shapes used to measure thermal conductivity in this study.



Figure 6. PEDB used for measuring thermal conductivity in the UNDGL.

Recommendations for Future Work in Minnesota

- 1) Continue to refine the new Minnesota heat flow map by:
 - a. continued collection of down hole temperature data as mineral exploration and water wells become available;
 - b. continued collection of granitic rock samples for geochemistry, radionuclide analyses, and thermal conductivity analyses;
- 2) In the selected area(s), drill “touch down” core holes, i.e., drill through the overburden and then drill (oriented drill core) 10-20 feet into the hard bedrock to define a reservoir by collecting samples for:
 - a. chemistry, including radionuclides analyses;
 - b. thermal conductivity;
 - c. fracture(s) analysis;
- 3) Provide data to potential geothermal energy producers who might conduct additional deeper drilling and reservoir development to determine the reservoir’s producing characteristics; and
- 4) Continue to educate the public on the benefits of geothermal energy.

ACKNOWLEDGEMENTS

This project was primarily made possible by funding provided by the Office of Energy Security of the MN Department of Commerce grant through the use of XCEL Energy Renewable Development Funds (Laws of Minn. 2007, Ch 57, article 2, sec 3 subd6). We wish to thank Mr. Ken Brown and Ms. Ann Zechbauer for their effective oversight of this project and willingness to answer questions.

The first author thanks Josh and Anna Crowell, who assisted in the well logging efforts, and other members of the University of North Dakota, Geophysical Laboratory (UNDGL) who assisted in making this project happen. Gratitude is expressed to the Department of Natural Resources, Division of Waters, Messrs. James A. Berg, Michael MacDonald, and Scott R. Pearson for providing access to observation water wells and related data. Additional thanks are given for the funding and support from the Association of American State Geologists-DOE funded grant to Minnesota (Dr. Harvey Thorleifson, Director) to collect additional data. Gratitude is expressed for the additional data collection funding from the Initiative for Renewable Energy and the Environment grant to Dr. Martin Saar, Department of Earth Sciences, University of Minnesota, Minneapolis and to Mr. Ben Tutolo, who also collected downhole temperature data on this grant.

We want to thank Messrs. G. Wagoner, T. Levar, C. Maly, and Miss Sara Chelbeck, all of NRRI-UMD, for their assistance with well logging and well location.

A very special thank you goes out to all Minnesota property owners who allowed us to sample wells and collect rock samples. In particular, we extend our gratitude to Mr. Thomas Chrisfield of CenterPoint Energy, Minneapolis, MN for access to their wells and well logs over the Wakefield Gas Storage Facility.

The stored drill core at the Hibbing Drill Core Library, Minnesota Department of Natural Resources, Division of Lands and Minerals was a very valuable asset for collecting rock samples from across the State for this study.

Finally, to Minnesota Senator Yvonne Prettner-Solon (current Lt. Governor, State of Minnesota), Senator Ellen Anderson, and Minnesota Representative Bill Hilty for making funding of this project possible, and to other senators and representatives who saw the usefulness of this research to Minnesota.

TABLE OF CONTENTS

EXECUTIVE SUMMARY	i
Recommendations for Future Work in Minnesota.....	ix
ACKNOWLEDGEMENTS	ix
LIST OF TABLES	xii
LIST OF FIGURES	xiii
LIST OF APPENDICES.....	xviii
1. INTRODUCTION	1
1.1 Geothermal Energy	1
Section 1.1.5 General Economics of Establishing an EGS System.....	6
1.2 Previously Assessed Geothermal Resources in Minnesota	9
1.3 Minnesota Geology.....	11
1.4 Heat Flow.....	14
1.5 Previous Research of Heat Flow in Minnesota and Canadian Shield.....	18
1.6 Climate Effect on Heat Flow	21
2. RESEARCH METHODS	22
2.1 Temperature Gradient Measurements.....	22
2.2 Thermal Conductivity	27
2.3 Radioactivity Measurements.....	30
2.4 Calculating Temperatures at Depth and Geothermal Resources	32
3. OVERVIEW OF NEW HEAT FLOW MEASUREMENTS	33
3.1 Climate Changes Affecting Heat Flow	33
3.1.1 Recent Warming Affecting the Gradient	33
3.1.2 Post-Glacial Warming Affecting the Gradient	37
3.2 New Heat Flow Measurements.....	40
3.3 New Heat Flow Map.....	43
3.4 Assessment of Heat Flow Data.....	43
3.5 Temperatures at Depth and Electrical Geothermal Resources of Minnesota	51
4. RECOMMENDATIONS FOR FUTURE WORK IN MINNESOTA.....	52
REFERENCES	53
APPENDICES	57

LIST OF TABLES

Table 1. Heat flow provinces for the United States. Contribution of mantle heat flux and the thickness of the radioactive layer are given (Roy et al., 1968).18

Table 2. List of wells and drill holes run by the groups for the project showing which wells were run as duplicates as checks for the data from the different equipment used on the project.101

LIST OF FIGURES

Figure 1a.	The Blackwell and Richards map of 2004 (below) was developed to show heat flow ranges for the continent and uses a range of 15-150+ mW m ⁻² . MN has a range 25-55 mW m ⁻² . Applying the same range employed for the national study to Minnesota shows the difference in results for maps using the same scale (above). Changing scale to take advantage of the additional data collected for this project allows for finer granularity. These improved data use a heat flow range of 20-115 mW m ⁻²	ii
Figure 1b.	Final heat flow map of Minnesota using a different-colored temperature scale to illustrate the greater heat flow detail in the new map. Note the presence of the Mid-Centiment Rift (blue color) and high heat flow areas in west-central Minnesota in Otter Tail-Wilkin counties, in southwest Minnesota in Murray-Nobles-Pipestone-Rock counties, and in central Minnesota in Pope County. (Vertical colored scale in mW m ⁻² and vertical and horizontal scales on the map represent latitude and longitude.).....	iii
Figure 2.	New depth (5-10km) versus temperature (°C) maps based on the new heat flow map of Minnesota	iv
Figure 3.	Comparison of temperature data (°C) at 6.5 km from Tester et al. (2006 – at the top left and right) and this study. Note the local increases in temperature and detail at the same depth with the new data. The colored vertical scale is temperature in degrees Celsius. Horizontal and vertical axes on the map are in degrees latitude and longitude.....	v
Figure 4.	Hand crank used to lower temperature probe into the wellbore.....	vii
Figure 5.	Various sample shapes used to measure thermal conductivity in this study.....	viii
Figure 6.	PEDB used for measuring thermal conductivity in the UNDGL.....	viii
Figure 7.	Schematics of dry steam, flash steam, and binary power plant technology to utilize hot fluids to generate electricity. Source: Geothermal Technologies Program (2011).	3
Figure 8.	Concepts of an EGS reservoir using crystalline basement rocks. A closed looped reservoir is created through hydraulic stimulation, allowing for fluid to circulate and extract heat. The fluid then is flashed to steam where it powers a turbine, generating electricity. Source: U.S. Department of Energy Geothermal Technologies Program (2008).	4
Figure 9.	Diagram of a geothermal power generating facility showing: 1) an injection well undergoing hydrofracturing; 2) an additional borehole with downhole seismometers to record the locations of the microfractures by recording the microseismicity; and 3) a recovery well that brings the heated fluids (100-150°C water or CO ₂) to the surface power generating facility (after Zhao et al., 2011).	7
Figure 10.	The various stages of EGS exploration, development, production and financing versus risk tolerance (Eliasson and Smith, 2011).	8

Figure 11.	Levelized costs of selected power producing technologies (Blodgett and Slack, 2009).....	9
Figure 12.	Geothermal resources of the U.S. EGS resources in Minnesota are least favorable or N/A in cases of the black shaded area where temperatures are >150°C at 10 kilometers Source: Roberts (2010).....	10
Figure 13.	Geologic map of Minnesota. Labels are provided to describe locations of mafic and felsic rock bodies.....	12
Figure 14.	Locations and subdivisions of the Superior Province. The Wawa-Abitibi, Wabigoon, Quetico, and Minnesota River Valley Gneiss are all different geologic terranes making up the Precambrian Bedrock in Minnesota. Modified from Wyman and Kerrich (2009) with permission.	13
Figure 15.	Geology and geographical extent of the Midcontinent Rift System through North America. Modified from Holm et al. (2007).....	15
Figure 16.	Heat flow map of the United States. Source: Blackwell and Richards (2004).	17
Figure 17.	Heat flow measurements of the Canadian Shield with outlines of subprovinces. Source: Mareschal and Jaupart (2004).....	20
Figure 18a.	Locations of wells logged for temperature and rock sample locations measured for thermal conductivity and radioactivity. Horizontal and vertical axes on the map are in degrees latitude and longitude.....	23
Figure 18b.	Location of wells and exploration drill holes probed by more than one instrument.....	24
Figure 19.	A DNR well sampled for temperature gradient measurements.....	25
Figure 20a.	Hand crank used to lower temperature probe into the wellbore.....	26
Figure 20b.	During the latter half of the project NRRI used an automated Scintrex temperature probe to collect data.	26
Figure 20c.	Down hole temperature made by the Dept. of Earth Sciences at the University of Minnesota (mock setup to illustrate equipment).....	27
Figure 21.	PEDB used for measuring thermal conductivity in the UNDGL.....	28
Figure 22.	Various sample shapes used to measure thermal conductivity in this study.....	28
Figure 23.	A sample between the two brass plate sandwiches applying steady thermal gradients for measurement of thermal conductivity.....	29
Figure 24.	Canberra Germanium detector housed within lead shielding to measure the radioactive heat content of the crushed rock samples.	31
Figure 25.	Pint sized containers used to house the crushed rock sample to measure radioactivity.....	31
Figure 26.	Screenshot of the digital spectrum from 40keV to >10MeV to determine concentrations of the radioactive elements.	32

Figure 27.	Change in temperature from the mean over the past 100+ years in regions 2 and 3 from data acquired from The National Data Climatic Center (http://www.ncdc.noaa.gov/oa/ncdc.html).	34
Figure 28.	Climate divisions of Minnesota from the National Climatic Data Center. Data from each region was used in temperature forcing to determine the extent of perturbations caused by recent warming.	35
Figure 29.	Recent warming perturbations affecting the nine different climate regions in Minnesota. Regions are 1-9 respectively from left to right.	36
Figure 30.	DNR Well 52007 corrected for recent warming in Zone 8. The blue line is the data logged in the borehole and the red line is the log corrected for recent warming after subtracting out the signal.	38
Figure 31.	Extent of the Laurentide Ice Sheet over Minnesota. Minnesota sat on the edge of the ice sheet and may have exhibited colder temperatures on the margins (Lusardi, 1997).	38
Figure 32.	Heat flow measurements (diamonds), are systematically lower than the heat flow calculated from radioactivity (dots). This difference gives further evidence that a correction for post-glacial warming needs to be applied. The colored vertical scale is heat flow in mW m^{-2} . Horizontal and vertical axes on the map are in degrees latitude and longitude.	39
Figure 33.	Both 12 and 15 degree warming causes major perturbations down to 2000 meters. At the surface, temperature gradients are affected by 30-40%.	41
Figure 34.	Heat flow-heat production relationship of the Canadian Shield showing the different geologic provinces. Heat flow intercept is 33 mW m^{-2} and a slope of 9.1 km for the thickness of the radioactive layer. Modified from Perry et al. (2006).	42
Figure 35.	New heat flow map of Minnesota using both traditional heat flow measurements (diamonds) and calculated heat flow measurements (dots) based on the Q-A relationship. The colored vertical scale is heat flow in mW m^{-2} . Horizontal and vertical axes on the map are in degrees latitude and longitude.	44
Figure 36.	First attempt at a heat flow map based on regionally corrected data with newly acquired data in the first year of this study. The colored vertical scale is heat flow in mW m^{-2} . Horizontal and vertical axes on the map are in degrees latitude and longitude.	45
Figure 37.	Second attempt of the heat flow map using nine heat flow sites and data acquired from the whole rock and trace element analysis. The colored vertical scale is heat flow in mW m^{-2} . Horizontal and vertical axes on the map are in degrees latitude and longitude.	46
Figure 38.	Third attempt of the heat flow map of Minnesota. Anomalies are most likely unrealistic because heat flow variations are large over short distances. The colored vertical scale is heat flow in mW m^{-2} . Horizontal and vertical axes on the map are in degrees latitude and longitude.	47

Figure 39.	Heat flow locations on the geologic map of Minnesota. These data were used to create the new heat flow map of Minnesota by averaging the heat flow data over the geologic terrane it represented. (Base map source: http://tin.er.usgs.gov/geology/state/state.php?state=MN .)	48
Figure 40.	Histogram of the Radioactive Heat Production in this study throughout Minnesota.	49
Figure 41.	Heat flow measurements located on general outlines of the Wabigoon, Wawa-Abitibi, Quetico, MRV, and Midcontinent Rift System.	50
Figure 42.	Energy available and power potential at varying depths in Minnesota.	52
Figure 43.	Temperature Map of Minnesota at a Depth of 4 Kilometers. The colored vertical scale is heat flow in mW m^{-2} . Horizontal and vertical axes on the map are in degrees latitude and longitude.	58
Figure 44.	Temperature Map of Minnesota at a Depth of 5 Kilometers. The colored vertical scale is heat flow in mW m^{-2} . Horizontal and vertical axes on the map are in degrees latitude and longitude.	59
Figure 45.	Temperature Map of Minnesota at a Depth of 6 Kilometers. The colored vertical scale is heat flow in mW m^{-2} . Horizontal and vertical axes on the map are in degrees latitude and longitude.	60
Figure 46.	Temperature Map of Minnesota at a Depth of 7 Kilometers. The colored vertical scale is heat flow in mW m^{-2} . Horizontal and vertical axes on the map are in degrees latitude and longitude.	61
Figure 47.	Temperature Map of Minnesota at a Depth of 8 Kilometers. The colored vertical scale is heat flow in mW m^{-2} . Horizontal and vertical axes on the map are in degrees latitude and longitude.	62
Figure 48.	Temperature Map of Minnesota at a Depth of 9 Kilometers. The colored vertical scale is heat flow in mW m^{-2} . Horizontal and vertical axes on the map are in degrees latitude and longitude.	63
Figure 49.	Temperature Map of Minnesota at a Depth of 10 Kilometers. The colored vertical scale is heat flow in mW m^{-2} . Horizontal and vertical axes on the map are in degrees latitude and longitude.	64
Figure 50.	Thermal Conductivity Map of Precambrian Bedrock in Minnesota. The colored vertical scale is thermal conductivity in $\text{W}/(\text{m}\cdot\text{K})$. Horizontal and vertical axes on the map are in degrees latitude and longitude.	65
Figure 51.	Depth to Precambrian bedrock. Overburden consists of glacial till and sedimentary rocks. The colored vertical scale is in meters. Horizontal and vertical axes on the map are in degrees latitude and longitude.	66
Figure 52.	This map is arbitrarily divided into regions of the State to better illustrate graphically the various plots of the chemistry in the diagrams to follow. The circles are the granitic rock sample locations.	90
Figure 53.	A Floyd-Winchester plot of ZrTiO_2 versus Nb/Y (ppm) illustrating the types of granitic and other rocks in each region (Floyd and Winchester, 1975).	91

Figure 54.	Ab-An-Or plot illustrating the type of granitic rock the samples in each region (Barker, 1979). Calculated from a CIPW norm (Terra Softa, Inc., 2002). Sample IDs represent individual samples only, due to a limited pool of sample symbols available in Igppt.	92
Figure 55.	Shands index gives an idea of the alkalinity of granitic rocks. Alkaline igneous rocks can have higher U, Th, and K, as well as Rare Earth Elements (Maniar and Piccoli, 1989). Sample IDs represent individual samples only, due to a limited pool of sample symbols available in Igppt.	93
Figure 56.	Differentiation of tectonic origin of the granitic samples using the Shands Index. Anorogenic granites (upper right in diagram) can have higher uranium, thorium, and rare earth elements that contribute to heat flow. I- and S-granites indicate more tectonically active environments, i.e., related to subduction processes (Whalen et al., 1987). Sample IDs represent individual samples only, due to a limited pool of sample symbols available in Igppt.	94
Figure 57.	Relationship between U+Th (ppm) versus K ₂ O (wt. %) in granitic samples in various regions of the State (This Study). The higher the values on each axis should indicate more radioactive heat generation. Note the linear relationships in the various regions. Sample IDs represent individual samples only, due to a limited pool of sample symbols available in Igppt.	95
Figure 58.	Wells and drill holes investigated during project.	99
Figure 59.	Wells measured for geothermal temperature data.	100
Figure 60.	The header information supplied for each hole measured includes name and location data for each hole, operators for the measurement and on what date. For angled drill hole, which are common in exploration drilling, the depth is corrected to true vertical depth from the cable measurement using deviation data supplied by the exploration company.	105
Figure 61.	Set up and operation of downhole temperature collection equipment, winter 2010, Duluth Metals Nokomis Cu-Ni-PGE deposit, drill hole MEX-3.	106
Figure 62.	Recording of downhole temperature data, winter 2010, Duluth Metals Nokomis Cu-Ni-PGE deposit, drill hole MEX-3.	106
Figure 63.	Granitic samples collected to determine the heat flow in Minnesota using thermal conductivity and radionuclide analyses.	108
Figure 64.	Granite samples used for geochemistry and thin sections.	109

LIST OF APPENDICES

APPENDIX A: Temperature at Depth (4-10 km), Conductivity, and Sediment Thickness
Maps57

APPENDIX B: Heat Flow Observation Data67

APPENDIX C: Thermal Conductivity and Radioactivity Data.....72

APPENDIX D: Equations Used for Zones 1-9 in Minnesota to correct for recent
warming.....85

APPENDIX E: Petrography and Geochemistry of Collected Granite Samples87

APPENDIX F: NRRI Field Collection Data97

1. INTRODUCTION

Low heat flow has been previously reported in Minnesota ($40 \pm 6 \text{ mW m}^{-2}$) and the Superior Province of the Canadian Shield ($42 \pm 8 \text{ mW m}^{-2}$) (Perry et al., 2010). This study finds that the low heat flow in Minnesota is due to heat flow measurements made in the mafic rocks of the Mid-Continent Rift System (MCRS) and lack of correction for post-glacial climate changes. The radioactive component is critical; particularly in Minnesota, where most of the published heat flow sites (3 of 4 sites on land, and 168 in Lake Superior (Roy et al., 1968; 1972; Hart et al., 1994)) are located within the MCRS, creating a bias in the data. The rift is a massive mafic intrusive complex that extends from the surface to the Moho and has characteristically low radioactive heat production. Thus, there is a sampling problem where heat flow has not been measured in the granitic terranes in Minnesota.

Post-glacial climatic changes affect temperature gradients in the upper two kilometers of the crust (Jessop, 1971), and this has not been consistently accounted for in previously published heat flow values (Roy et al., 1968; 1972; Hart et al., 1994). Thermal gradient measurements in Minnesota require re-analysis to account for the effects of micro-climates at the drill holes, including modification of the temperature gradients by recent climate change and by post-glacial warming. Because the temperature has increased 15°C since the last glaciation, temperature gradients are underestimated by 25-40%.

This study presents several lines of evidence to show that heat flow in the region has been underestimated and that geothermal potential in the region is not insignificant. Surface heat flow, q (mW m^{-2}), is the sum of heat flow from the mantle, q_0 , and radioactive heat production, A ($\mu\text{W m}^{-3}$), from U, Th, and K in the crust ($q = q_0 + A \cdot b$). The parameter, b , has units

of length and has been determined to be 9.1 km for the Canadian Shield and a mantle heat flow is approximately 33 mW m^{-2} (Levy et al., 2010). The changes in heat production affect heat flow over short distances in the Canadian Shield (Jaupart and Mareshal, 2007).

New heat flow measurements, and the sampling of over two hundred rock samples, were obtained from cores and outcrops for ^{238}U , ^{232}Th , and ^{40}K concentrations and thermal conductivity in Minnesota. Based on corrections for post-glacial warming, this study finds the average heat flow in Minnesota to be $44.1 \pm 6.6 \text{ mW m}^{-2}$. This is similar to heat flow measurements in the Quetico, Wawa-Abitibi, and Wabigoon Superior Subprovinces in Canada. The same geologic subprovinces are found in Minnesota.

Previously published maps of the U.S. suggest that because of low heat flow values, the potential for developing Enhanced Geothermal Systems (EGS) in Minnesota may be absent (Roberts, 2010). Newly acquired data on heat flow, thermal conductivity, and radiogenic heat production, allows for an assessment of the EGS resources, at depths of 4 to 10 kilometers, for Minnesota. Using the newly acquired data and by correcting heat flow values for climatic changes, temperatures of 150°C are found at much shallower depths, increasing the amount of Minnesota's EGS resources.

1.1 Geothermal Energy

Using geothermal energy directly or indirectly can provide many uses, including electricity generation and heating or cooling of your home. When exploring for geothermal energy, understanding the heat flow in the area is the primary source for evaluating and understanding geothermal resources. In the near future, heat from the Earth may be the solution to our energy

demands, both domestically and abroad. Over the past couple of decades, researchers have been refining and determining the total heat flux of the Earth. Estimates of 44.2 ± 1 TW ($1 \text{ TW} = 1 \times 10^{12}$ Watts) was given by Pollack et al. (1993). Later, other estimates were reported by Jaupart and Mareschal (2007) to be 46 ± 3 TW, and then refined to 47 ± 1 TW by Davies and Davies, (2010). These estimates represent the massive amount of natural energy that is wasted and lost into Earth's atmosphere. A fraction of this energy could help supply all, or a majority of the world's energy demands.

Reported by the U.S. Energy Information Administration (2010), energy consumption will grow 49% by 2035. This demand will most likely grow faster than the amount of renewable energy being constructed; not to mention the number of renewable energy power plants that are needed to help phase out fossil fuels and nuclear producing electrical plants. The rise of fossil fuel costs, electricity prices, and demand for energy, will benefit the implementation of geothermal power plants economically.

Geothermal is more attractive than wind or solar when developing sustainable energy. Unlike wind or solar, geothermal does not have to rely on the wind to blow or the sun to shine. In other words, the power is available 24 hours a day, 7 days a week, making it a renewable base load power supply. Having such a large amount of power within the Earth will help supply our future energy. Not only could it supply our energy needs, but also help diminish fossil fuel emissions such as CO_2 into the atmosphere, and lessen the need for domestic and foreign crude oil.

Today, most people are aware of the concept of geothermal for heating and cooling but are unaware of geothermal energy for electrical generation. This lack of knowledge may be due to the lack of government funding for geothermal projects compared to wind and solar. It could also be

attributed to our human nature. Everyone sees the sunshine and feels the wind blow. Very few know about the power beneath their feet.

A new growing trend in North America is the use of geothermal heat pumps. Depending on the varying seasons, it can heat and cool your house. However, the geothermal concept has been around for quite some time. The oldest use of geothermal energy dates back to 11,000 B.C. written on clay pots in ancient Japan, and progressively through time by the Romans for space heating and mineral extraction (Fridleifsson, 2001). However, Prince Piero Ginori Conti at Larderello, Tuscany, first developed the use of geothermal energy for electrical purposes in 1904 (Fridleifsson, 2001). Although a large and vast resource is available to generate electricity, very little is utilized today. Geothermal resources have been identified all over the world and utilized in many countries, but the geothermal market supplies only a small fraction of the overall need worldwide, with the U.S. producing only 3,086 MW (GEA, 2010).

The concept of utilizing geothermal energy for electrical needs is quite simple. Utilizing natural steam for electricity has been around for over a century. By using water, either liquid or steam, as the primary medium of transporting the heat from the Earth, the hot fluid is used to turn a turbine and generate electricity. There are three different types of power plants, depending on the temperature and nature of the source. These plants include dry steam, flash steam, and binary power plants (Fig. 7). First, dry steam plants use steam to directly turn the turbines. Second, flash steam is hot water that has been brought from a high-pressure reservoir and flashes to steam at the surface where it, in turn, will turn the turbines. Third, binary power uses typically cooler temperature geothermal fluids (90°C - 100°C) that exchange heat with an organic fluid, e.g., Rankine and Kalina Cycle engines, that

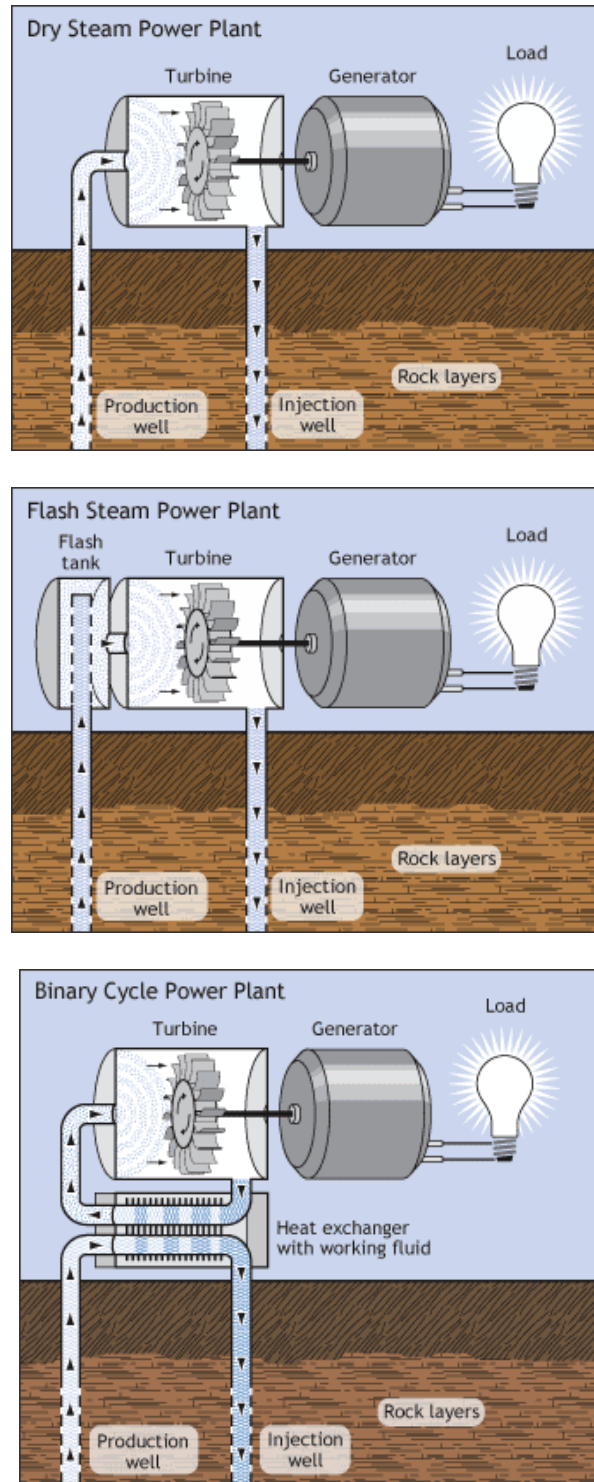


Figure 7. Schematics of dry steam, flash steam, and binary power plant technology to utilize hot fluids to generate electricity. Source: Geothermal Technologies Program (2011).

flashes to steam and turns the turbine to generate power. If efficiencies for binary power plants increase, utilizing this technology may help in developing geothermal in areas that were previously ruled out for geothermal electrical production. (This situation includes Minnesota if fluid flows of more than 1,000 gallons per minute at 90°C are produced and are economic, but that flow rate is difficult to achieve in enhanced geothermal systems (EGS; McKenna et al., 2005)). Although all three plants are different, they all share similar concepts, and depend on different temperature and pressure characteristics of the geothermal reservoir.

As renewable energy becomes a bigger part in fueling the Earth’s growing electrical demand, geothermal could make the largest impact. With basically an infinite supply of

“fuel” in the Earth, geothermal can be developed virtually anywhere as base load power at reasonable drilling depths. Geothermal electrical power will create a buffer between fossil fuel price fluctuations and nuclear plant retirements (Tester et al., 2006). Continued funding by government programs will most likely help in facilitating geothermal power plants in the near future.

In order to fully implement geothermal globally, technology to create Enhanced or Engineered Geothermal Systems (EGS) is a necessity. This concept of creating a geothermal reservoir in deep, hot, crystalline bedrock may be the solution for implementing geothermal in almost any area (Fig. 8). In order to create an EGS reservoir, hot, dry rock is stimulated, i.e., fractured, in such a way to increase porosity and permeability through a fracture network.

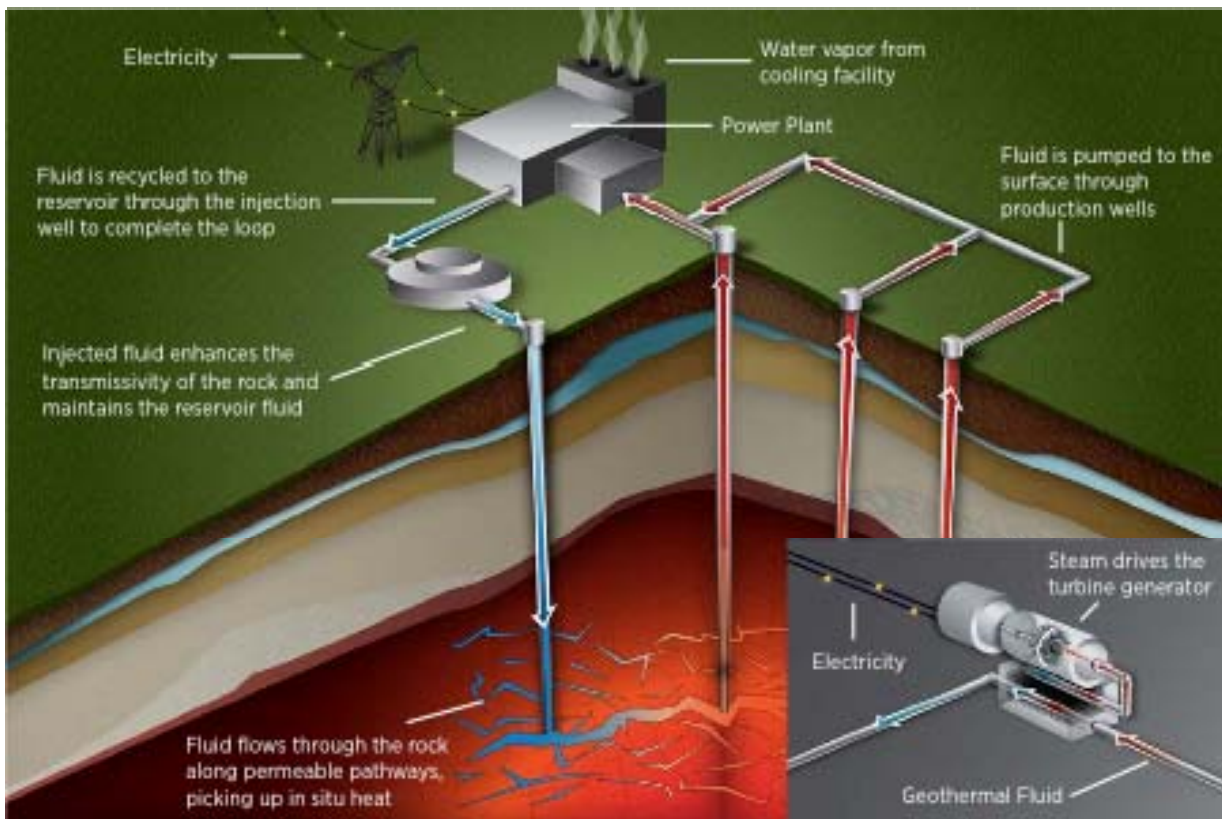


Figure 8. Concepts of an EGS reservoir using crystalline basement rocks. A closed looped reservoir is created through hydraulic stimulation, allowing for fluid to circulate and extract heat. The fluid then is flashed to steam where it powers a turbine, generating electricity. Source: U.S. Department of Energy Geothermal Technologies Program (2008).

This fracture network is then limited to a certain volume of rock, where fluid is circulated within the fractures to extract the heat from the newly developed reservoir. Fluid is then circulated through a network of production and injection wells to maintain reservoir pressure and fluid volumes large enough to sustain electrical production on the megawatt (MW) scale. With new technology, EGS could produce 100 gigawatts of electricity in the next 50 years with reasonable investments from independent developers and government funding for research and development (Tester et al., 2006).

EGS reservoir creation has been tested and demonstrated in many locations, e.g., U.S., Europe, and Australia (Tester et al., 2006). Lack of funding in the past decade has hampered development domestically, and technology transfer has been limited (Tester et al., 2006). The most notable of EGS tests in the U.S. took place at Fenton Hill, NM in the 1970s. Over the past decade, development of EGS worldwide has had successes showing that EGS is technically feasible at rock depths between 3 and 5 km (Tester et al., 2006). Accomplishments in the industry include, connected fracture networks in large volumes of rock in excess of 2 km³, circulation of fluid in the fractured networks without large pressure losses at commercial rates, and power generation at the surface from the EGS reservoir (Tester et al. 2006).

Wyborn (2011) reports that prior to establishing fluid circulation in the Innamincka granite in northern South Australia, seven other EGS programs in granites were evaluated to determine the critical reservoir characteristics that were needed to establish fluid circulation. Some of these characteristics from Wyborn (2011) are:

1. Stimulation in granite rock resulting from water injection with no added

- chemicals to enhance rock fracture permeability by 2-3 orders of magnitude;
2. Increased permeability resulting from increased fracture porosity associated with slippage on existing natural fractures during the stimulation;
3. The extent of the resulting reservoir can be accurately mapped by acoustic (micro-seismic) monitoring of the fracture slippages;
4. The orientation of the reservoir is strongly dependent on the relative directions of the three principle rock stress axes;
5. The stimulation pumping pressures required were 50-75% of the minimum principle stress for the depth of reservoir creation in accord with geomechanical theory, and are therefore lower than those required to open tensile fractures (fracking);
6. The size of the resulting stimulated reservoir is proportional to the volume of water injected. New space created by the increase in fracture porosity associated with the micro-seismic events is taken up by the injected water; and
7. Most projects up to 2002 were carried out in strike-slip and normal faulting stress regimes with minimum stress direction horizontal and the resulting reservoirs were oriented close to vertically.

The specific factors that control the amount of the heat resource that can be recovered as heat or converted into electricity or needed to forecast the EGS potential, or to manage the heat resources are (after Philips, 2000; Tester et al., 2007):

1. initial rock temperature;
2. maximum temperature drop that can be tolerated by the heat/power plant, i.e., the reservoir abandonment temperature;
3. the volume of rock that can be accessed and stimulated;

4. the active or effective heat-exchange area (controlled by the length, width, and spacing of the existing and stimulated fractures); and
5. the flow rate of the water or CO₂ through the connected fractures, which in turn are controlled by:
 - a. permeability;
 - b. temperature;
 - c. porosity/connected porosity;
 - d. fluid path(s);
 - e. fluid pressure;
 - f. rock volume fractured;
 - g. fracture spacing, orientation, and fluid loss;
 - h. rock volume attainable by drainage; and
 - i. pattern of injection and producer wells.

There have been significant accomplishments and some drawbacks and difficulties in producing the reservoir either from engineering or environmental setbacks. Issues include fluid flow short-circuiting, geochemical impacts, induced seismicity, injection pressures, and fluid loss (Tester et al., 2006). If some of these negative impacts are better understood through research and development, geothermal energy will prove to be more economical and competitive. In the near future, geothermal energy will likely help create a sustainable future domestically and abroad. This concept seems quite simple, but technological advances in the industry are needed to improve our understanding of engineering and environmental issues.

Section 1.1.5 General Economics of Establishing an EGS System

Based upon the initial work by Tester et al. (2006), there are very few geothermal

wells deeper than 2.75 km. The major costs of establishing a geothermal electrical power generating system are: 1) exploration drilling, e.g., in Minnesota to >7 km to locate sufficient temperature and natural fracture systems in a given area; 2) production drilling; and 3) injection well drilling of 2 or more boreholes – one for injection of fluids and a second or more for recovery of heated fluids (Fig. 9). For lower grade geothermal resources, like in Minnesota, Tester et al. (2006) estimates that these drilling costs are 60% of the cost of constructing a power generation facility (capital costs). Tester et al. (2006) based geothermal drilling costs on deep drilling for oil and gas, and these authors indicate the cost of the geothermal wells will be 2 to 5 times the cost of similar oil or gas wells. For example, Tester et al. (2006) estimate that 7.5 km well would cost about \$12 million to drill and complete for production, which would be applicable to potential Minnesota targets. This estimate comes from costs of drilling deep oil and gas wells in 2006, i.e., costs may vary with the introduction of new drilling technologies.

A power generation installation would require a minimum of two wells with a minimum flow rate (water or CO₂) of 2,000 gpm at 150°C. Exploration drilling to determine bottom hole temperatures and fractures systems would proceed the production phase (Fig. 10).

Technological advancements in drilling, reservoir stimulation, and binary power plant efficiency must be met in order to reduce costs (including return on investment for development and production) under \$0.065 per kWh, assuming tax incentives [2.0 cents/kWh] (Mims, 2009).

According to Eliasson and Smith (2011), there are 3 economic stages in establishing a 50MW enhanced geothermal electrical generation plant: 1) identification of a site [\$0.5-1.0 million]; 2) exploration –

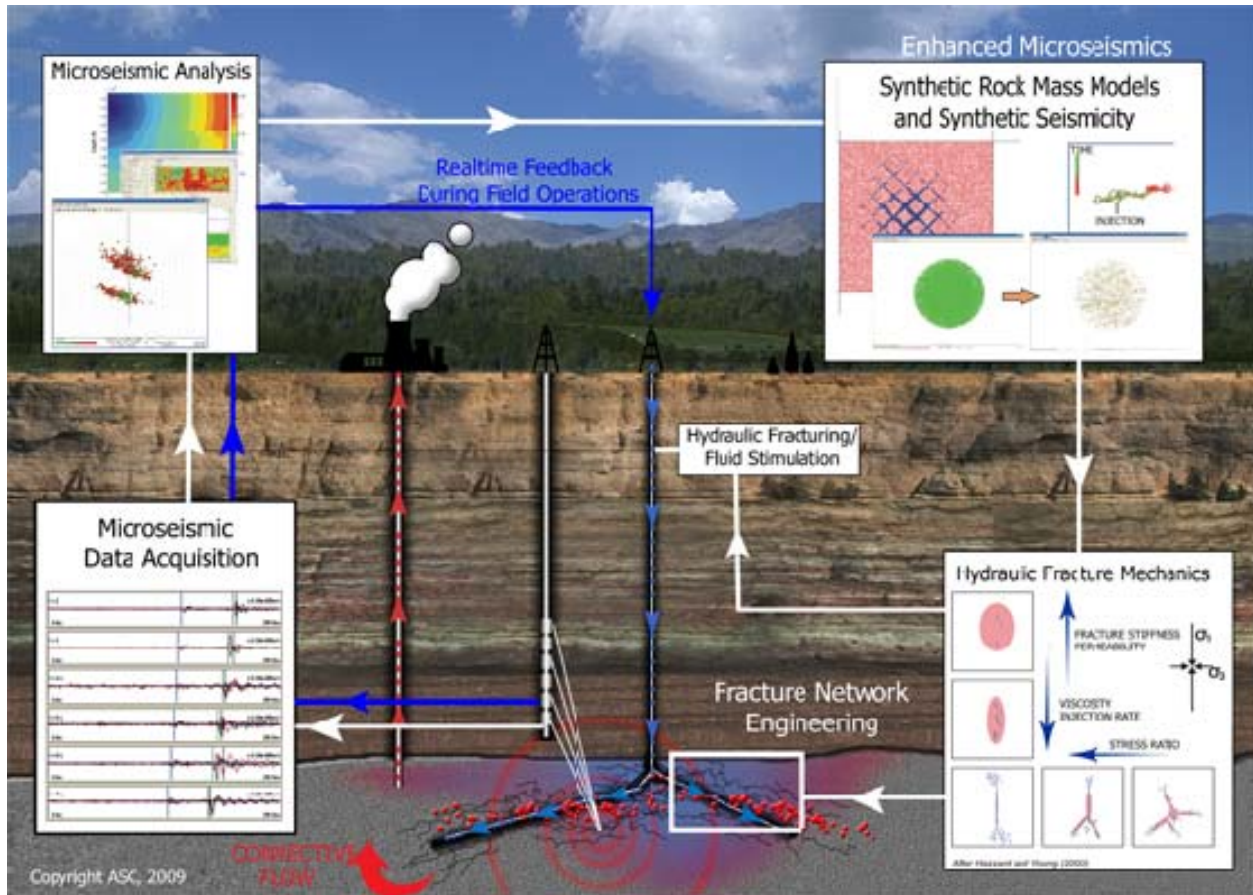
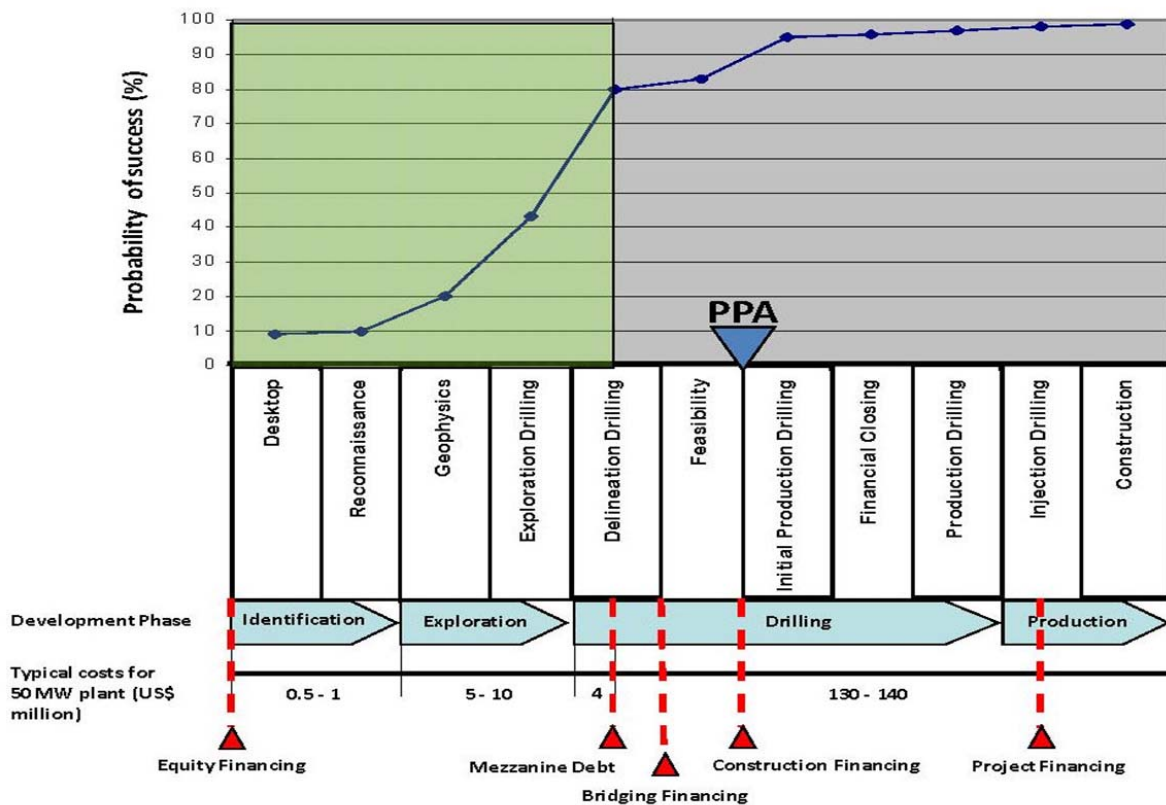


Figure 9. Diagram of a geothermal power generating facility showing: 1) an injection well undergoing hydrofracturing; 2) an additional borehole with downhole seismometers to record the locations of the microfractures by recording the microseismicity; and 3) a recovery well that brings the heated fluids (100-150°C water or CO₂) to the surface power generating facility (after Zhao et al., 2011).

geophysics and initial drilling [\$5-\$10 million]; and 3) delineation drilling, including a feasibility study, initial production drilling, financial closing, and production drilling (injection drilling) and plant construction [\$134-\$144 million].

Blodgett and Slack (2009) state that the California Energy Commission in 2007 estimates placed the levelized generation costs for a 50 MW geothermal binary plant at \$92 per megawatt hour and for a 50 MW dual flash geothermal plant at \$88 per megawatt hour, which over the lifetime of the plant can be competitive with a variety of technologies, including natural gas (Fig.

11). As the figure illustrates geothermal energy plants with either a dual flash or binary (organic Rankine or Kalina cycle engines, respectively) plants are the lowest levelized cost of other types of renewable energy on a \$/MWh basis. Technological advancements in drilling, reservoir stimulation, and binary power plant efficiency must be met in order to reduce costs (including return on investment for development and production) under \$0.065 per kWh, assuming tax incentives [2.0 cents/kWh; Lund et al., 2010] (Mims, 2009).



Source: Deloitte, *Geothermal Risk Mitigation Strategies Report*, for the US Department of Energy, February 2008

Figure 10. The various stages of EGS exploration, development, production and financing versus risk tolerance (Eliasson and Smith, 2011).

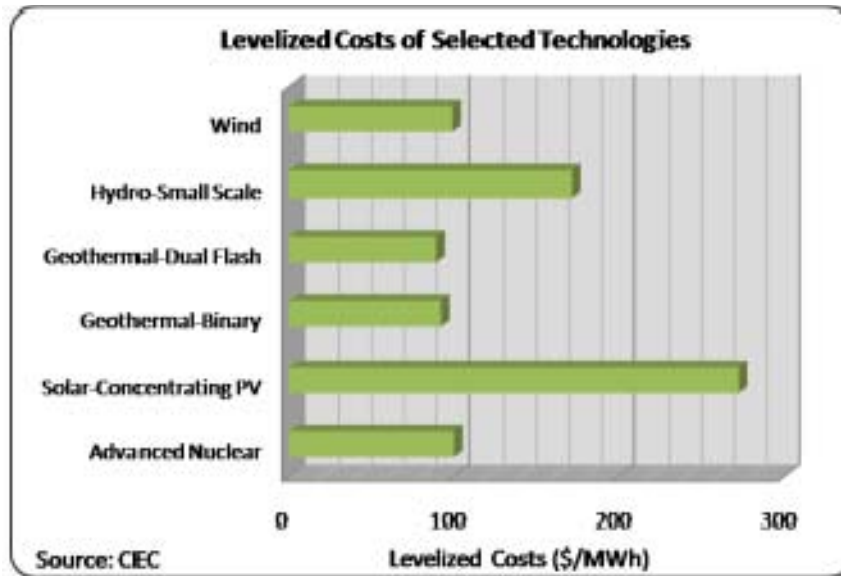


Figure 11. Levelized costs of selected power producing technologies (Blodgett and Slack, 2009).

1.2 Previously Assessed Geothermal Resources in Minnesota

Being situated in the stable North American craton, low temperatures are encountered compared to the western continental margin. Few have tried to quantify the electrical geothermal resources available in Minnesota because of the low heat flow resulting in low temperatures at depths and the small amount of energy available for EGS production. The estimated EGS resources for Minnesota are presented in a 2006 report issued by MIT (Tester et al., 2006), and maps produced by the National Renewable Energy Lab (Fig. 12). In both cases, Minnesota is seen having a “low” geothermal resource and developing geothermal in the upper 10 km is highly unlikely.

With a previous estimate of 35,789 EJ, this quantity is enough energy to produce 6,161 MW at a 2% recovery factor (Tester et al., 2006). Although this is a large amount of energy available from 3-10 km, it is low compared to other areas of the U.S. To

develop EGS, temperatures of 150°C are accessible only at depths 8.5 km and deeper, resulting in an engineering problem withdrawing heat at depths lower than 5 km (Tester et al., 2006). Minnesota ranks 49th, before New Hampshire in the U.S. in the amount of energy available for EGS applications based upon current resource calculations (Tester et al. 2006).

As previously mentioned, there is a bias in the data towards low heat flow values in Minnesota. Because heat flow values are low, it reflects an estimation of what the temperatures are at 3-10 km, and the available energy at these depths. New heat flow, thermal conductivity, and radioactivity measurements are made in this study to better quantify the resource and produce more reliable and likely temperature maps at depths of 4-10 km (Fig. 2 and Appendix A). Heat flow measured from conventional methods and heat flow estimated from radioactive heat generation will permit further quantifying of the resource, aiding in future exploration for high heat flow areas.

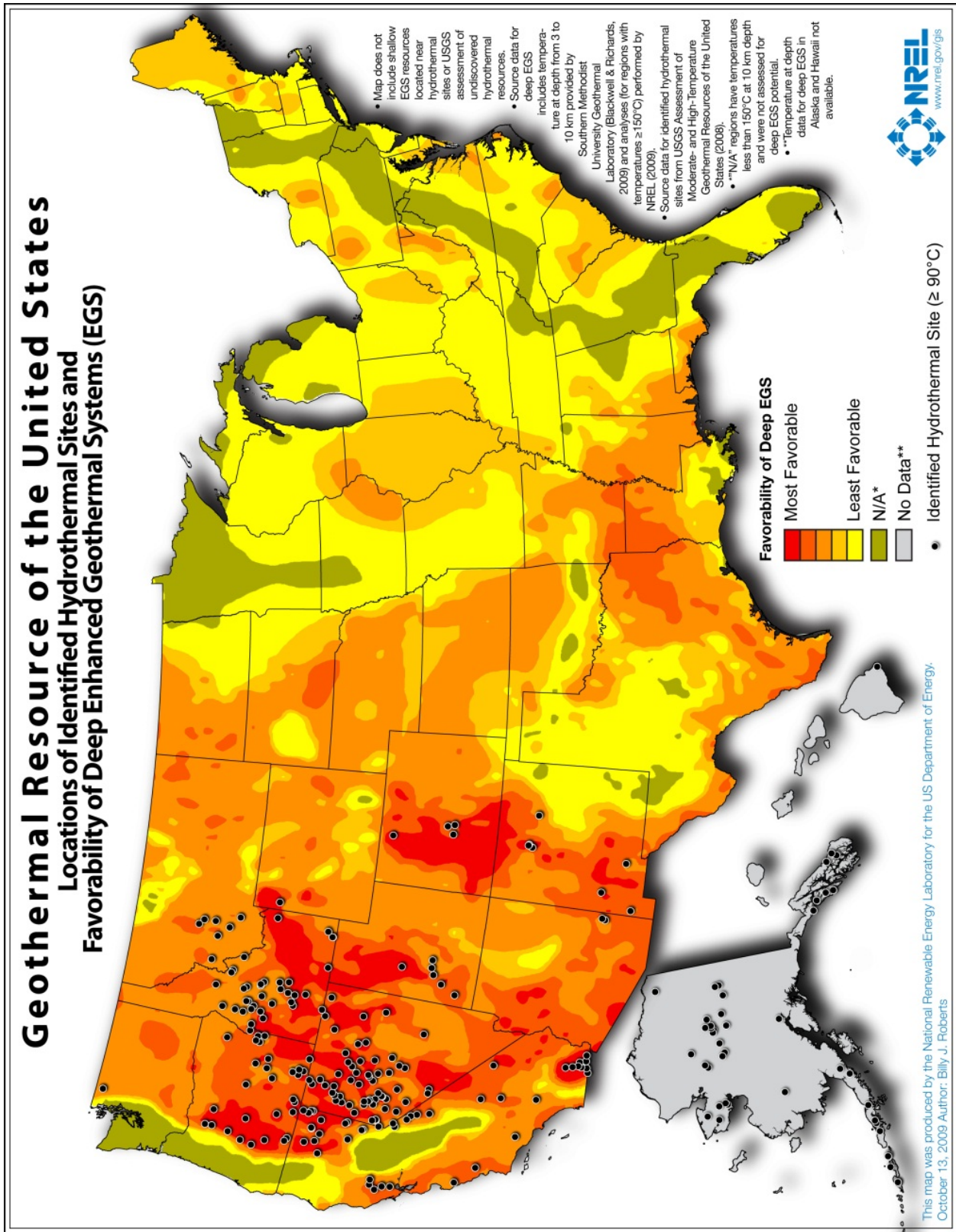


Figure 12. Geothermal resources of the U.S. EGS resources in Minnesota are least favorable or N/A in cases of the black shaded area where temperatures are $>150^{\circ}\text{C}$ at 10 kilometers Source: Roberts (2010).

High heat generation in the granitic and gneissic rock will have higher temperatures and will be the best candidate for developing geothermal resources in Minnesota. Optimistically, resources in the granitic plutons will be available at depths near six kilometers for engineering feasibility. Reaching the 150°C isotherm near a 6 km depth is a drastic difference than the 8.5-10 km previously estimated. Advancing EGS technology for the future could potentially aid in developing geothermal electrical resources in Minnesota.

1.3 Minnesota Geology

Geology plays a very important role in the heat transport throughout the Earth. This geological role is mainly due to the characteristics of the basement rocks, including thermal conductivity and radiogenic heat production. Ideally, heat flow will be higher in felsic than in mafic rocks due to the difference in radioactive heat production in stable continental areas. Both rock types are characteristically found throughout Minnesota. Along with geology, understanding the climate history can also affect temperature gradients. Extensive episodes of glaciation have occurred in Minnesota, affecting the gradient substantially since the last glacial maximum (LGM) and should be corrected appropriately at each heat flow site.

Located almost entirely in the Superior Province of the Canadian Shield, Minnesota contains some of the oldest rocks on Earth. The stratigraphic column of Minnesota provides information on various geologic events spanning from 3,600 Ma ago to today. Seen on the geologic map of Minnesota, this time span includes the

accretion of island arcs and microcontinents, followed by mountain building, rifting, deposition, erosion, and glaciation (Fig. 13).

Subdivided by lithology, structure, metamorphism, and geophysical characteristics, many different subprovinces make up the Superior Province of the Canadian Shield (Fig. 14). The Wawa-Abitibi, Wabigoon, and Quetico subprovinces are present in Minnesota and extend further into Canada. The Minnesota River Valley (MRV), a micro continent composed of gneiss, is part of the same assemblage making up the Canadian Shield. Although these terranes are different by the supracrustal rocks and plutonic rocks they contain, the east-west structural trends are similar due to the several orogenic events that occurred during accretion.

The Wabigoon and Wawa-Abitibi subprovinces, 2.7 Ga in age, are composed of alternating greenstone belts with sedimentary sequences intruded by large granitoid bodies located in northern Minnesota (Henry et al., 1998; Morey and Sims, 1976). Gravity and aeromagnetic maps (Chandler, 1990) show these subprovinces trend to the northeast as narrow curvilinear anomalies. Exposed in some areas, these belts are 100 km wide and 900 km east to west through Minnesota, Ontario, and Manitoba. The Wabigoon subprovince consists of greenstone belts, batholithic complexes, and plutons (Card, 1990). The plutonic batholithic complexes range from ultramafic and mafic to granitoid intrusions. Mainly, the Wabigoon and Wawa-Abitibi subprovinces consist of 2/3 plutonic rocks and 1/3 supracrustal rocks, including greenstone belts unconformably overlain by alluvial and fluvial sediments (Card, 1990).

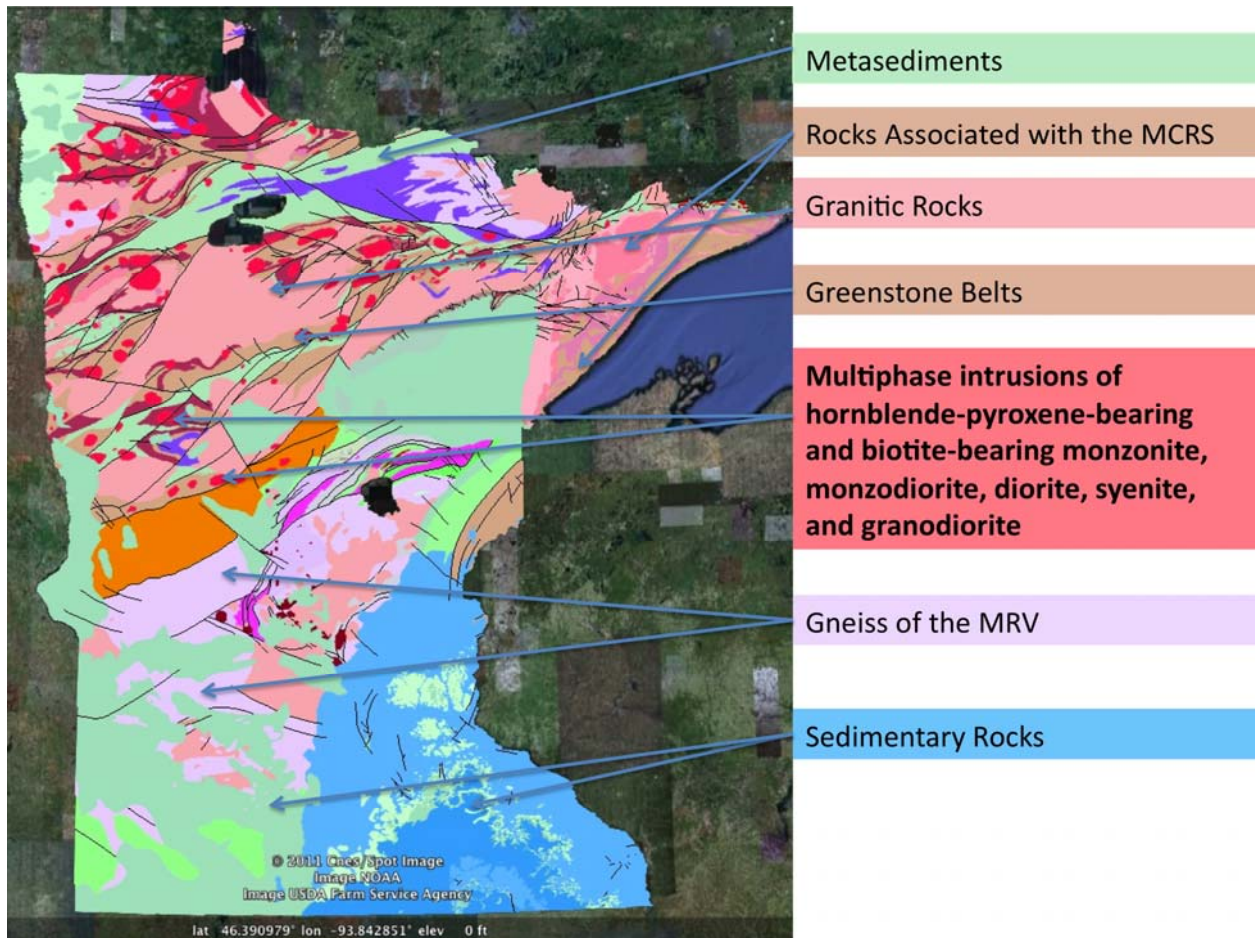


Figure 13. Geologic map of Minnesota. Labels are provided to describe locations of mafic and felsic rock bodies.



Figure 14. Locations and subdivisions of the Superior Province. The Wawa-Abitibi, Wabigoon, Quetico, and Minnesota River Valley Gneiss are all different geologic terranes making up the Precambrian Bedrock in Minnesota. Modified from Wyman and Kerrich (2009) with permission.

Different than the former subprovinces, the Quetico is a metasedimentary belt with granitoid intrusions. Although the subprovinces are separated into different terranes, structural trends seem to be similar due to the orogenic events that took place during the Archean. The Quetico is bounded by the Wabigoon to the north and Wawa-Abitibi to the south in Minnesota. Primarily, the Quetico subprovince is composed of low to medium grained metasediments with some gneissic rocks derived from wacke and siltstone (Card, 1990). The metasediments increase in metamorphic grade from greenschist facies at the margins to amphibolite facies near the axial regions (Perry et al., 2006). Structurally, the Quetico is an accretionary prism. The accretionary prism accreted onto the Wabigoon and was later compressed by the Wawa arc (Card, 1990). Almost three fourths of the subprovince consists of plutonic and gneissic rocks with the remaining one fourth consisting of low to medium grade supracrustal rocks (Card, 1990).

South of the Wawa-Abitibi Subprovince is the MRV gneissic terrane (Fig. 14). Gneisses are most likely volcano-plutonic in origin, a separate micro continent (Card, 1990). At some point the MRV was accreted to the Superior Province during the Penokean orogeny approximately 1.88 Ga (Holm et al., 2007). Mostly, these rocks consist of an interlayered sequence of migmatitic granitic gneiss, amphibolitic gneiss, and pelitic gneiss, creating broad magnetic and gravity anomalies (Morey and Sims, 1976). The MRV has synclinal and anticlinal structures with an eastward plunging axis (Morey and Sims, 1976).

After erosion exposed the granites formed during the Penokean orogeny, rifting started to occur in North America around 1,100 Ma ago (Holm et al., 2007). The arc-shaped rift extends from the lower peninsula of Michigan, up through Lake Superior, down through eastern Minnesota, and into Kansas (Fig. 15). During this time, mafic

magma rose to the surface forming basalts in the sea floor and covering the land with lava flows. Soon after, the Duluth Complex, composed of gabbros and other coarse grained igneous rocks, intruded the lava flows and crystallized beneath the surface.

With a violent and extensive history during the Precambrian, very little history remains from the Phanerozoic and Cenozoic. During the Paleozoic, sandstones, limestones and shales were deposited throughout Minnesota during six episodes of flooding (Mossler, 2008). Presently, most of the Paleozoic section was eroded in the state, except in the southeastern portion and in some areas of the northwest. Another advancement of seas deposited sediment in northwestern Minnesota during the Jurassic and then again in the western part of the state during the Cretaceous. Erosion during the Tertiary was followed by glaciation as the climate cooled between 1.8 Ma and 10ka. During that time four major glacial advancements occurred. These advancements covered the land with glacial till and created many depositional features, including the kettle lakes that give rise to Minnesota's nickname, "The Land of 10,000 Lakes."

1.4 Heat Flow

Extensive heat flow studies have helped scientists understand geologic processes, including subduction, rifting, volcanism, maturation of fossil fuels, and mantle convection. Using heat flow data with other geophysical techniques, geologists are able to support research on the past and present thermal nature of the Earth. In this study, heat flow helps in understanding the thermal regime of tectonically stable areas such as the Canadian Shield, the effects of past climates on borehole temperature measurements, and the resource possibilities of harnessing heat as a sustainable energy source through geothermal technology.

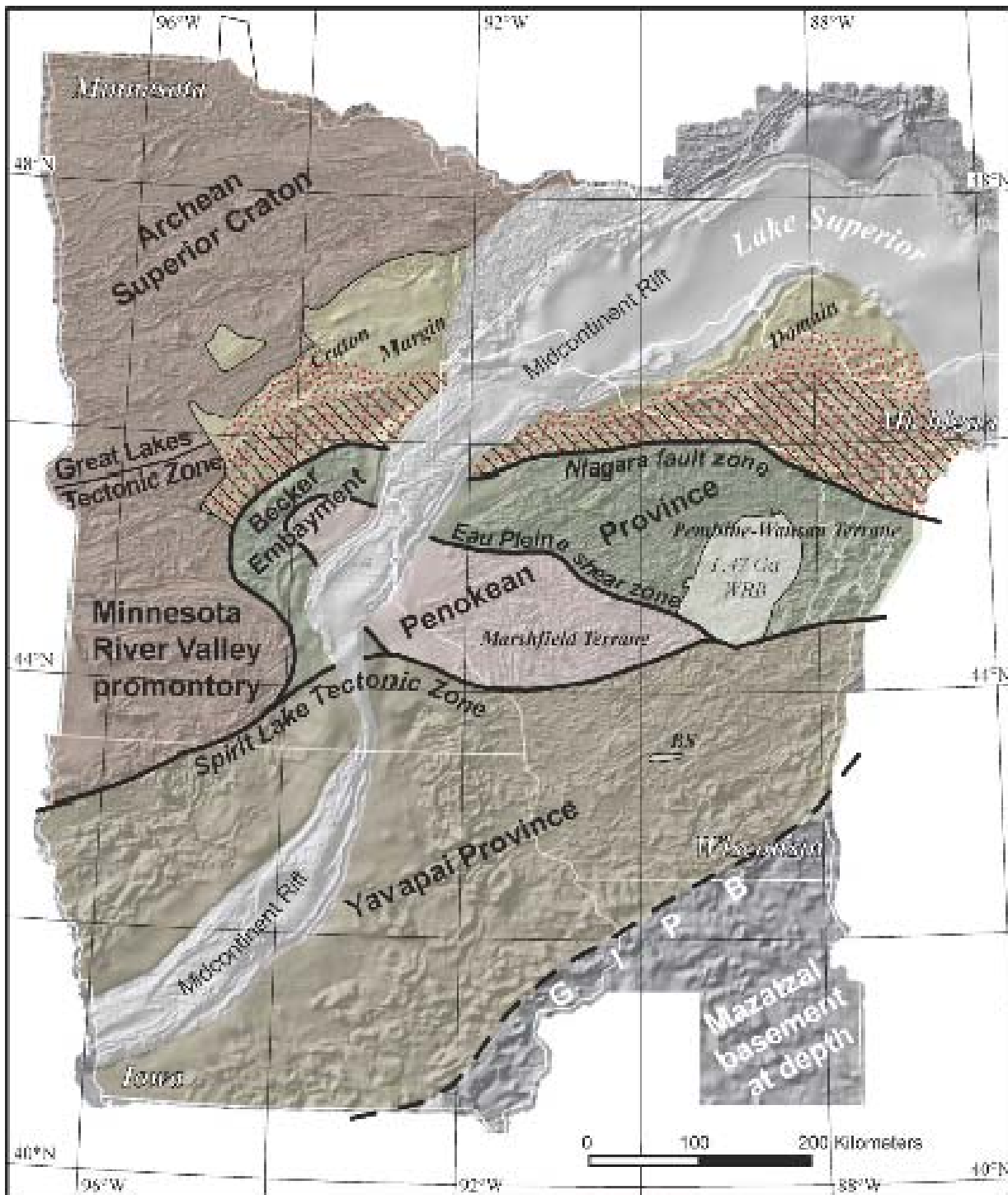


Figure 15. Geology and geographical extent of the Midcontinent Rift System through North America. Modified from Holm et al. (2007).

To fully understand the heat flow of an area, Roy et al. (1968) noted that heat flow measurements in an area “requires a spacing of measurements on the horizontal scale comparable with the dimensions of geological units or crustal thickness, some tens of kilometers.” In other words, in order to understand heat flow in a particular area, heat flow measurements should be made routinely close to one another, i.e., 10 kilometers. Although these conditions would be ideal, temperature gradient measurements are made in wells of opportunity, including water, oil and gas, or mineral exploration wells. Wells of opportunity tend to concentrate heat flow measurements in certain areas creating a sampling bias. This ideal spacing is met in a few places and has provided rough outlines of geothermal provinces (Roy et al., 1968). Even though a large number of measurements have been made throughout the Earth, many areas are left uncovered and understudied.

Defined mathematically:

$$q = \lambda \Gamma \quad (\text{Eq. 1.4.1})$$

Where q is heat flow, λ is thermal conductivity, Γ is geothermal gradient. Heat flow is the transport of heat from a warmer area to a cooler one. The primary means of heat flow in the crust occurs as heat conduction from one rock unit to another, but at times, heat will flow by convection as fluid flows through pores and fractures within geologic units of the Earth. Although conduction is the primary source of heat transport in the crust and convection in the mantle, heat flow will not be uniform everywhere due to the geologic diversity of the Earth.

Heat sources in the crust occur from the mantle conducting heat to the surface, or about 60% of the present heat flow. The other 40% is attributed to the radioactive decay of ^{238}U , ^{232}Th , and ^{40}K , naturally

occurring within the Earth’s crust. Through radioactive decay, energy is given off through alpha, beta, or gamma particles, as well as neutrinos and antineutrinos. Heat generation in the crust is defined exponentially:

$$A = A_0 e^{\frac{-z}{b}} \quad (\text{Eq. 1.4.2})$$

where z is depth, A_0 is the measured surface heat production, and b is the thickness of the radioactive layer.

Due to the diverse nature of the crust, both of these heat sources are distributed unevenly throughout the globe. Mantle conduction will contribute a higher percentage of the heat flow around volcanic and tectonically active areas, and will be lower in tectonically stable areas like the Canadian Shield. Radiogenic isotopes are going to be concentrated in felsic bodies unlike those mafic in origin. Other sources of heat occur from frictional heating along major faults and the exothermic metamorphic and diagenetic processes. However, these latter sources are localized and contribute very little heat.

Geology in the U.S. is diverse, causing variations in heat flow from east to west (Fig. 16). Differences can be constrained to heat flow provinces defined by Roy et al. (1968). These provinces include the Basin and Range, Sierra Nevada, and Eastern United States. A heat flow province is defined by the characteristic relationship between heat flow and heat production where the tectono-thermal history is somewhat similar within a certain area (Blackwell, 1971; Beardsmore and Cull, 2001). The characteristic relationship of heat flow and heat production can be defined linearly by $q = q_0 + Ab$, where q is the surface heat flow, q_0 (the intercept) is the heat flow from the mantle, b (the slope) is the thickness, and A is the radioactive heat production of plutonic rocks. Mantle heat

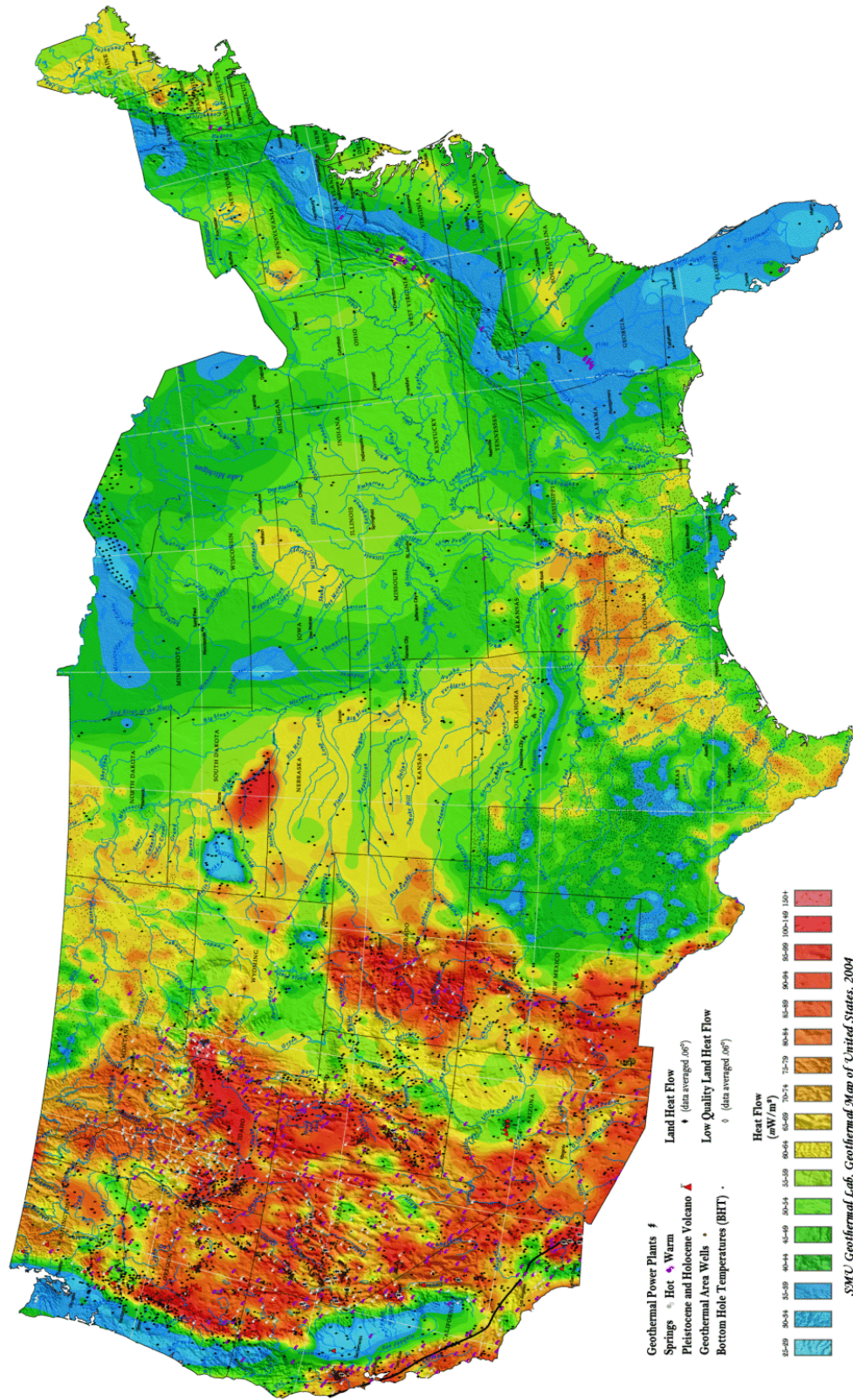


Figure 16. Heat flow map of the United States. Source: Blackwell and Richards (2004).

flow and the relative thickness for the three heat flow provinces in the U.S. are shown in Table 1. Using the linear relationship, the heat flow province concept is acceptable when modeling shallow subsurface temperatures within the crust (Beardsmore and Cull, 2001).

In the Eastern U.S., 40% fewer heat flow measurements are made in comparison to the Western U.S. (Gosnold, 1990). This difference is largely due to the extensive studies done in tectonically active areas where heat flow can differ drastically laterally, unlike the stable areas of the Eastern U.S. Attributed to predictability caused by the variation of radioactive decay, the Eastern U.S. is left understudied compared to the Western U.S. Previous research (see discussion below), on heat flow in the Canadian Shield and Minnesota is very limited. This lack of research is due to the number of wells made available for temperature logging throughout this area. In addition to temperature gradient measurements in wells and exploration drill holes, this study will use measurements of thermal conductivity and radioactivity data to better constrain and understand heat flow in Minnesota and the amount of EGS resources available.

1.5 Previous Research of Heat Flow in Minnesota and Canadian Shield

Prior to this study, there were only four heat flow measurements in Minnesota (Roy

et al., 1968; 1972). These measurements were either made in the mafic rocks of the MCRS or in shallow lakes. One heat flow measurement, near Bemidji, MN, was made outside the MCRS (37 mW m^{-2}), while the other three measurements were made in the MCRS near Ely, St. Paul, and Duluth (average: $40 \pm 6 \text{ mW m}^{-2}$). Other research in the MCRS includes 162 heat flow measurements using marine techniques in Lake Superior (Hart et al., 1994). Heat flow values in Minnesota are low compared to the continental average, 70.9 mW^{-2} , and those corresponding to other Precambrian rocks, 50.5 mW^{-2} (Davies and Davies, 2010). Low heat flow in Minnesota is most likely caused by the following two reasons: 1) past heat flow measurements were made in mafic rocks of the MCRS (mafic rocks tend to have low radiogenic heat production, unlike the granitic and gneissic rocks that make up much of the Canadian Shield); and 2) post-glacial climatic changes have affected temperature gradients up to 30% in the upper two kilometers of the crust, and these data were either not known or were not taken into account.

One of the previous measurements in Minnesota was made using traditional borehole techniques at Ely. The other three were measured using oceanographic techniques on land in small lakes. Previously, other oceanographic techniques in large lakes, including Lake Superior by Hart and Steinhart (1965), proved to be more successful with isothermal bottom water in unconsolidated sediments.

Table 1. Heat flow provinces for the United States. Contribution of mantle heat flux and the thickness of the radioactive layer are given (Roy et al., 1968).

Heat Flow Province	Mantle Heat Flux (mW m^{-2})	Thickness (km)
Eastern U.S.	33.5	7.5
Basin and Range	58.7	9.4
Sierra Nevada	16.8	10

However, using the same techniques in small lakes usually have large and uncertain corrections. Roy et al. (1972) noted that this method was still unproven since there were no conventional measurements made near any of these locations. Allis and Garland (1979) used the same techniques in the Canadian Shield and noted that the values were highly perturbed. However, these measurements were overcorrected and were systematically higher than traditional land techniques and should be deemed unreliable (Rolandone et al., 2003). Much consideration should be taken into account when using the previous values measured in the small lakes when investigating heat flow in Minnesota. Most likely the heat flow values should not be considered when doing any further study on heat flow in Minnesota as they create both highs and lows when contouring the data.

Due to the lack of research and the uncertainty of the heat flow measurements made in the shallow lakes, very little is known about heat flow variances in the same subprovinces in Minnesota. If the shallow lake measurements are disregarded, only one reliable heat flow site represents what we know about heat flow in Minnesota. Most likely heat flow is similar to the other measurements in the Superior Province and is higher outside the Midcontinent Rift System.

Research on heat flow in Minnesota is not extensive, but a considerable amount of research has been done in the same Superior subprovinces in Canada that are present in Minnesota (Fig. 17). Higher heat flow, compared to the current measurements in Minnesota, is present in the Wabigoon, Quetico, and Wawa Subprovinces of the Superior Province measured in Ontario and Manitoba (Levy et al., 2010). Lithology and age of these subprovinces is similar as they extend into Minnesota. Heat flows for the subprovinces are 40.3 mW m^{-2} , 46.6 mW m^{-2} and 45.1 mW m^{-2} respectively (Perry et al., 2006). Measurements made in these sub-

provinces, would be more representative of the heat flow in northern Minnesota. Heat flow measured in the subprovinces would be a general assumption of heat flow in Minnesota since variations in the Canadian Shield geology can be highly variable, but generally heat flow follows the systematic geology of each subprovince (Perry et al., 2010). Extending southward into Minnesota heat flow could be suggestively higher near the edges than the center of the North American craton caused by thinning of the lithosphere, implying a greater heat flux from the mantle (Perry et al., 2010). If true, heat flow would be higher in the Superior subprovinces trending to the southwest in Minnesota than what is measured in Manitoba and Ontario.

Most of the plutonic rocks in the Wawa-Abitibi subprovince are large granitic batholiths and gneissic complexes (Card, 1990). In Canada, the Wawa has a heat flow of 45.1 mW m^{-2} and an average heat generation of $0.85 \text{ } \mu\text{W m}^{-3}$ (Perry et al., 2006). This value is 12% greater than the heat flow measured in Minnesota. Similar geologically to the Wawa-Abitibi subprovince, the Wabigoon has an average heat flow of 40.3 mW m^{-2} and a heat generation of $0.63 \text{ } \mu\text{W m}^{-3}$. With similar geology to the Wawa-Abitibi, high heat flow will be concentrated in high radioactive granitic intrusions throughout the province.

Radioactive elements are depleted in the Wabigoon and Wawa-Abitibi compared to the Quetico metasedimentary belt (Perry et al., 2010). Higher radioactivity in the metasediment belts is common throughout the Canadian Shield (Perry et al., 2010). With an average radioactivity of $0.95 \text{ } \mu\text{W m}^{-3}$, heat flow averages 46.5 mW m^{-2} (Perry et al., 2006). The common characteristic for the Superior Province and the rest of the Canadian Shield is that the mantle heat flux has little variance and perhaps may be higher near the southern margin (Perry et al., 2010). Heat flow variances throughout the Canadian Shield are going to commonly be

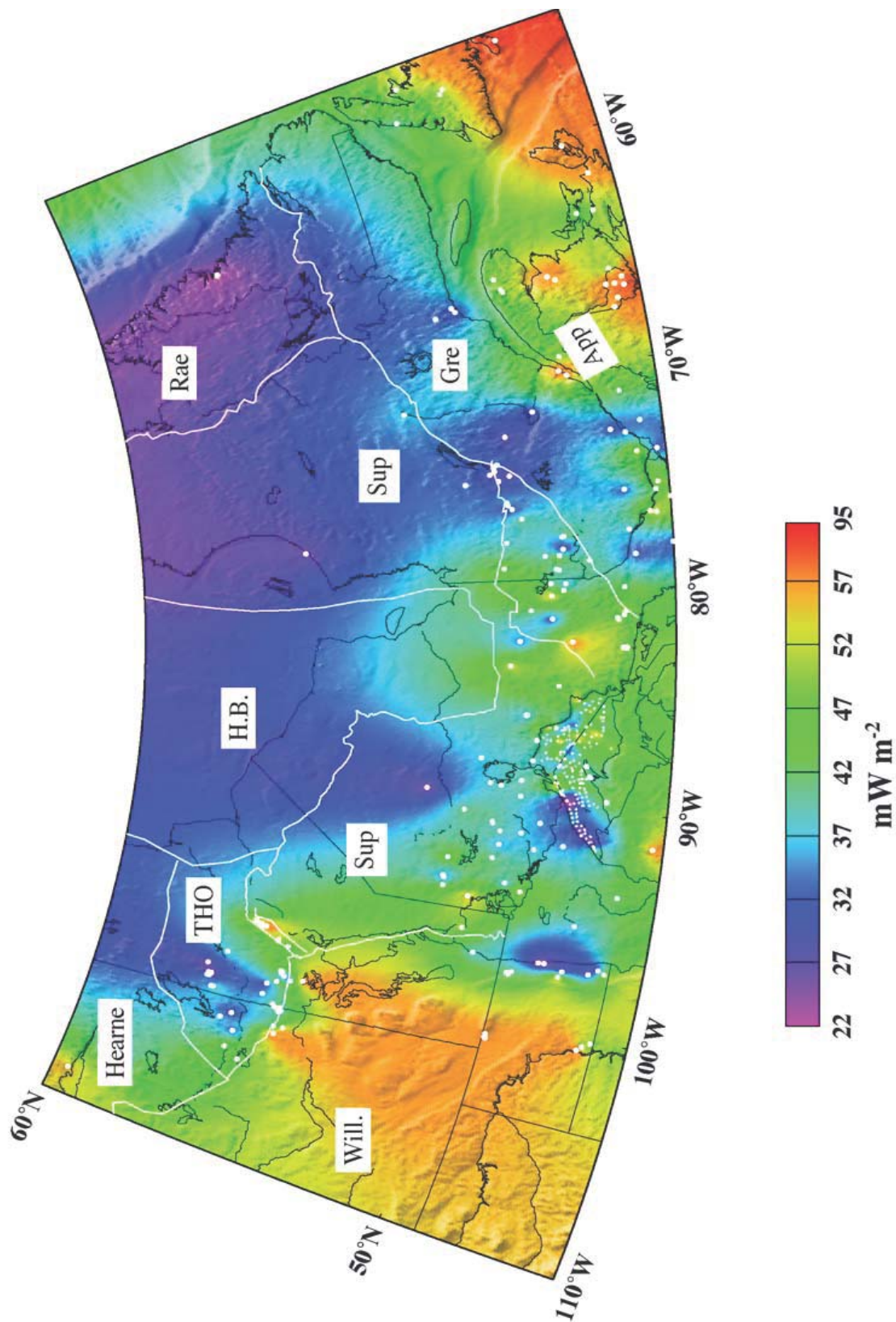


Figure 17. Heat flow measurements of the Canadian Shield with outlines of subprovinces. Source: Mareschal and Jaupart (2004).

attributed to changes in heat production due to changes in lithology in the different crustal rocks of the subprovinces.

Another characteristic of the Superior Province is that high heat flow in the granitic intrusions of the subprovinces will tend to form positive anomalies with heat flow exceeding 50 mW m^{-2} (Perry et al., 2010). Due to the nature of higher heat generation in the granitic intrusions, heat flow will be higher in many of the plutonic bodies throughout the state, but may not represent the bulk statistics of heat flow. Radioactivity measurements in granitic plutons in Minnesota yield average heat generations of $2.17 \mu\text{W m}^{-3}$ for the Vermillion Massif, and $2.24 \mu\text{W m}^{-3}$ for the Giants Range Batholith (Rye and Roy, 1978). Heat flow values for these areas would be very similar to other plutons in Canada based on the heat flow heat production relationship. Radioactive heat production of the metasediments of the Quetico in Minnesota is an average of $0.90 \mu\text{W m}^{-3}$ (Rogers et al., 1969) and would also yield similar heat flow values of measurements made in Ontario. Since mantle heat flow is fairly consistent and radioactivity is the controlling mechanism of heat flow variations in the Canadian Shield, heat flow should be greater in areas of high heat production.

1.6 Climate Effect on Heat Flow

As previously discussed, low heat flow in Minnesota is attributed to the measurements made in low radioactive areas of the MCRS and the uncertainty of the perturbation of the measurements made in the shallow lakes in Minnesota. Another reason heat flow measurements are low could be attributed to perturbation of the gradients caused by warming since recent glaciations. This perturbation of the gradient has been known for quite some time (Hotchkiss and Ingersoll, 1934), and heat

flow measurements have been published ignoring the subject. This perturbation occurs in data collected in the Canadian Shield and in the northern latitudes of North America. Not accounting for the perturbation will underestimate the true heat flow.

Initially, Jessop (1971) developed a correction for such perturbations where in extreme cases amounted up to 10% in southern Canada and the northern U.S. This correction accounted for temperatures at the base of the glacier and the present ambient temperature. Although glaciated areas are of initial concern, non-glaciated areas are open to just as much speculation for correction as well (Jessop, 1971). If non-glaciated areas are affected, a large number of heat flow measurements made throughout the world, especially those in shallow boreholes, may have to account for such a correction.

The amount of warming varies by latitude and a correction should be applied to temperature gradients measured in glaciated areas. Warming can vary by latitude and longitude based on the paleo temperature and the present day temperature. Jessop (1971), with good reason, assumed the base of the glacier is near the pressure point of melting (-1°C). Annually, Minnesota has an average ambient temperature of $6\text{-}7^\circ\text{C}$ indicating a warming of $7\text{-}8^\circ\text{C}$ since the LGM. More recent investigations (Chouinard and Mareschal, 2009) using data from deep boreholes confirmed the temperature at the base of the ice sheet to be near the pressure point of melting, but temperatures near the edge of the ice sheet may have actually been cooler or -4 to -6°C . This measurement would indicate a warming of $10\text{-}15^\circ\text{C}$ in Minnesota. With other supportive evidence this warming has been confirmed by a pollen analyses in Manitoba indicating a warming of nearly 15°C (Ritchie, 1983), and climate modeling also indicated a warming of $15\text{-}20^\circ\text{C}$ (Ganopolski et al., 1998; Schneider von Deimling et al., 2006).

The high degree of warming gives strong support that temperature gradients made near the surface (upper 2000 m) should have a temperature correction, dependent on depth, on the basis of 15°C warming since the retreat of the Laurentide ice sheet 9-12 ka ago. The correction developed in this study is similar to the one developed by Majorowicz and Wybraniec (2010) for temperature gradients in Europe.

2. RESEARCH METHODS

The University of North Dakota Geothermal Lab (UNDGL) and the Natural Resources Research Institute (NRRI) of the University of Minnesota Duluth conducted sample analysis and temperature measurements. The UNDGL and NRRI have the capabilities and equipment to analyze heat flow and geothermal resources in Minnesota that include a thermistor temperature probe for temperature gradient measurements, a gamma ray spectrometer to measure radioactivity, and two portable electronic divided bar (PEDB) apparatuses for measuring thermal conductivity. A total of 795 wells were inspected for temperature gradient measurements. Of the 795 wells inspected, over 100 boreholes were measured. About half of these wells had noise disturbances creating isothermal or perturbed gradients and could not be used in heat flow calculations. In this study, 57 new measurements were made and were compiled into 31 new heat flow sites (Appendix B). Additional data from 199 drill core and outcrop samples were analyzed for rock conductivity and radioactivity (Fig. 18 and Appendix C). One hundred rock and drill core samples were also analyzed for whole rock and trace elements including U and Th (Appendix E – Excel spreadsheet).

2.1 Temperature Gradient Measurements

Wells in Minnesota for temperature logging are difficult to find. Most likely wells are either too shallow or inaccessible. This situation is typical in most cases for heat flow studies. Wells available for temperature logging are wells of opportunity, and are rarely drilled for the sole purpose of making temperature gradient measurements. By permission from the Minnesota Department of Natural Resources (DNR) and from mining companies (Rio Tinto, Duluth Metals, and PolyMet Mining), 46 measurements were made in DNR water observation wells and 11 in exploratory mining wells for use in this study.

Only wells that were in excess of 100 meters were measured in this study. This reduced any perturbation affecting the temperature gradient caused by land disturbance and the effects of recent and past climate changes. Gathered from the Minnesota County Well Index (CWI) database online, on the Minnesota Department of Health website maintained by the Minnesota Geological Survey (MGS), information for the wells included location, depth, and static water level for wells drilled in Minnesota. The database also contains a lithology log recorded during drilling. Most wells in Minnesota are shallow and pump water from shallow aquifers. Of the hundreds of wells located in the CWI, only a select number were deeper than 100 meters, and only a few were available for temperature logging (Fig. 19).

Temperature measurements were logged at 1 meter and 10 meter depth intervals using a thermistor probe calibrated to $\pm 0.001^\circ\text{C}$. Logging consisted of two or more individuals lowering the temperature probe into the well and recording the results given in Ohms using a resistance meter.

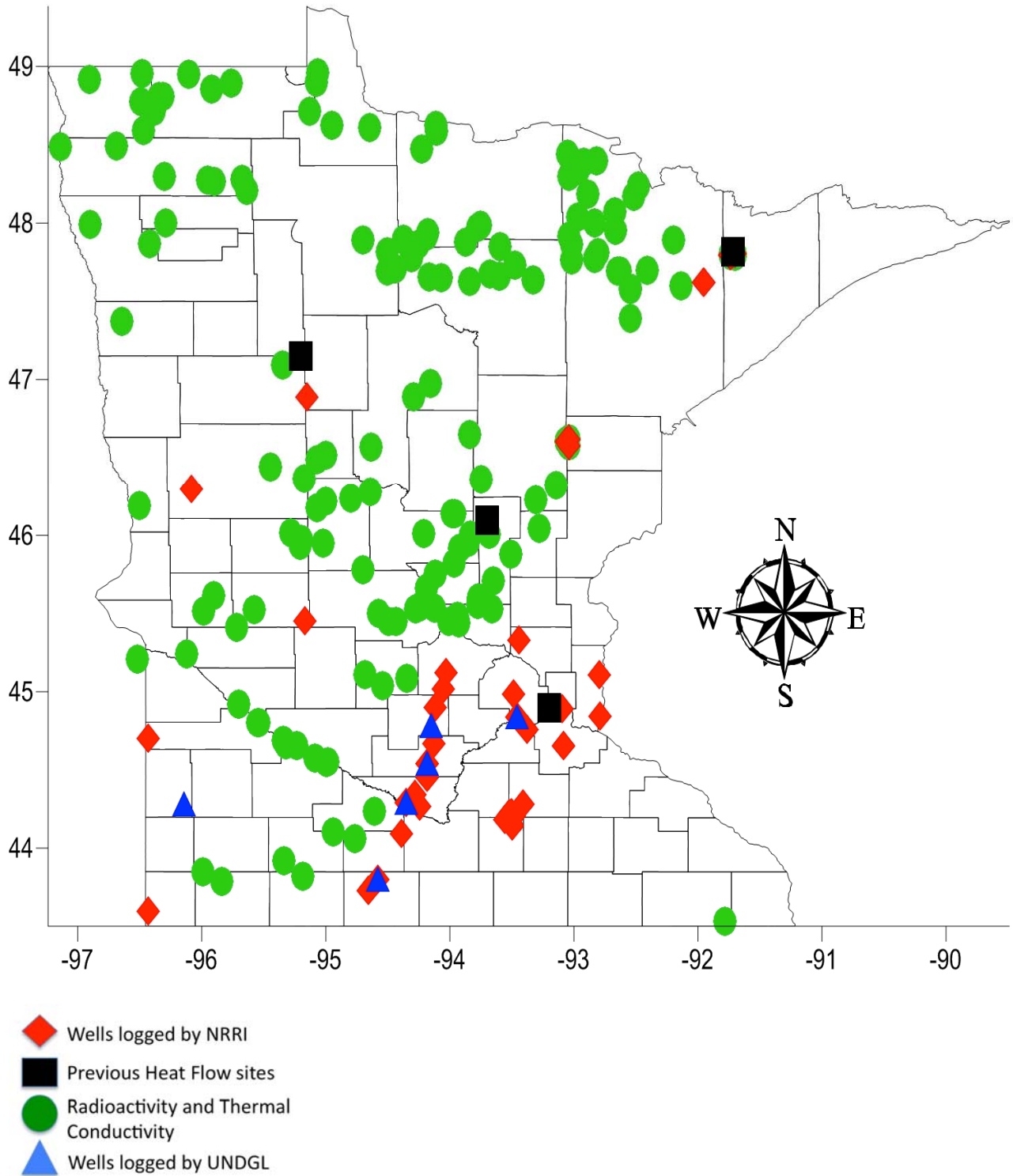


Figure 18a. Locations of wells logged for temperature and rock sample locations measured for thermal conductivity and radioactivity. Horizontal and vertical axes on the map are in degrees latitude and longitude.

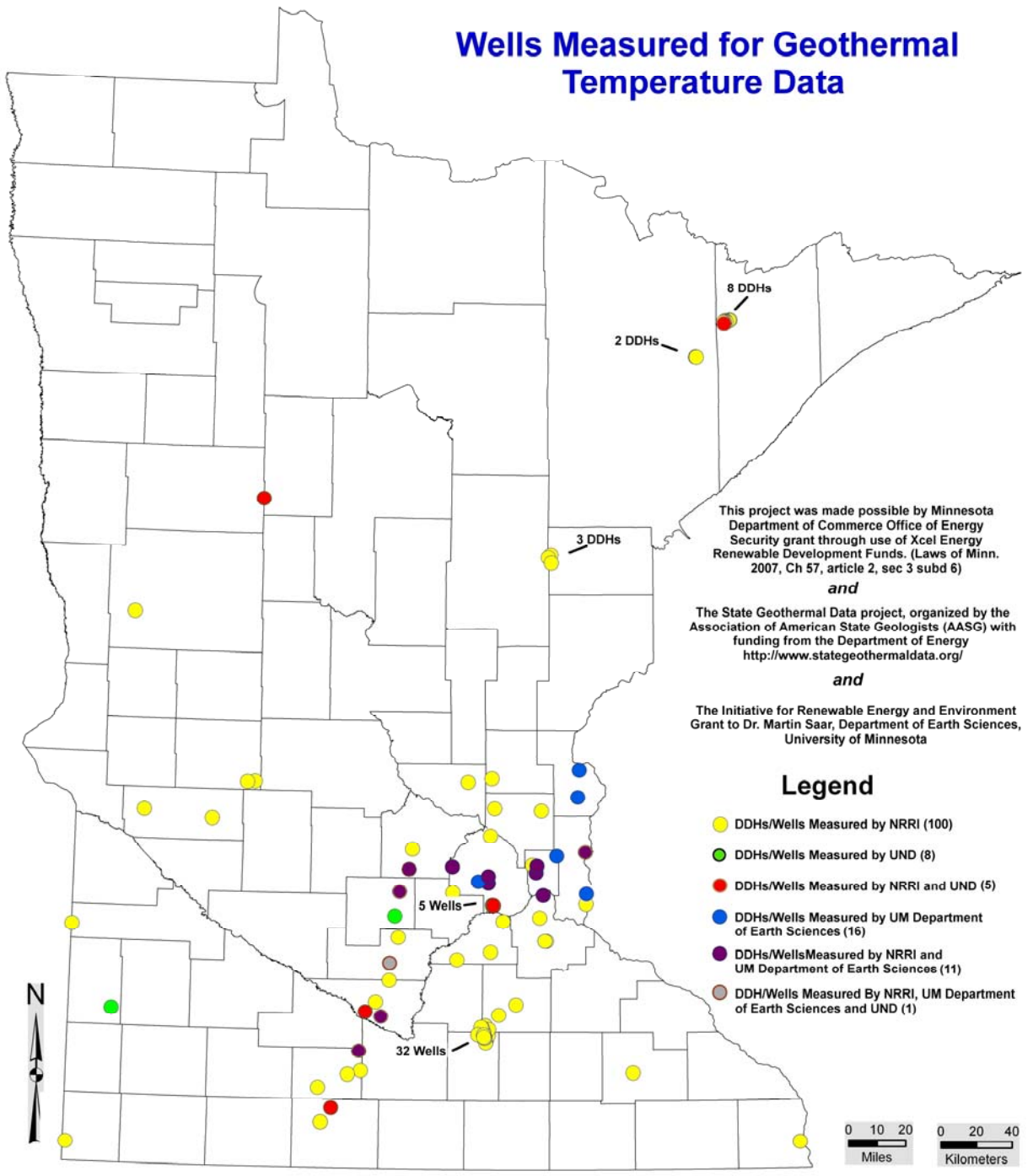


Figure 18b. Location of wells and exploration drill holes probed by more than one instrument.



Figure 19. A DNR well sampled for temperature gradient measurements.

Measurements were recorded going down the borehole to minimize circulation and fluid flow as opposed to logging from the bottom up. The thermistor is lowered using a manual hand crank reel with ~300 meters of 5 mm diameter cable (Fig. 20a; Appendix F, Figs. 61 and 62). NRRI used a Scintrex automated downhole probe (Fig. 20b) to collect data in the latter portions of the project. Some wells and drill holes were probed by several instruments (Figs. 18b, 20c) to compare the data from different probes to standardize the results (see Appendix F for downhole temperature data).

Gradients were calculated by plotting temperature versus depth in a stable part of the borehole. A linear trend line was then fit to the stable part of the profile, producing a gradient for use in calculating heat flow. Approximately forty profiles were not used in this study as water flow in the well produced isothermal temperature profiles, resulting in a gradient of zero (Appendix D).

Gradients were then corrected for perturbations caused by climate changes since the retreat of the Laurentide ice sheet 9-12 ka ago. The calculation is a depth dependent calculation similar to the one developed by Majorowicz and Wybraniec (2010). The equation developed by Carslaw and Jaeger (1959) to model temperature variations and the effect they propagate into the ground defined:

$$T_{\ominus} = T_0 \operatorname{erfc} \left(\frac{z}{\sqrt{4\kappa t}} \right) \quad (\text{Eq. 2.1.1})$$

where T_{\ominus} is the departure from original equilibrium temperature at depth z , T_0 is the change in surface temperature, κ is thermal diffusivity, $\operatorname{erfc}(\mathbf{x})$ is the complimentary error function, and t , time, was used to determine the temperature at different depths. This function allows for a depth dependent correction for the temperature



Figure 20a. Hand crank used to lower temperature probe into the wellbore.



Figure 20b. During the latter half of the project NRRI used an automated Scintrex temperature probe to collect data.

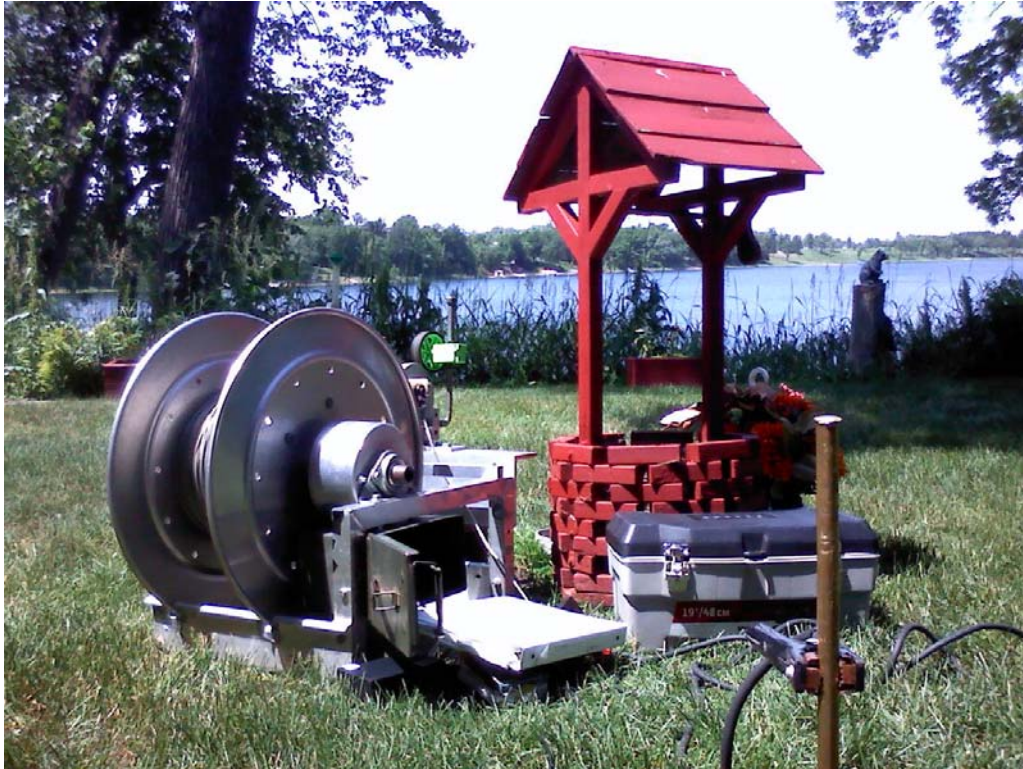


Figure 20c. Down hole temperature made by the Dept. of Earth Sciences at the University of Minnesota (mock setup to illustrate equipment).

gradients in Minnesota based on a T_0 of 15°C . Of the wells measured in this study, gradients are underestimated by 30-35% due to the shallow depth at which they were measured. Shallow parts of the gradient (<100 m) were also corrected for recent warming affects. This signal was minimal and affected the gradient slightly. Data was compiled from the National Climatic Data Center (2011) for the nine different regions of Minnesota given by the website.

2.2 Thermal Conductivity

Traditionally, thermal conductivity measurements are made on core of the well logged for temperatures. This situation was the case for the wells logged at the Rio Tinto, Duluth Metals, and PolyMet Mining Cos. exploratory wells. For the MN DNR observation wells logged, core was not available. In these instances, a well log was

provided, determining the individual lithologies at different depth intervals. This well log allowed for conductivities to be assumed based on the log or assumed from measurements of similar material.

Thermal conductivity was measured on Precambrian mafic and felsic igneous rocks, as well as some metamorphic gneiss and quartzite in Minnesota (Figs. 18, 21). Approximately 199 rock samples were collected at various locations in Minnesota and analyzed for thermal conductivity. Rock samples were collected from outcrop samples or along road cuts in northern Minnesota. Drill core samples were also collected from various wells for analysis. After preparing the sample, thermal conductivity measurements in the vertical direction were made using two portable electronic divided bar (PEDB) apparatuses made by Hot Dry Rocks Pty Ltd (Figs. 21-23).



Figure 21. PEDB used for measuring thermal conductivity in the UNDGL.



Figure 22. Various sample shapes used to measure thermal conductivity in this study.



Figure 23. A sample between the two brass plate sandwiches applying steady thermal gradients for measurement of thermal conductivity.

Samples were prepped and prepared at the UNDGL using a Felker Tile Master saw to cut samples to a thickness of approximately 20 mm. Also, the tile saw was used to cut outcrop rocks to a square or rectangular shape to fit in the PEDB. After cutting the samples into a desired thickness and shape, the samples were smoothed using a Hillquist thin section machine. Smoothing allowed for the samples to have good contact between the rock surface and the brass plates that apply the heating and cooling sources (Fig. 23). The samples were then put under vacuum for 8 hours in a Precision Scientific Model 25 Vacuum Pump. After 8 hours under vacuum, water was put into the vacuum chamber to saturate the samples for 12 hours and allow for water to fill the pores. Saturation allowed for more realistic in-situ conditions for proper measurement.

Samples were then measured using a digital caliper to determine the volume of

the sample and coated with Vaseline before measurement in the PEDB. The Vaseline allows for contact between the sample and the brass plates by filling in any irregularities at the surface. Next, the samples are hand tightened between the brass plates. To maintain a vertical heat flow, the samples are insulated to prevent any air circulation that could heat or cool the sample.

Thermal conductivity is determined by:

$$\lambda = \frac{d}{R} \quad (\text{Eq. 2.2.1})$$

λ = thermal conductivity

d = thickness of the sample in mm

$R = (A (\Delta T - c)) / (a (\text{diameter} + b))$

A = surface area of sample in mm²

$\Delta T = (T_2 - T_3) / ((T_1 - T_2) + (T_3 - T_4))$

where $T_1, T_2, T_3,$ and T_4 are temperatures of the brass plates measured by the

thermocouples, and a,b, and care calibration constants.

The PEDB measures thermal conductivity by applying a steady thermal gradient across a rock sample between two “sandwiches” consisting of two brass plates and a polycarbonate layer in the middle. Each “sandwich” acts as a heating or cooling source allowing for measurement of the thermal gradient across the sample. Thermocouples are imbedded into each of the four plates and are recorded using the PicoLog computer program. By knowing the conductivity of the polycarbonate, thermal conductivity can be calculated by measuring the ratio of the thermal gradient across the sample, relative to the thermal gradient across the polycarbonate (Fig. 23). Equilibrium of the sample usually takes 5-15 minutes, depending on the samples’ conductivity. To reduce error, a fused silica disk of known conductivity was run daily to maintain error within a reasonable 5%. This procedure allowed for high accuracy of the thermal conductivity measurements made in this study.

2.3 Radioactivity Measurements

Samples collected for thermal conductivity were also measured for radioactivity to determine radiogenic heat production and further calculate heat flow based on the Q-A relationship. Over 186 samples were sampled, including mafic and felsic rocks alongside road cuts, outcrops, quarries, and drill core from mineral exploration drill holes in Minnesota. Measurements were made using a Canberra gamma-ray spectrometer detecting gamma rays using a standard electrode germanium detector (Fig. 24).

A majority of the samples were prepped before being sent to the UNDGL from the NRRI in Duluth, MN. Samples were crushed in a rock crusher to pea size particles. Both

samples from NRRI and those prepped at the UNDGL were put into pint size containers containing ~800 g of material (Fig. 25). The containers were then sealed and stabilized until the Radon was in equilibrium for detection by the germanium detector.

In real time, the data are analyzed by a Model DSA-1000 digital spectrum analyzer and saved to a digital file displaying a spectrum from 40keV to >10MeV (Fig. 26). Samples and the detector are housed within lead shielding to help minimize noise from background gamma rays. Some noise is detected from the room housing the GeLi detector, but is subtracted out to maximize accuracy of the rock sample measurement.

The spectrum displays a number of energy peaks given off by elements contained in the rock sample. Of most importance are the concentrations of Uranium, Potassium, and Thorium, which contribute to natural radiogenic heat production within the Earth. The integral for each element’s energy peaks is acquired to calculate concentrations for the radioactive elements. Using a spreadsheet, developed from standards provided by Southern Methodist University, concentrations in parts per million (ppm) for U and Th and %K can be calculated after removing the background radiation. Background was determined over a twenty-four hour period in the UNDGL. Calibrating the matrices for the spreadsheet calculation allowed for this component to be factored out, improving results.

Radioactive heat production (A_0) can then be calculated for each sample depending on the various concentrations of radioactive elements using the following equation:

$$\text{Radioactive heat generation} = (\text{element abundance in rock}) * (\text{density}) * (\text{heat generation factor}) \quad (\text{Eq. 2.3.1})$$



Figure 24. Canberra Germanium detector housed within lead shielding to measure the radioactive heat content of the crushed rock samples.



Figure 25. Pint sized containers used to house the crushed rock sample to measure radioactivity.

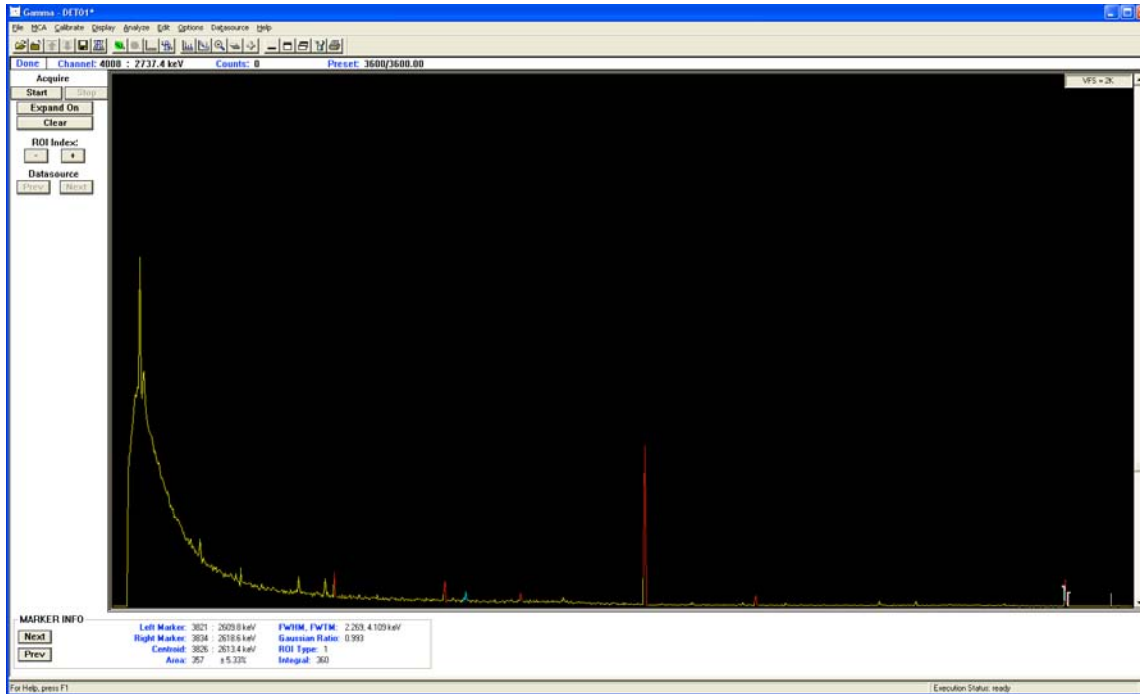


Figure 26. Screenshot of the digital spectrum from 40keV to >10MeV to determine concentrations of the radioactive elements.

where element abundance is measured in ppm for U and Th and % for K and the heat generation factor is $96.7 \cdot 10^{-6}$, $26.3 \cdot 10^{-6}$, and $3.5 \cdot 10^{-9}$, for U, Th, and K respectively. The heat generation factor is based on thermal energy released during radioactive decay. Calculating A_0 and using the Q-A linear heat relationship equation, heat flow can be calculated for each individual sample location.

2.4 Calculating Temperatures at Depth and Geothermal Resources

Temperatures and geothermal resources are calculated using measurements from the previous described methods for depths 4-10 kilometers using the format developed by Beardsmore et al. (2010). Heat flow, heat generation, sediment thickness, ambient temperature, and thermal conductivity are all parameters taken into account when estimating Minnesota's EGS resources and temperatures at depth.

The following equation was used to calculate temperatures at 4-10 km depth:

$$T_z = T_s + (q_s(z - S) / \lambda_B) - A_B((z - S) / (2\lambda_B)) \quad (\text{Eq. 2.4.1})$$

where T_z is the temperature at depth z ; T_s the temperature at the top of the Precambrian basement; q_s the heat flow at the top of the Precambrian basement; S the sediment thickness; λ_B the thermal conductivity of the Precambrian basement; and A_B the radiogenic heat production of the Precambrian basement (Beardsmore et al., 2010). Sediment thickness in Minnesota mostly consists of glacial till and Paleozoic sedimentary rocks in the southeast. Using the information from deep wells in the CWI (www.health.state.mn.us/divs/eh/cwi/index.html), sediment thickness was determined for the sedimentary rocks and glacial till varying from 0-500 meters. The lack of sedimentary rocks will have a small effect on temperatures compared to other areas in the U.S. where sedimentary basins are present.

Temperature maps then determined available heat and power potential for temperatures >150°C for a 1000 meter thick block of crust. The available heat was calculated using Eq. (2.4.2):

$$H = \rho C_p V_c (T_z - T_r) 10^{-18} \quad (\text{Eq. 2.4.2})$$

where **H** is the available heat; **ρ** the density; **C_p** the specific heat; **V_c** the volume of each grid cell; **T_z** the calculated temperature at depth **z**; and **T_r** the reference temperature (Beardsmore et al., 2010).

Power potential can then be calculated converting the amount of heat to energy in MW. Using Golden Software's Surfer 10, maps were generated using the Kriging gridding method for temperature, available heat, power potential, sediment thickness, thermal conductivity, and radioactive heat generation. By making the grids the same size, Surfer 10 is able to combine the grids using the equations above to calculate maps for temperature, available heat, and power potential.

3. OVERVIEW OF NEW HEAT FLOW MEASUREMENTS

3.1 Climate Changes Affecting Heat Flow

Wells logged in this study had abundant noise in the upper 100 meters pertaining to seasonal variations or long-term temperature variations caused by glacial retreat, recent warming, or vegetation disturbances. Although most of the noise is filtered out below 100 meters, additional noise occurred from fluid flow in the borehole producing isothermal gradients. Because of these reasons, only a select number of boreholes were used for heat flow calculations, and were corrected appropriately for post-glacial disturbances affecting the upper 2000 meters of the crust. If well logs went uncorrected for post-glacial warming effects, the new heat flow values would average 33.8

mW m⁻², resulting in heat flow considerably lower than the average of the Superior Province or of the previous measurements in Minnesota. Special care was taken when correcting the gradients for recent warming and post-glacial warming signals. Recent warming changes have not been accounted for in previous heat flow studies and while the noise disturbs the 0-120 m interval, this noise in some instances, can be corrected using climate data over the past 100 years from The National Climatic Data Center (<http://www.ncdc.noaa.gov/oa/ncdc.html>).

3.1.1 Recent Warming Affecting the Gradient

Recent warming in some cases is minimal, but it is still taken into account for correcting perturbations of the gradient in the upper 100 meters. As a controversial subject, recent warming is human and natural drivers affecting our climate, such as increasing of greenhouse gases and aerosols (IPCC, 2007; Fig. 27). Using a UNDGL in-house software, temperature data since 1895 is forced into the subsurface. These data taken from the National Climatic Data Center has been compiled over nine different regions (Fig. 28) in Minnesota, showing different effects for each area. Each region has had different amounts of warming, but the warming is more subtle in the north than in the south.

Warming affects primarily the upper 100 meters by 1 degree in extreme cases near the surface in region 1 where region 3 has been affected the least (Fig. 29). Although warming is attributed to increasing greenhouse gasses, other human drivers affect it as well. Region 1 is a large agricultural area compared to that of region 3, which is heavily forested. Warming varies from each region because there are different effects controlling it. In the past century, vegetation has been removed throughout Minnesota for industrial and agricultural

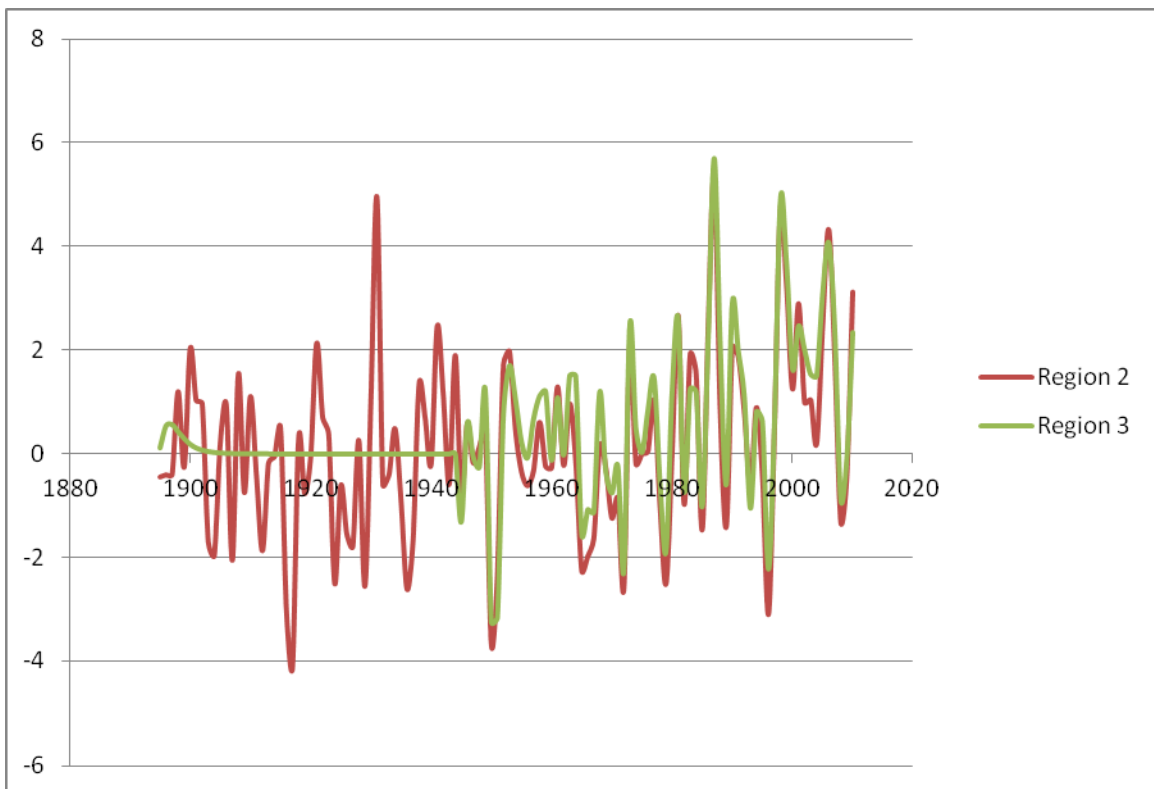


Figure 27. Change in temperature from the mean over the past 100+ years in regions 2 and 3 from data acquired from The National Data Climatic Center (<http://www.ncdc.noaa.gov/oa/ncdc.html>).

Minnesota

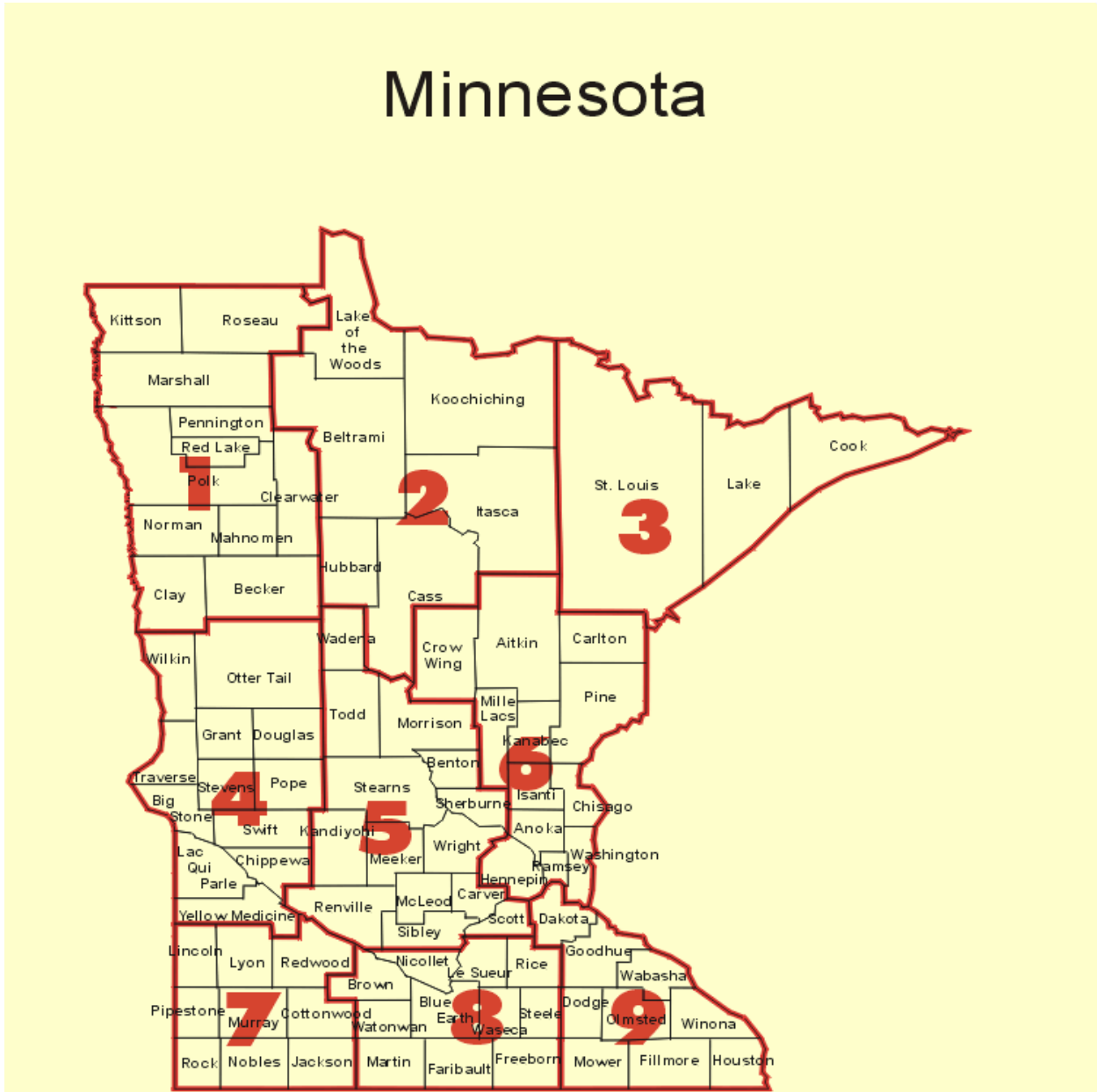


Figure 28. Climate divisions of Minnesota from the National Climatic Data Center. Data from each region was used in temperature forcing to determine the extent of perturbations caused by recent warming.

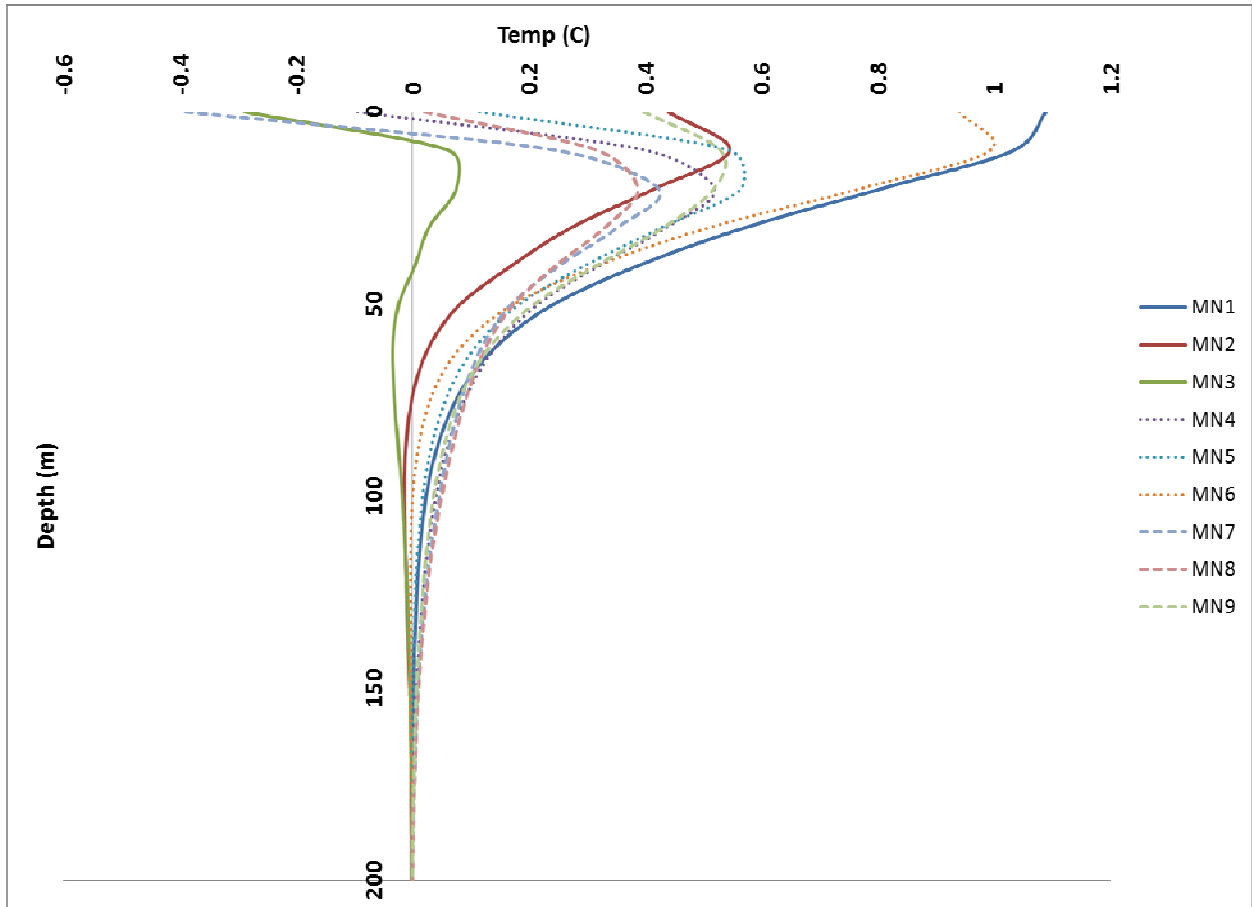


Figure 29. Recent warming perturbations affecting the nine different climate regions in Minnesota. Regions are 1-9 respectively from left to right.

purposes, allowing for larger amounts of warming to occur than just those caused by greenhouse gasses. The removal of trees and vegetation has allowed the ground to warm up from the abundance of sunlight, creating a larger correction. In northern Minnesota, the state is heavily forested and has warmed from just the effects of greenhouse gasses. Although different areas of the state have more extreme warming than other areas, both need to be accounted for and corrected in the measured gradients in this study. By fitting a polynomial to each curve (Appendix D), gradients measured had the signal subtracted out according to region and depth, allowing for a more proper and linear gradient for calculating heat flow (Fig. 30).

3.1.2 Post-Glacial Warming Affecting the Gradient

Heat flow corrections for post-glacial warming perturbations have been systematically corrected in Canada using the correction developed by Jessop (1971). However, this correction applies an adjustment to heat flow at the surface and is not depth dependent. Depending on the diffusivity and conductivity of the rock, the amplitude of the signal decreases at different rates with increasing depth. The calculation used in this study is a depth dependent calculation similar to the one developed by Majorowicz and Wybraniec (2010) using Equation 2.1.1 developed by Carslaw and Jaeger (1959) to model temperature variations and the effect they propagate into the ground. In this study, an in-house UNDGL heat flow software (ARC) and a T_0 of -15 was used to determine the extent the warming signal has on the temperature gradient. If gone uncorrected, heat flow would increase down the borehole. This increase would not occur due to the depletion of radioactivity and the steady state principles of heat flow.

Understanding the extent of the warming since the last glaciation is a difficult variable to constrain to a general area. Temperatures at the base of the ice sheets that once covered North America can be variable depending on the accumulation of snow, flow of ice, and geothermal heat flux (Rolandone et al., 2003). Currently, glaciated areas on Earth have basal glacier temperatures ranging from 0°C in Antarctica to -16°C in Greenland (Rolandone et al., 2003). In general, temperature profiles interpreted from deep borehole data conclude that during the LGM temperatures did not fall much below 0°C, but may have been -4 to -6°C at the margins measured from a borehole near Sept-Iles, Quebec (Chouinard and Mareschal, 2009; Mareschal et al., 1999; Rolandone et al., 2003.)

Minnesota, located on the margins of the Laurentide Ice Sheet (Fig. 31), more than likely experienced similar temperatures to Sept Iles, Quebec. Ambient temperatures in Minnesota vary by latitude and range from 4-9°C from north to south. Using -4 to -6°C as the temperatures during the LGM, a temperature change of 10-15°C has occurred since the retreat of the Laurentide Ice Sheet. This degree of warming has been further confirmed in nearby states and provinces from a deep borehole in the Pierre Shale (Gosnold et al., 2005), pollen analyses in Manitoba (Ritchie, 1983), and recent modeling of the surface temperature during the Pleistocene (Ganopolski et al., 1998; Schneider von Deimling et al., 2006). Furthermore, if heat flow values were left uncorrected, they would be systematically lower than the calculated heat flow values from radioactivity (Fig. 32). The supportive evidence indicates that the lower limit of -15°C is the likely degree of warming that has occurred and is used as the T_0 in Eq. 2.1.1.

Using a T_0 of -15°C since the retreat of the Laurentide Ice Sheet, a stable gradient

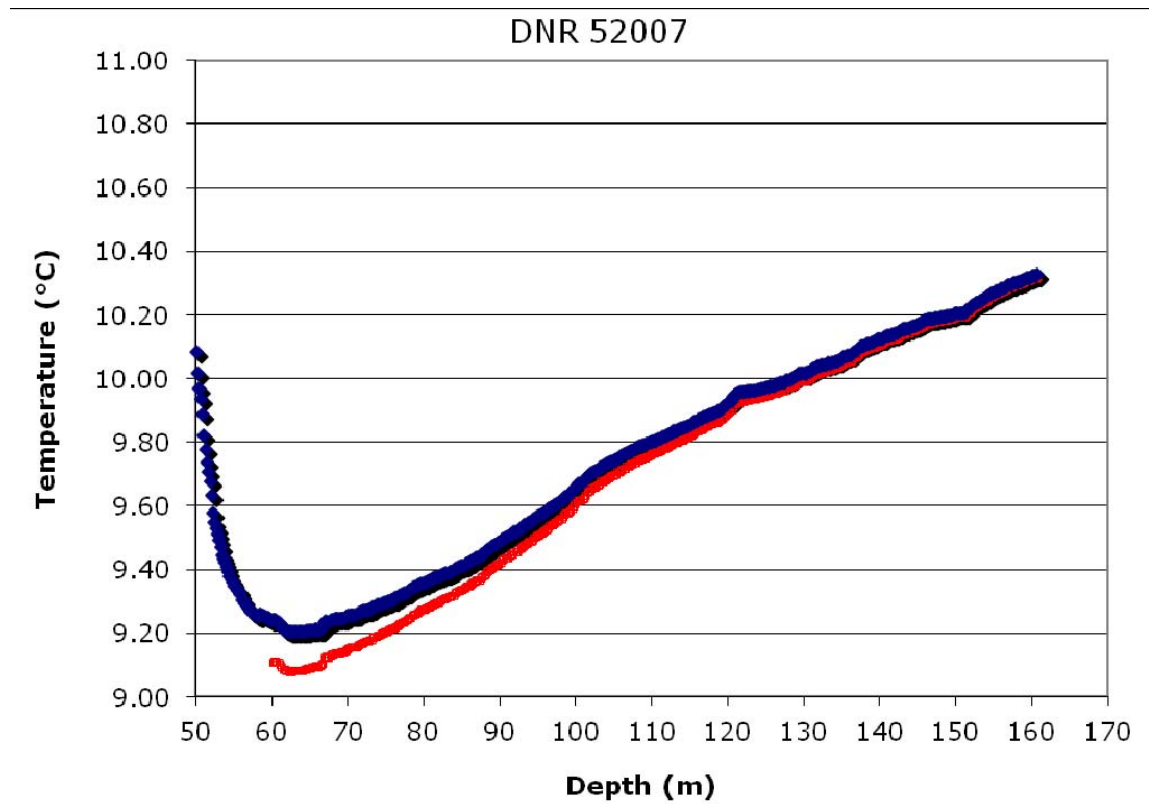


Figure 30. DNR Well 52007 corrected for recent warming in Zone 8. The blue line is the data logged in the borehole and the red line is the log corrected for recent warming after subtracting out the signal.

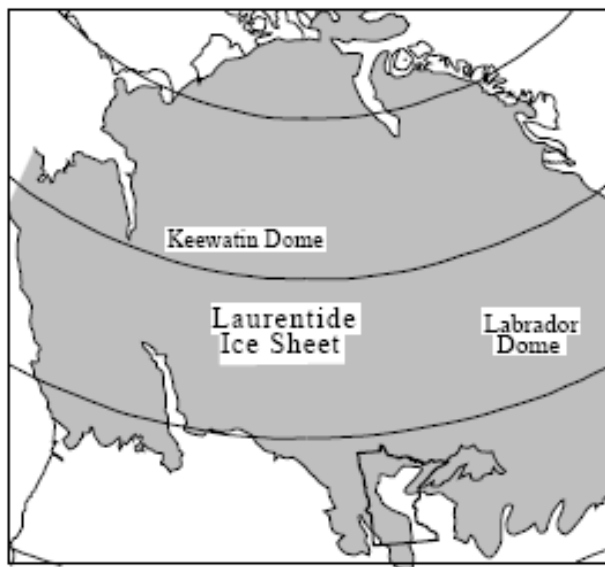


Figure 31. Extent of the Laurentide Ice Sheet over Minnesota. Minnesota sat on the edge of the ice sheet and may have exhibited colder temperatures on the margins (Lusardi, 1997).

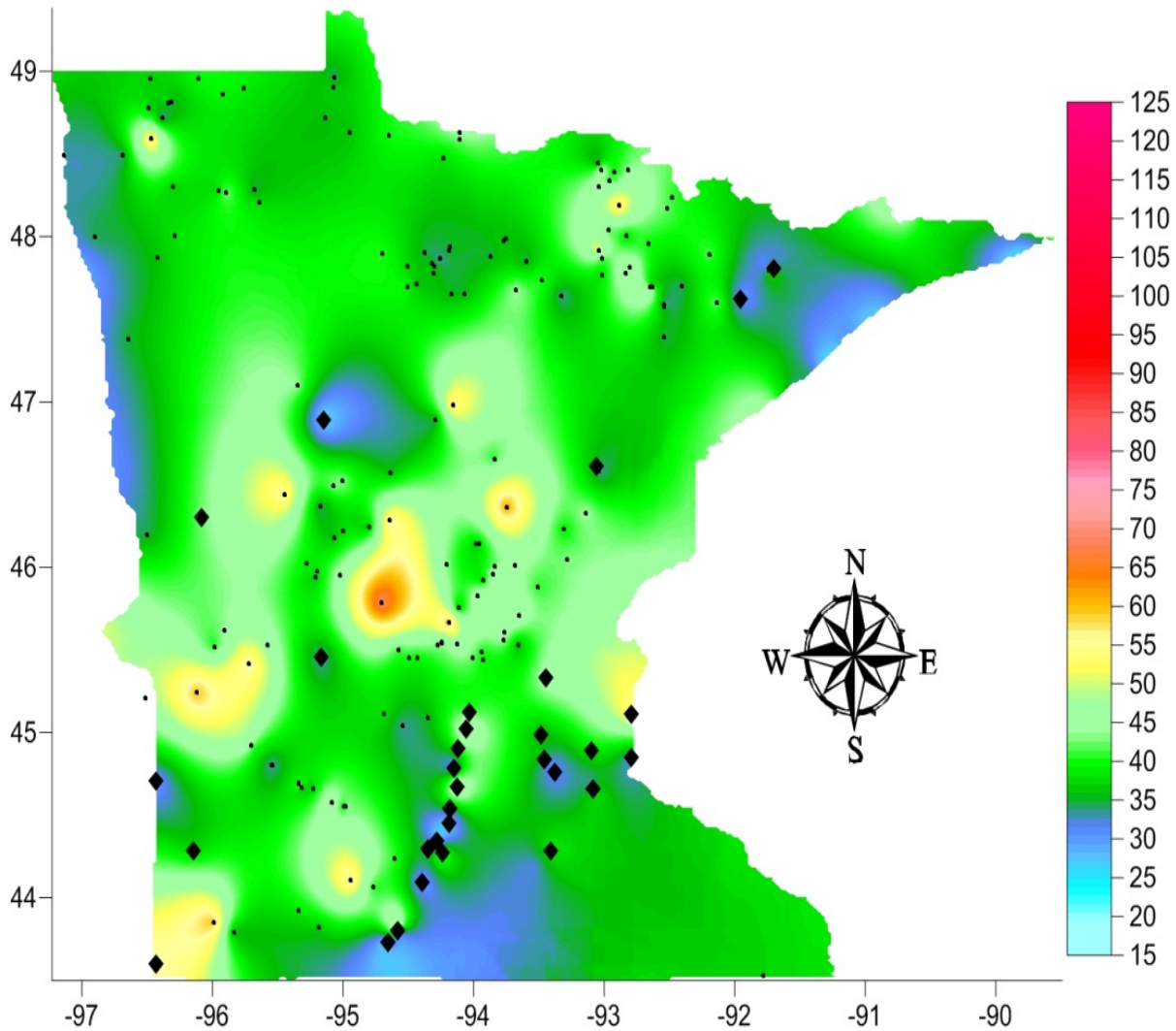


Figure 32. Heat flow measurements (diamonds), are systematically lower than the heat flow calculated from radioactivity (dots). This difference gives further evidence that a correction for post-glacial warming needs to be applied. The colored vertical scale is heat flow in mW m^{-2} . Horizontal and vertical axes on the map are in degrees latitude and longitude.

can be affected nearly 40% at the surface (Fig. 33). By taking a stable steady state gradient, and changing the surface temperature by 15 degrees, the ARC software allows for a steady state heat flow transfer over a large volume (km^3). This software produces curvatures in the gradient. Seen in Figure 33, the curvature is minimal, but considerably lower than a measurement taken at a deeper depth. Fitting a polynomial to the correction curve, $y = -4\text{E-}23x^6 + 8\text{E-}19x^5 - 3\text{E-}15x^4 - 2\text{E-}11x^3 + 2\text{E-}07x^2 - 0.0005x + 0.4173$, to wells logged in this study can be corrected appropriately depending on the depth of the heat flow measurement recorded. In all cases, heat flow measurements exceeded 100 meters, but were less than 400 meters due to the depth of the wells and logging cable. Because of these shallow depths of measurement, corrections were between 30-35%. By further applying the correction to several other heat flow measurements in nearby provinces and states from the International Heat Flow Commission (IHFC) database (<http://www.heatflow.und.edu/data.html>), eliminates the contouring of uncorrected and corrected datasets. Some heat flow observations were already corrected for post-glacial warming in Canada. In this case, the corrected values published by the original author from the IHFC database were used in contouring the data.

3.2 New Heat Flow Measurements

New heat flow data has been acquired, enlarging the once biased database with an additional 31 new heat flow observation sites (Appendix B) and 186 heat flow values calculated from radioactivity based on the Q-A relationship (Appendix C). Prior to this study, reports of heat flow in Minnesota were biased due to the location of the measurements in the MCRS, as well as the uncertainty of the measurements made in

shallow lakes by the original authors (Roy et al., 1968; 1972). All heat flow measurements in this study were also corrected for recent warming as well as warming since the retreat of the Laurentide Ice Sheet. Perturbations caused by post-glacial warming were not accounted for in previous studies, but recently have been systematically corrected in other areas of the Superior Province (Mareschal et. al., 2000; Rolandone et. al., 2002; Rolandone et al., 2003; Perry et al., 2004).

Previously, heat flow reported for Minnesota was $40 \pm 6 \text{ mW m}^{-2}$ from the four heat flow measurements made in shallow lakes and the Ely site. This study finds that the heat flow average from the newly 31 acquired heat flow sites is $44.1 \pm 6.6 \text{ mW m}^{-2}$. This value is slightly higher than the previous measurements and similar to the rest of the Superior Province. Although the new heat flow average is similar to previous measurements, some heat flow values calculated from radioactivity exceed 50 mW m^{-2} . Due to the low mantle heat flow, heat flow measurements in the Canadian Shield are highly sensitive to crustal heat production, discrediting the previous conception that heat flow variations in cratons is minimal and has no pattern (Perry et al., 2010).

Two types of data were used in contouring the new heat flow map of Minnesota. These data included 31 newly acquired traditional heat flow observations and heat flow calculated from radioactive heat production based on the Q-A relationship. Furthermore, data gathered from the International Heat Flow Database (<http://www.heatflow.und.edu/data.html>) allowed for contouring of heat flow values in adjacent states and provinces, after correcting for post-glacial warming effects.

Many authors have studied heat flow in the Canadian Shield and have enough data to present a linear heat flow heat production relationship (Perry et al., 2006). The Superior Province of the Canadian Shield

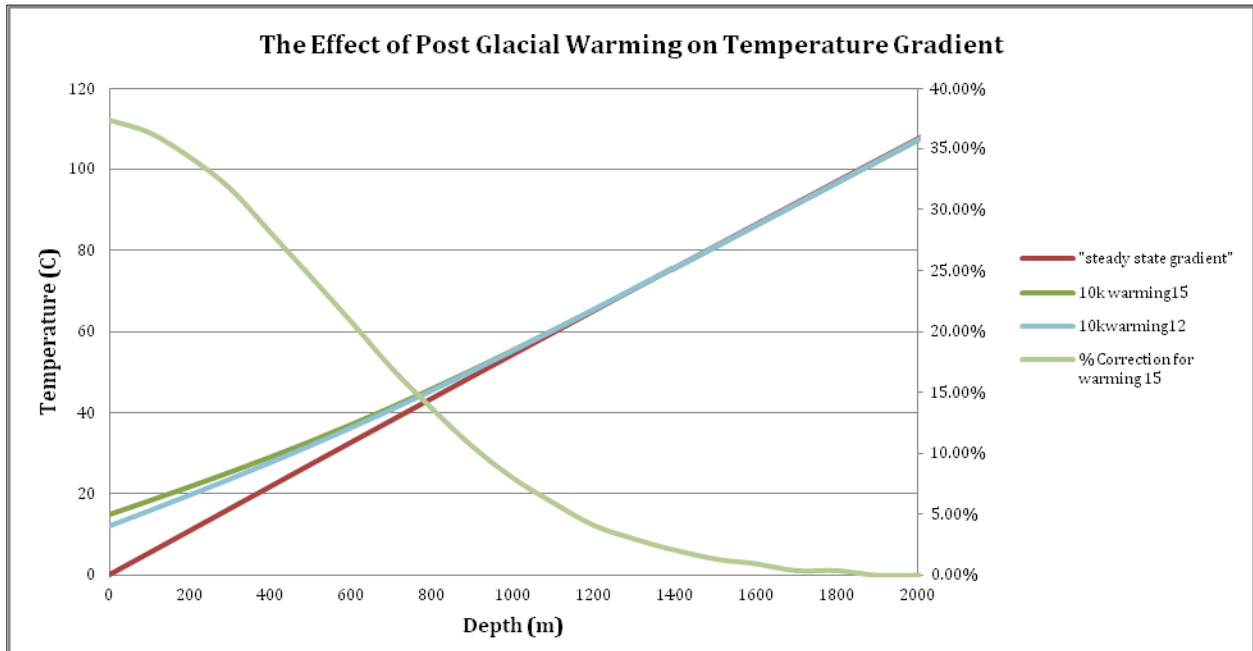


Figure 33. Both 12 and 15 degree warming causes major perturbations down to 2000 meters. At the surface, temperature gradients are affected by 30-40%.

has a remarkable linear Q-A relationship with an intercept of 33 mW m^{-2} (Levy et al., 2010; Fig. 34). This intercept is very similar to the same intercept of the eastern U.S. However, the thickness of the radioactive layer for the Eastern U.S., 7.5 km (Roy et al., 1968), is thinner than the thicker crust of the Canadian Shield, 9.1 km (Perry et al., 2006), allowing for higher crustal heat production. Using an intercept value of 33 mW m^{-2} and a thickness of 9.1 km for the radioactive layer, heat flow values are calculated based on radiogenic heat production calculated from the concentrations of U, K, and Th. Using measurements of radioactivity for calculating heat flow is a concept that was used by Kukkonen (1993), while studying heat flow of the Fennoscandian Shield. Mainly, the convenience of collecting rock samples for measurement and the lack of deep wells accessible for temperature measurements prevents a data bias where only boreholes are present. Although heat flow values calculated on the Q-A relationship cannot

wholly substitute for traditional heat flow measurements, this method provides reasonable data where temperature gradient data does not exist (Kukkonen, 1993). In this study, a majority of the heat flow observation sites were made in the southern end of the state and in mineral exploratory wells. If heat flow would have been calculated and mapped on the heat flow observations alone, a sampling bias would again have occurred.

Wells for temperature logging in this study were chosen with great care. A majority of the new heat flow observations were located in southern Minnesota in upper sediments not penetrating the Precambrian basement rock. These wells were found to have stable gradients and allowed for reliable temperature gradients. However, core was unavailable for thermal conductivity measurements. Although a thermal conductivity measurement is a critical component to calculating heat flow, a well log is available where the temperature measurements were conducted. Extensive

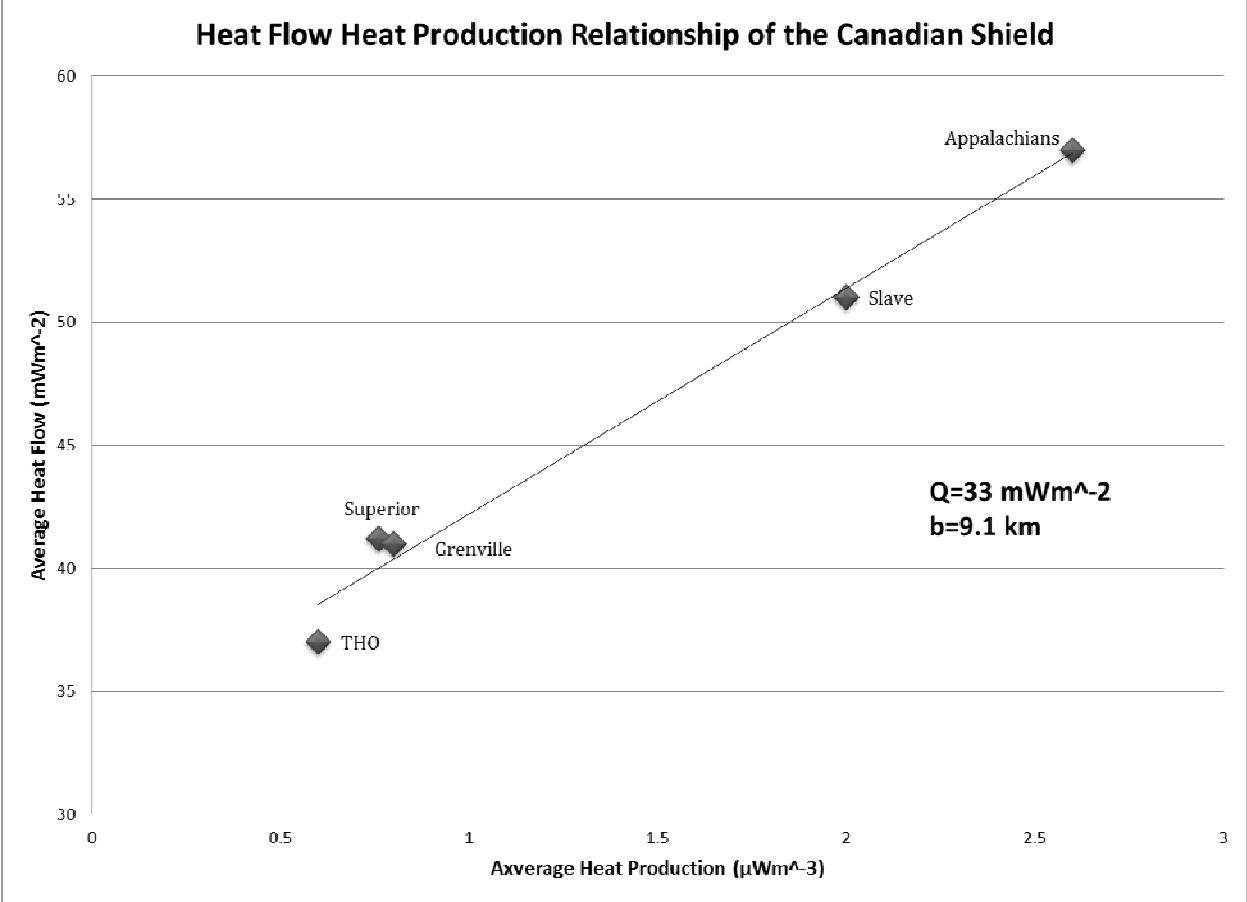


Figure 34. Heat flow-heat production relationship of the Canadian Shield showing the different geologic provinces. Heat flow intercept is 33 mW m^{-2} and a slope of 9.1 km for the thickness of the radioactive layer. Modified from Perry et al. (2006).

studies on clastic rocks and sediment types allow for the conductivity of these wells to be estimated based on the well log provided (Beardsmore and Cull, 2001; Gosnold et al., 2010). Primarily, wells penetrated interbedded sandstone and shale units with assumed thermal conductivity values of 3.5 and 1.2 W/(m*K), respectively. The remaining wells were logged in crystalline bedrock in the MCRS in northeastern Minnesota with core available courtesy of mining companies. These wells were deeper and experienced stable gradients with core available for thermal conductivity measurements providing for higher accuracy in the heat flow calculations.

3.3 New Heat Flow Map

A new heat flow map (Fig. 35) has been constructed from 217 data points using both the heat flow observations and heat flow calculated from radioactivity based on the concepts of the Q-A relationship. Acquiring the data gradually over the past two years has allowed for the heat flow maps to evolve from different contouring attempts. Previously-published maps used only the 4 heat flow sites and regional data to contour data for the state (Fig. 16). The previously-published maps were then used in calculating the EGS resources, as heat flow is the driving parameter for temperature calculations at depth. The newly acquired heat flow data allows for a more realistic assessment of EGS resources in Minnesota.

Due to gradually acquiring data, the heat flow map in this study has undergone multiple changes. First attempts utilized only heat flow observations made from heat flow measurements made in the first year of this study (Fig. 36). This effort included heat flow measurements from the mining exploratory wells and from six heat flow sites made in the DNR observation wells. A second attempt utilized the same heat flow observation data as well as data acquired

from the whole rock and trace element analysis (Fig. 37). After acquiring more data from the 186 measurements made on crushed rock samples from the gamma-ray spectrometer, a third map was created along with the final data set of 31 heat flow sites (Fig. 38). This third map and data set was going to be used as the final map to further calculate temperatures and EGS resources. However, it produced bulls-eyes in many areas caused from large changes in radioactivity over short distances.

A fourth and final attempt resulted in averaging the data over the specific rock type it represented. The 217 data heat flow points acquired in this study was posted onto the geologic map of Minnesota (Fig. 39). Data points covered the state almost uniformly representing various lithologies including gneiss, MCRS mafic rocks, granitic plutons, metasediments, and greenstone belts. Data points measured in the geologic terrane it represented were then averaged over the geologic body regionally. This averaging eliminated the high heat flow changes over short distances allowing for a more realistic and interpretation of heat flow based on the changes of radioactivity on a subprovince scale.

3.4 Assessment of Heat Flow Data

Previously credited as having some of the lowest heat flow values in North America, heat flow in Minnesota is still is considerably lower than the mean for continents of 65 mW m⁻² (Pollack et al., 1993). Radioactive elements seem to be depleted in a majority of the rocks measured in this study, resulting in low heat flow values (Fig. 40). Low radioactivity is most likely caused by the age of the rocks and the crustal formation and stabilization process of the Canadian Shield (Perry et al., 2006). However, some of the granites and gneissic rocks are still highly radioactive with a total heat generation exceeding 3 μW m⁻³,

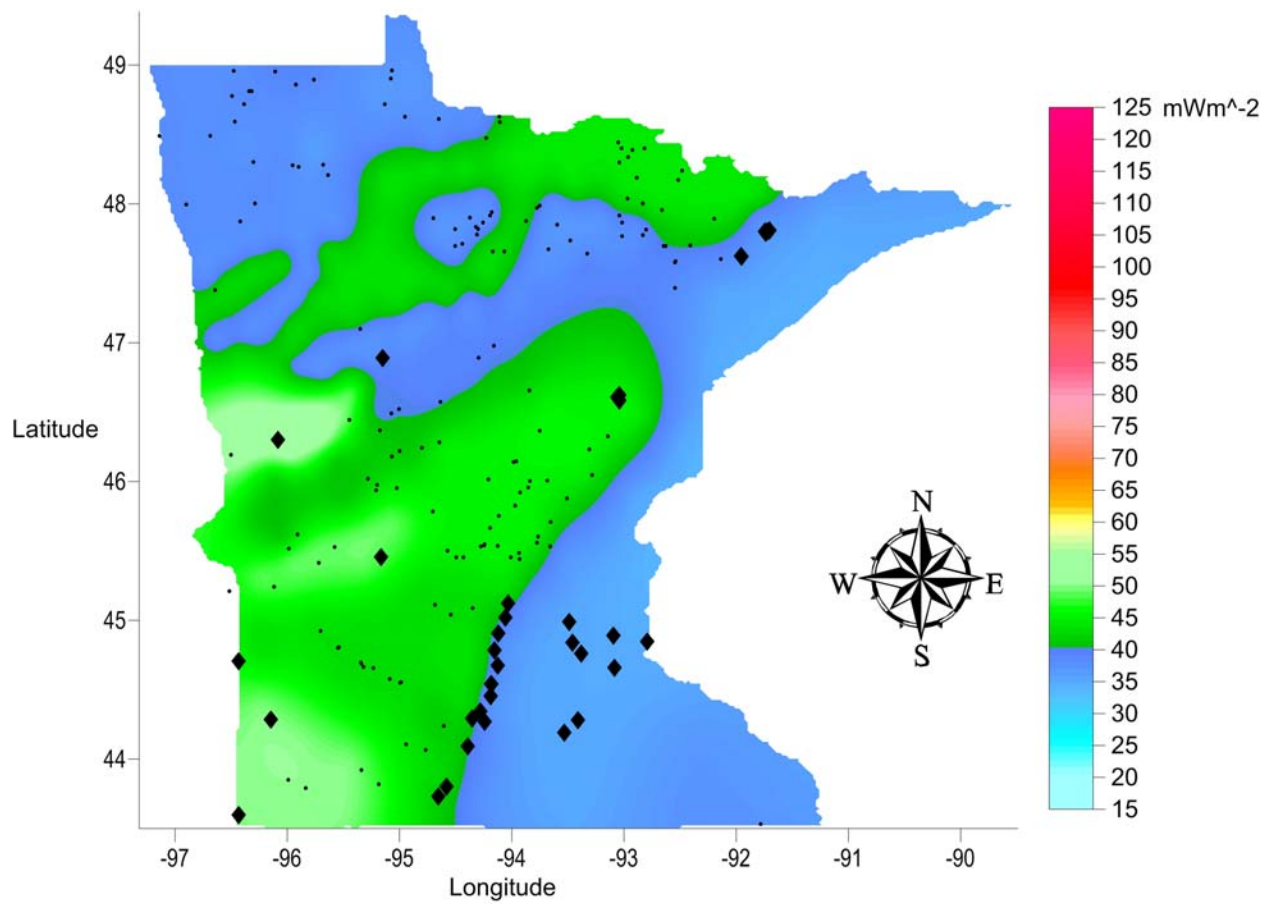


Figure 35. New heat flow map of Minnesota using both traditional heat flow measurements (diamonds) and calculated heat flow measurements (dots) based on the Q-A relationship. The colored vertical scale is heat flow in mW m^{-2} . Horizontal and vertical axes on the map are in degrees latitude and longitude.

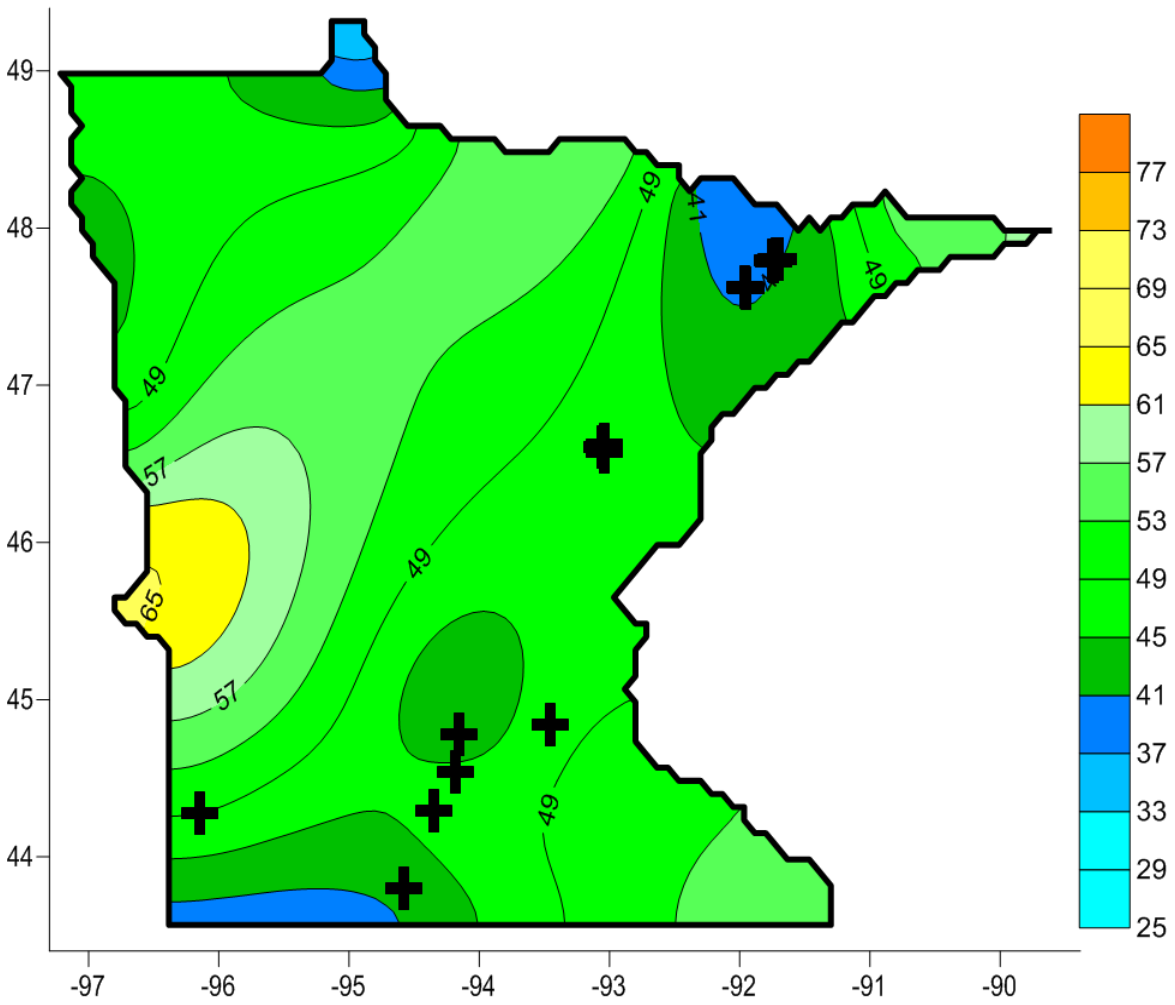


Figure 36. First attempt at a heat flow map based on regionally corrected data with newly acquired data in the first year of this study. The colored vertical scale is heat flow in mW m^{-2} . Horizontal and vertical axes on the map are in degrees latitude and longitude.

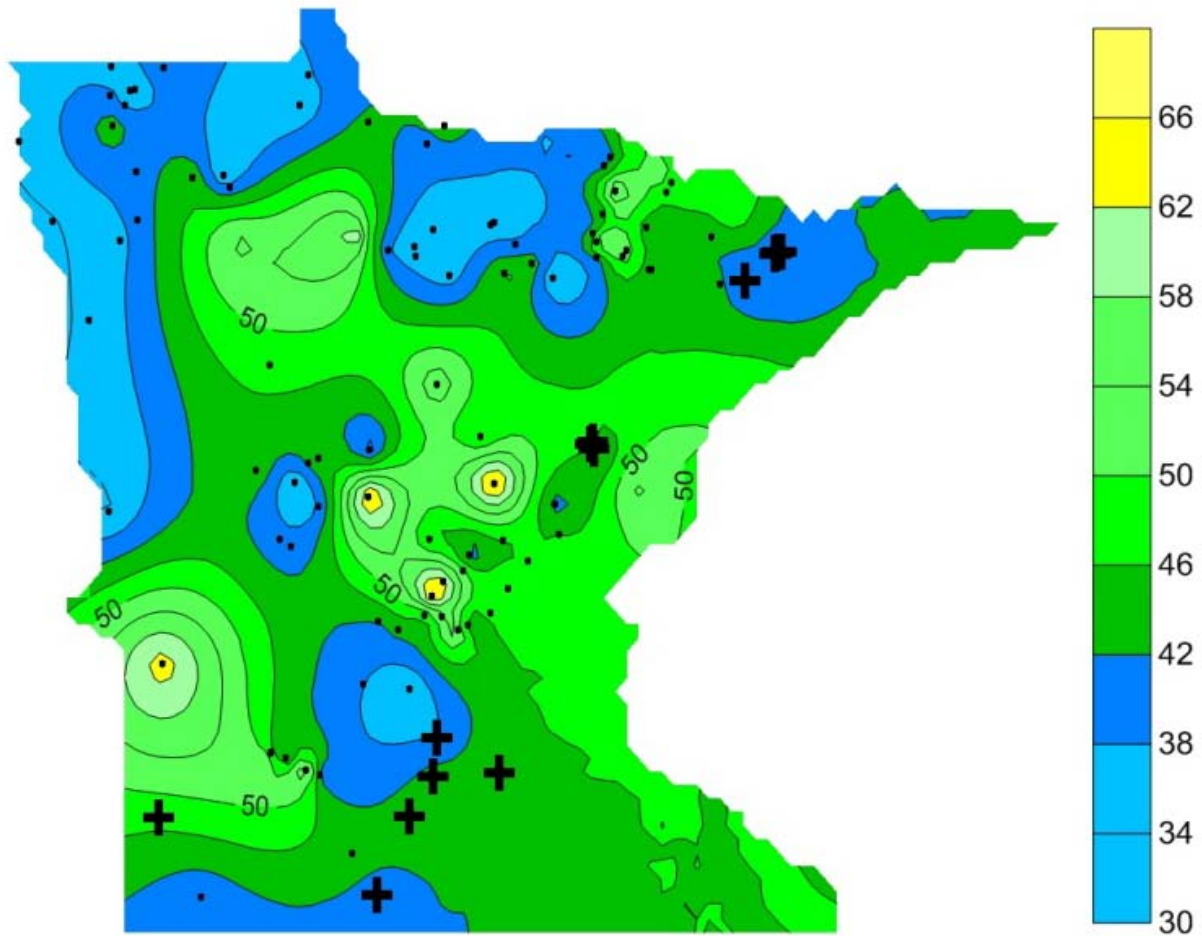


Figure 37. Second attempt of the heat flow map using nine heat flow sites and data acquired from the whole rock and trace element analysis. The colored vertical scale is heat flow in mW m^{-2} . Horizontal and vertical axes on the map are in degrees latitude and longitude.

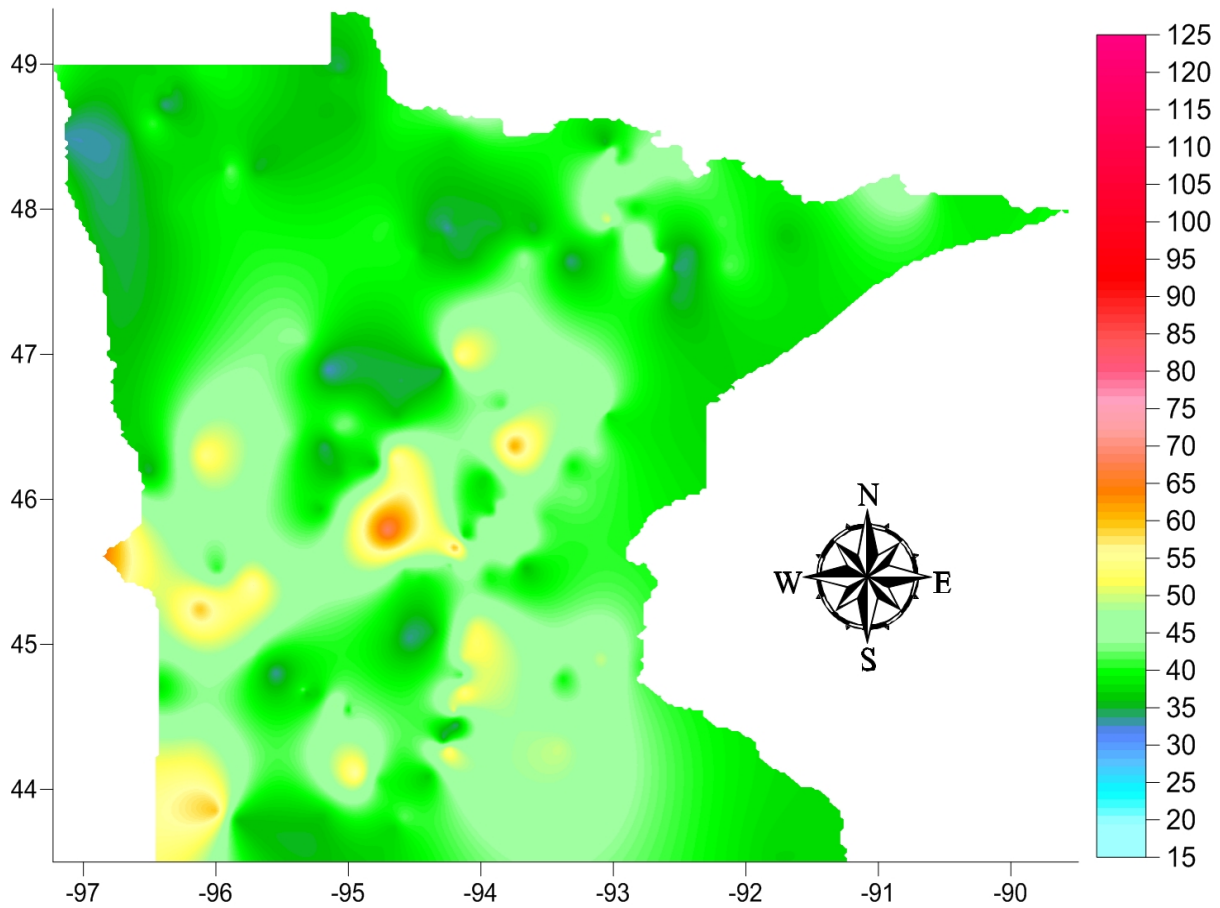


Figure 38. Third attempt of the heat flow map of Minnesota. Anomalies are most likely unrealistic because heat flow variations are large over short distances. The colored vertical scale is heat flow in mW m^{-2} . Horizontal and vertical axes on the map are in degrees latitude and longitude.

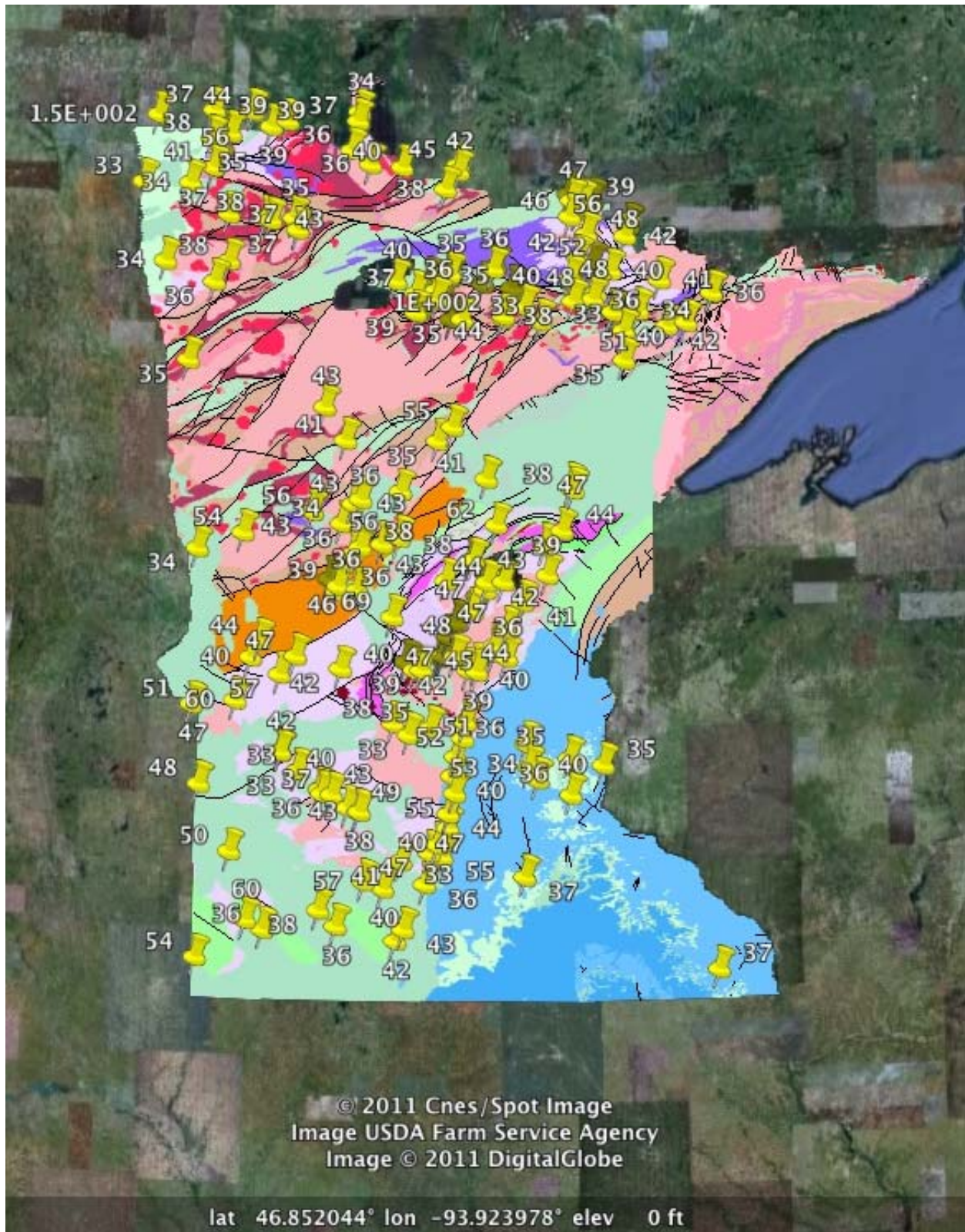


Figure 39. Heat flow locations on the geologic map of Minnesota. These data were used to create the new heat flow map of Minnesota by averaging the heat flow data over the geologic terrane it represented. (Base map source: <http://tin.er.usgs.gov/geology/state/state.php?state=MN.>)

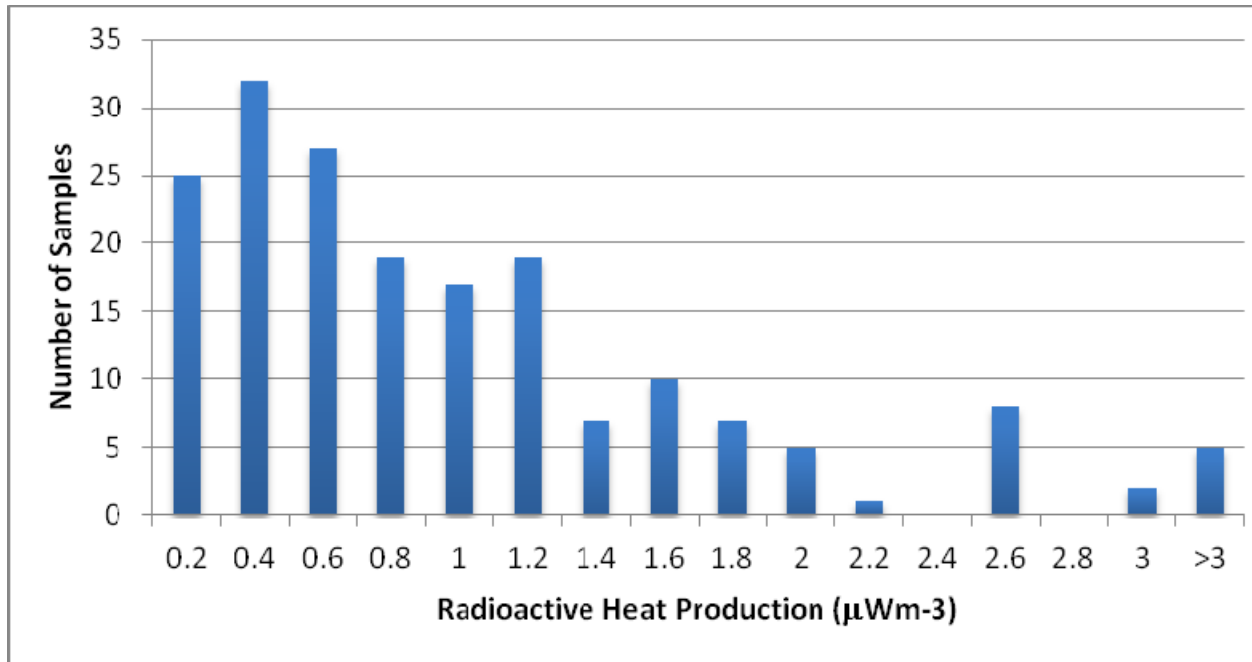


Figure 40. Histogram of the Radioactive Heat Production in this study throughout Minnesota.

resulting in heat flows ranging from 50-60 mW m^{-2} (Appendix C). Other rocks analyzed had a radioactive heat production of 7-12 $\mu\text{W m}^{-3}$ with calculated heat flow values exceeding 100 mW m^{-2} . These extremely high values most likely are not characteristic of the area as a whole and were left out when contouring the heat flow map due to the large anomalies created.

Before heat flow values were corrected for post-glacial warming, they were systematically lower than the heat flow values calculated from radioactive heat production. These data could be interpreted two different ways: 1) either heat flow is unaffected by post-glacial warming and heat flow calculated from radioactivity is overestimated; or 2) heat flow is underestimated due to post-glacial warming, and heat flow calculated from radioactivity is accurate based on the Q-A relationship of the Canadian Shield. As presented earlier in this study, the latter is more accurate. Because the heat flow map lacks large anomalous areas, using the Q-A calculated data confirms the accuracy of the data for

use in the heat flow map. Although there are few measurements of radioactivity near the boreholes, this method still needs to be tested to prove the calculated measurements are valid.

On a subprovince scale, heat flow in Minnesota varies between the different geologic terranes. To see differences on a subprovince scale, heat flow values were plotted on rough outlines of each subprovince (Fig. 41). In the Superior Province, the Wawa-Abitibi, Wabigoon, and Quetico have heat flow values of 39.4 ± 6.0 , 38.3 ± 4.6 , and $43.7.8 \pm 5.2$, mW m^{-2} respectively. The MCRS and Minnesota River Valley gneiss, 36.8 ± 2.6 mW m^{-2} and 46.1 ± 7.63 mW m^{-2} respectively, exhibit similar heat flow values. Heat flow in the Wawa-Abitibi, Wabigoon, and Quetico in Minnesota are similar to those measurements made on the same subprovinces in Canada.

The Quetico and MRV terranes exhibit higher heat flow values than the other terranes found in Minnesota. As hypothesized, the MCRS has significantly

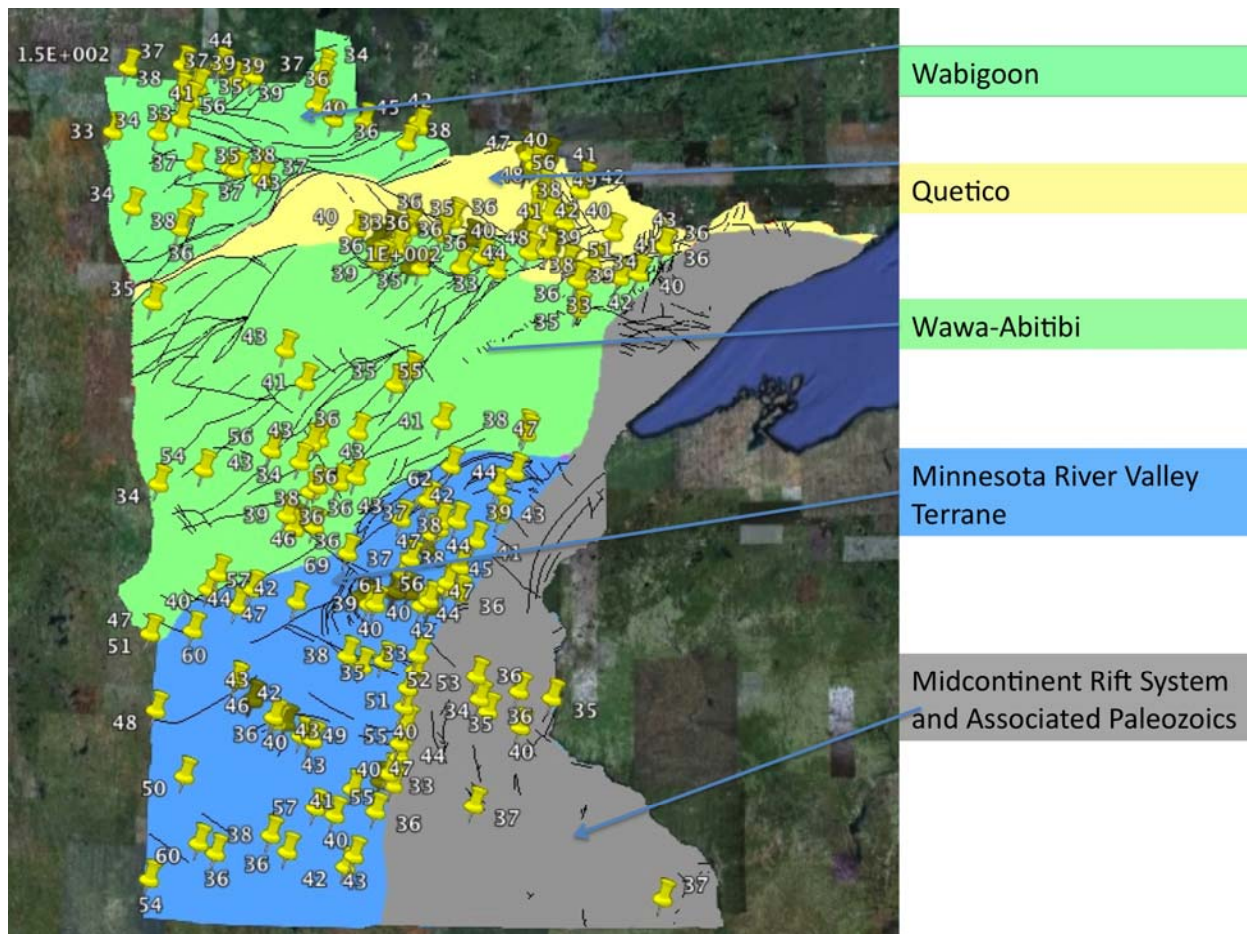


Figure 41. Heat flow measurements located on general outlines of the Wabigoon, Wawa-Abitibi, Quetico, MRV, and Midcontinent Rift System.

low heat flow resulting from low radioactive heat production from the mafic rocks. The Quetico and MRV both have a higher heat generation than the Wabigoon and Wawa-Abitibi terranes, resulting in different heat flows from one terrane to another. Therefore, the changes in heat flow on a subprovince scale are based on changes in radioactivity, similar to the rest of the Canadian Shield.

Although no other studies have analyzed heat flow in the MRV, it is very similar to the rest of the shield, with depleted radioelements due to the age of rocks. However, heat flow in the MRV has some highly radioactive areas where heat flow

exceeds 60 mW m^{-2} , based on the calculated radioactivity. These areas have the highest geothermal potential and may need further investigation using traditional techniques in the highly radioactive areas.

Most of the heat flow measurements are made using radioactivity and the Q-A relationship, heat flow from the mantle, and the thickness of the radioactive layer. The thickness of the radioactive layer, extent of the post-glacial warming signal, and the contribution of heat flow from the mantle is still not wholly understood in Minnesota. Further investigations would help in refining these data, and the effect these parameters have on the data collected in this study.

3.5 Temperatures at Depth and Electrical Geothermal Resources of Minnesota

Temperature maps have been created at one-kilometer depth intervals from 4-10 km (Fig. 2 and Appendix A) using Eq 2.4.1. The results of the temperature maps are a reflection of the newly acquired heat flow data and thermal conductivity data, which are essential parameters when calculating temperatures at depth. Newly acquired heat flow data and thermal conductivity data have raised the 150°C isotherm to 7 kilometers or about 1.5 kilometers less than previous estimates.

Conductivity measurements were made in the UNDGL from drill cores and outcrop samples in order to understand the conductive nature of the Precambrian basement rock (Appendix A). Low conductivity, 1.5-2.3 W/(m*K), is present in the MCRS due to the dominance of mafic rocks. Outside the rift, the granitic and gneissic bedrock have higher conductivities, 2.3-3.4 W/(m*K).

Understanding the thermal conductivity allows for temperature gradient calculations at the top of the Precambrian basement, and extrapolating them down to a desired depth. In this study, the thermal characteristics of the rock are assumed to stay constant to a depth of 10 kilometers. Other variables affecting the calculation of temperatures to depths of 4-10 kilometers include sediment thickness (Appendix A) and radioactivity of the sedimentary layer. Sediment thickness in Minnesota is primarily thin overburden consisting of glacial till, except in areas where Paleozoic rocks filled in areas of the failed MCRS in the southeast part of the state, and will have a minimal effect on the calculation of the temperatures. Radioactivity of the sediment layer is low, typically $>1.0 \mu\text{W m}^{-3}$ (Beardsmore and Cull, 2001) and will also have a minimal effect in calculating temperatures at depth.

Converting the temperatures to available heat (given in exajoules, $1\text{EJ}=10^{18} \text{ J}$) and

power potential (MW) involves the use of equation 2.4.2. Temperatures in these calculations are $>150^\circ\text{C}$, the minimum temperature needed to economically produce electricity for EGS (Tester et al., 2006). As a result from the temperature maps, the available heat and power potential (Fig. 42) is over three times larger than previously assessed by MIT (Tester et al., 2006). That is 96,794 EJ or 18,409 of MW are available at depths greater than 6 km (assuming a 2% recovering factor) compared to the previous assessments of 6,161 MW at depths >8.5 km. Minnesota is also now similar in resources to other eastern U.S. states and is no longer the least favorable for future development for EGS.

With an abundant amount of resources for geothermal electrical power, the depth to the 150°C isotherm is still considerably deep, but can be reached by current drilling technologies. With heat flow high in the gneissic rocks of the MRV and granites of the Giants Range Batholith, and Vermillion Massif, these areas have the most potential for geothermal development in Minnesota. Further investigations of the MRV using both traditional heat flow observations and will further quantify this resource and determine if heat flow may be higher in some areas of the MRV.

Although the MRV is the best candidate for areas of geothermal development, technology to drill and create a geothermal reservoir at 6 km is still limited. Due to the high cost of drilling in crystalline bedrock, developing this geothermal resource is currently a high risk. Technological advancements in drilling, reservoir stimulation, and binary power plant efficiency must be met in order to economically utilize this heat for geothermal electrical power.

In conclusion, new heat flow measurements in this study have combined traditional heat flow methods, and new methods to eliminate a sampling bias that previously occurred. New heat flow

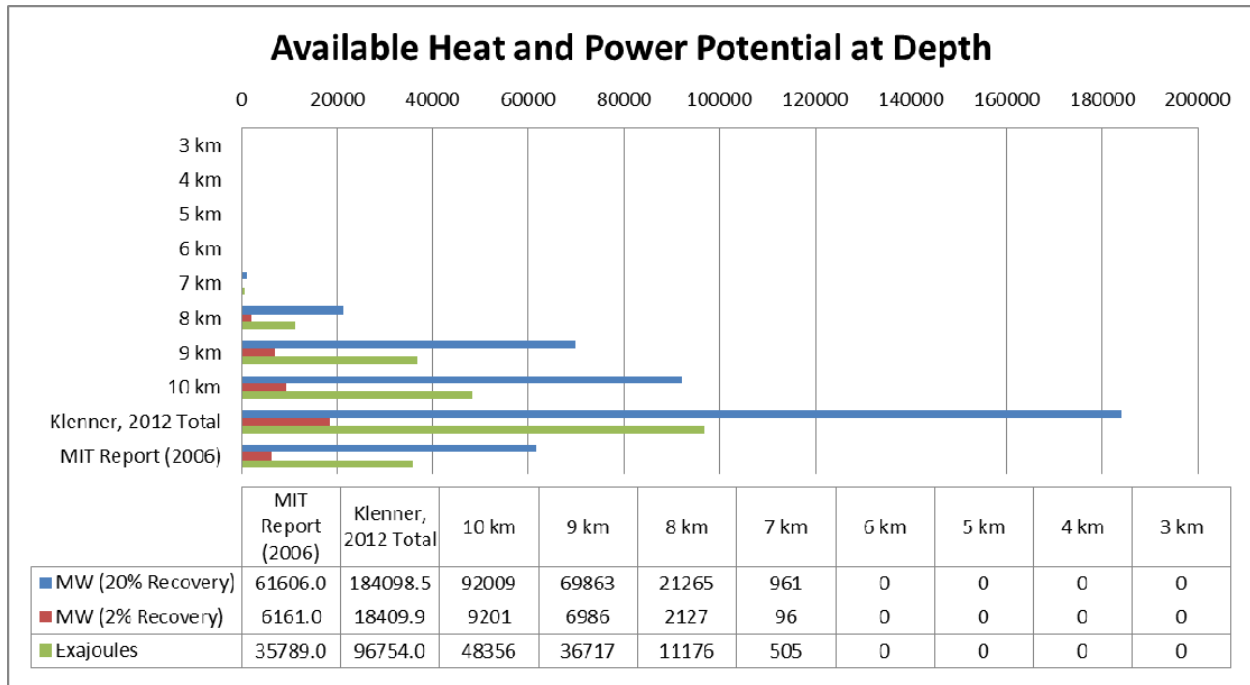


Figure 42. Energy available and power potential at varying depths in Minnesota.

measurements, thermal conductivity measurements and correcting heat flow data have raised the mean heat flow from 40 mW m⁻² to 44.1 mW m⁻², an increase of 10%. These values are also very similar to those found from measurements taken in the same Superior subprovinces in Manitoba and Ontario, Canada (Perry et al., 2006). Although heat flow values are still lower than the continental average, the 10% increase in heat flow has a positive effect on the EGS resources, especially in areas where heat flow exceeds 50 mW m⁻². Further research using deep boreholes to determine the extent of the post-glacial warming signal and more heat flow observations will give a better understanding of the mantle heat flux and the thickness of the radioactive layer. These data could give a better understanding of the thermal regime of the southwestern area of the Superior Province and the Minnesota River Valley subprovince. The vast amount of energy found in this study could essentially power Minnesota through clean base load power. Further heat flow studies will refine estimates of Minnesota's

heat flow, temperatures at depth, and EGS resources available.

4. RECOMMENDATIONS FOR FUTURE WORK IN MINNESOTA

1. Continue to refine the new Minnesota heat flow map by:
 - a. continued collection of down hole temperature data as mineral exploration and water wells become available; and
 - b. continued collection of granitic rock samples for geochemistry, radionuclide analyses, and thermal conductivity analyses;
2. In the selected area(s), drill “touch down” core holes, i.e., drill through the overburden and then drill (oriented drill core) 10-20 feet into the hard bedrock to define a reservoir by collecting samples for:
 - a. chemistry, including radionuclides analyses;

- b. thermal conductivity; and
 - c. fracture(s) analysis;
3. Provide data to potential geothermal energy producers who might conduct additional deeper drilling and reservoir development to determine the reservoir's producing characteristics; and
 4. Continue to educate the public on the benefits of geothermal energy.

REFERENCES

- Allis, R.G., and Garland, G.D., 1979, Heat flow measurements under some lakes in the Superior Province of the Canadian Shield: *Canadian Journal of Earth Sciences*, v. 16, p. 1951-1964.
- Beardsmore, G.R., and Cull, J.P., 2001, *Crustal Heat Flow, A Guide to Measurement and Modelling*: Cambridge University Press, Cambridge, New York, Melbourne, p. 324.
- Beardsmore, G.R., Rybach, L., Blackwell, D., and Baron, C., 2010, A Protocol for Estimating and Mapping Global EGS Potential: *Geothermal Resources Council Transactions*, v. 34, p. 301-312.
- Blackwell, D.D., 1971, The Thermal Structure of the Continental Crust: *Geophysical Monograph*, v. 14, p. 169-184.
- Blackwell, D.D., and Richards, M., 2004, *Geothermal Map of North America*: American Association Petroleum Geologist (AAPG), 1 sheet, scale 1:6,500,000.
- Blodgett, L. and Slack, K., eds., 2009, *Geothermal 101: Basics of Geothermal Energy Production and Use*: Geothermal Energy Association, Washington, D.C., 55 p.
- Boerboom, T.J., 1994, Alkalic Rocks in Northeastern Minnesota, *in* Southwick, D. (ed.), *Short Contributions to Minnesota Geology*: Minnesota Geological Survey, Report of Investigations 43, p. 20-38.
- Card, K.D., 1990, A review of the Superior Province of the Canadian Shield, a product of Archean accretion: *Precambrian Research*, v. 48, p. 99-156.
- Carslaw, H.S., and Jaeger, J.C., 1959, *Conduction of Heat in Solids*: Oxford University Press, New York, p. 510.
- Chandler, V. W., 1990, *Geologic Interpretation of Gravity and Magnetic Data over the Central Part of the Duluth Complex, Northeastern Minnesota*: *Economic Geology*, v. 85, p. 816-829.
- Chouinard, C., and Mareschal, J.-C., 2009, Ground surface temperature history in southern Canada: Temperatures at the base of the Laurentide ice sheet and during the Holocene: *Earth and Planetary Science Letters*, v. 277, p. 280-289.
- County Well Index, 2011, Minnesota Department of Health, 10 Dec. 2011, <<http://www.health.state.mn.us/divs/eh/cwi/>>.
- Davies, J.H., and Davies, D.R., 2010, Earth's surface heat flux: *Solid Earth*, v. 1, p. 5-24.
- Eliasson, L., and Smith, C., 2011, When smaller is better - Cost/Size/Risk analysis of geothermal projects: Geothermal Resource Council, Annual Meeting, San Diego, CA, Oct. 23-26, 2011. PowerPoint Presentation (<http://www.geothermal.org/powerpoints/11.html>).
- Fridleifsson, I.B., 2001, Geothermal energy for the benefit of the people: *Renewable and Sustainable Energy Reviews*, v. 5, p. 299-312.
- Ganopolski, A., Rahmstorf, S., Petoukhov, V., and Claussen, M., 1998, Simulation of modern and glacial climates with a coupled global model of intermediate complexity: *Nature*, v. 391, p. 351-356.
- Geothermal Energy Association, 2010, *Geothermal Energy: International Market Update* May, p. 77.
- Geothermal Technologies Program, 2011, U.S. Department of Energy, Energy

- Efficiency and Renewable Energy, 10 Dec. 2011, 37 p. http://www1.eere.energy.gov/geothermal/pdfs/evaluation_egs_tech_2008.pdf.
- Gosnold, W.D., 1990, Heat flow in the Great Plains of the United States: *Journal of Geophysical Research*, v. 95, p. 353-374.
- Gosnold, W., Lefever, R., Mann, M., Klenner, R., and Salehfar, H., 2010, EGS Potential in the Northern Midcontinent of North America: *Geothermal Resources Council Transactions*, v. 34, p. 355-358.
- Gosnold, W.D, Majorowicz, J., Šafanda, J., and Szewczyk, J., 2005, Has northern hemisphere heat flow been underestimated?: American Geophysical Union, Spring Meeting 2005, May 23-27, New Orleans, LA, abstract #T43D-01.
- Hart, S.R., and Steinhart, J.S., 1965, Terrestrial heat flow: Measurement in lake bottoms: *Science*, v. 149, p. 1499-1501.
- Hart, S.R., Steinhart, J.S., and Smith, T.J., 1994, Terrestrial Heat Flow in Lake Superior: *Canadian J. Earth Sciences*, v. 31, p. 698-708.
- Henry, P., Stevenson, R.K., and Gariépy, C., 1998, Late Archean mantle composition and crustal growth in the Western Superior Province of Canada: Neodymium and lead isotopic evidence from the Wawa, Quetico, and Wabigoon subprovinces: *Geochimica et Cosmochimica Acta*, v. 62, p. 143-157.
- Holm, D.K., Anderson, R., Boerboom, T.J., Cannon, W.F., Chandler, V., Jirsa, M., Miller, J., Schneider, D.A., Schulz, K.J., and Van Schmus, W.R., 2007, Reinterpretation of Paleoproterozoic accretionary boundaries of the north-central United States based on a new aeromagnetic-geologic compilation: *Precambrian Research*, v. 157, p. 71-79, doi: 10.1016/j.precamres.2007.02.023.
- Hotchkiss W.O., and Ingersoll L.R., 1934, Post-glacial time calculations from recent geothermal measurements in the Calumet copper mines: *Journal of Geology*, v. 42, p. 113-142.
- IPCC, 2007, Summary for Policymakers, *in* *Climate Change 2007: The Physical Science Basis*, Solomon, S., Qin, D., Manning, M., Chen, Z., Marquis, M. Averyt, D.B., Tignor, M., and Miller, H.L. (eds.): Cambridge University Press, Cambridge, United Kingdom and New York, N.Y., USA, 18p.
- Jaupart, C., and Mareschal, J.-C., 2007, Heat flow and thermal structure of the lithosphere, *in*, *Treatise on Geophysics*, Schubert, G. (ed.): Oxford, Elsevier Ltd., v. 6, p. 217-252.
- Jessop, A., 1971, The distribution of glacial perturbation of heat flow in Canada: *Canadian Journal Earth Science*, v. 8, p. 162-166.
- Kukkonen, I.T., 1993, Heat flow map of northern and central parts of the Fennoscandian Shield based on geochemical surveys of heat producing elements: *Tectonophysics*, v. 225, p. 3-13.
- Levy, F., Jaupart, C., Mareschal, J.-C., Bienfait, G., and Limare, A., 2010, Low heat flux and large variations of lithospheric thickness in the Canadian Shield: *Journal of Geophysical Research B: Solid Earth*, v. 115, p. 23.
- Lund, J.W., Gawell, K., Boyd, T.L., and Jennejohn, D., 2010, The United States of America county update: Stanford University, Stanford, California, *Proceedings, Thirty-Fifth Workshop on Geothermal Reservoir Engineering*, February 1-3, 2010, SGP-TR-188, 19 p.
- Lusardi, B.A., 1997, Quaternary Glacial Geology: Minnesota at a Glance: Minnesota Geological Survey, University of Minnesota.
- Majorowicz, J., and Wybraniec, S., 2011, New terrestrial heat flow map of Europe after regional paleoclimatic correction application: *International Journal of Earth Sciences*, v. 100, p. 881-887.

- Mareschal, J.-C., and Jaupart, C., 2004, Variations of surface heat flow and lithospheric thermal structure beneath the North American craton: *Earth and Planetary Science Letters*, v. 223, p. 65-77, doi: 10.1016/j.
- Mareschal, J.-C., Jaupart, C., Gariépy, C., Cheng, L.Z., Guillou-Frottier, L., Bienfait, G., and Lapointe, R., 2000, Heat flow and deep thermal structure near the southeastern edge of the Canadian Shield: *Canadian Journal of Earth Science*, v. 37, 399-414.
- Mareschal, J.-C., Rolandone, F., and Bienfait, G., 1999, Heat flow variations in a deep borehole near Sept-Iles, Québec, Canada: Paleoclimatic interpretation and implications for regional heat flow estimates: *Geophysical Research Letters*, v. 26, p. 2049-2052.
- McKenna, J., Blackwell, D., Moyes, C. and Patterson, P.D., 2005, Geothermal electrical power supply possible from Gulf Coast, Midcontinent oil field waters: *Oil and Gas Journal*, September 5, 2005, p. 34-40.
- Mims, C., 2009, Can Geothermal Power Compete with Coal on Price?: *Scientific American online*, 3 p.
- Morey, G.B., and Sims, P.K., 1976, Boundary between two Precambrian Terranes in Minnesota and its geologic significance: *Geological Society of America Bulletin*, v. 87, p. 141-152.
- Mossler, J.H., 2008, Paleozoic stratigraphic nomenclature for Minnesota: *Minnesota Geological Survey Report of Investigations*, v. 65, p. 75, 1 pl.
- National Climatic Data Center, 2011, National Oceanic and Atmospheric Administration, 10 Dec. 2011, <http://www.ncdc.noaa.gov/oa/ncdc.html>.
- Perry, H.K.C., Jaupart, C., Mareschal, J.-C., and Bienfait, G., 2006, Crustal heat production in the Superior Province Canadian Shield, and in North America inferred from heat flow data: *Journal of Geophysical Research B: Solid Earth*, v. 111, 20 p.
- Perry, H.K.C., Jaupart, C., Mareschal, J.-C., Rolandone, F., and Bienfait, G., 2004, Heat flow in the Nipigon arm of the Keweenawan rift, northwestern Ontario, Canada: *Geophysical Research Letters*, v. 31, doi:10.1029/2004GL020159.
- Perry, H.K.C., Rosieanu, C., Mareschal, J.C., and Jaupart, C., 2010, Thermal regime of the lithosphere in Canada: *Canadian Journal of Earth Science*, v. 47, p. 389-408.
- Pollack, H.N., Hurter, S.J., and Johnson, J.R., 1993, Heat flow from the Earth's interior: Analysis of the global data set: *Reviews of Geophysics*, v. 31, p. 267-280.
- Ritchie, J.C., 1983, The paleoecology of the central and northern parts of the glacial Lake Agassiz basin: *Geological Association of Canada, Special Paper*, v. 26, p. 157-170.
- Roberts, B., 2010, Geothermal Resource of the United States, 10 Dec. 2011, <http://www.nrel.gov/gis/pdfs/National%20Geothermal%20EGS%20Hydrothermal%20%202009.pdf>.
- Rogers, J.J.W., Condie, K.C., and Mahan, S., 1970, Significance of Thorium, Uranium and Potassium in some Early Precambrian Graywackes from Wyoming and Minnesota: *Chemical Geology*, v. 5, no. 3, p. 207-213.
- Rolandone, F., Jaupart, C., Mareschal, J.-C., Gariépy, C., Bienfait, G., Carbonne, C., and Lapointe, R., 2002, Surface heat flow, crustal temperatures and mantle heat flow in the Proterozoic Trans-Hudson Orogen: Canadian Shield: *Journal Geophysical Research*, v. 107, DOI: 10.1029/2001JB000698.
- Rolandone, F., Mareschal, J.C., Jaupart, C., Gosselin, C., Bienfait, G., and Lapointe, R., 2003, Heat flow in the western superior province of the Canadian shield: *Geophysical Research Letters*, v. 30, p. 39-1.

- Roy, R.F., Blackwell, D.D., and Decker, E.R., 1972, Continental heat flow, *in* Nature of the Solid Earth, Robertson, E.C. (ed.): McGraw-Hill, New York, NY, p. 506-544.
- Roy, R.F., Blackwell, D.D., and Birch, F., 1968, Heat generation of plutonic rocks and continental heat flow provinces: Earth and Planetary Science Letters, v. 5, p. 1-12.
- Rye, D.M., and Roy, R.F., 1978, Distribution of Thorium, Uranium and Potassium in Archean Granites From Northeastern Minnesota: American Journal Science, v. 278, p. 354-378.
- Schneider von Deimling, T.S., Held, H., Ganopolski, A., and Rahmstorf, S., 2006, Climate sensitivity estimated from ensemble simulations of glacial climate: Climate Dynamics, v. 27, p. 149-163.
- Stone, D., 2000, Temperature and pressure variations in suites of Archean felsic plutonic rocks, Berens River area, northwest Superior Province, Ontario, Canada: Canadian Mineralogist, v. 38, p. 455-470.
- Tester, J.W., Anderson, B., Batchelor, A., Blackwell, D., DiPippo, R., Drake, E., Garnish, J., Livesay, B., Moore, M.C., Nichols, K., Petty, S., Toksoz, N., Veatch, R., Augustine, C., Baria, R., Murphy, E., Negraru, P., and Richards, M., 2006, The future of geothermal energy: Impact of enhanced geothermal systems (EGS) on the United States in the 21st century. Massachusetts Institute of Technology, DOE Contract DE-AC07-05ID14517 Final Report (FGE2006), 209 p.
- Wyborn, D., 2011, Enhanced Geothermal Systems (EGS) – Where Are We Now (abs.): American Geophysical Union, Fall meeting, San Francisco, CA, Dec. 5-8, 2011.
- Wyman, D., and Kerrich, R., 2009, Plume and arc magmatism in the Abitibi subprovince: Implications for the origin of Archean continental lithospheric mantle: Precambrian Research, v. 168, p. 4-22, doi: 10.1016/j.precamres.2008.07.008.
- U.S. Department of Energy Geothermal Technologies Program, 2008, An Evaluation of Enhanced Geothermal Systems Technology, http://www1.eere.energy.gov/geothermal/pdfs/evaluation_egs_tech_2008.pdf.
- Zhao, X., Reyes-Montes, J.M., Andrews, J.R., and Young, R.P., 2011, Optimized EGS reservoir stimulation using microseismic and numerical methods (abs.): Geothermal Resources Council, Annual Meeting, October 23-26, 2011, San Diego, CA. PowerPointPresentation (<http://www.geothermal.org/powerpoints11.html>).

APPENDIX A:

Temperature at Depth (4-10 km), Conductivity, and Sediment Thickness Maps

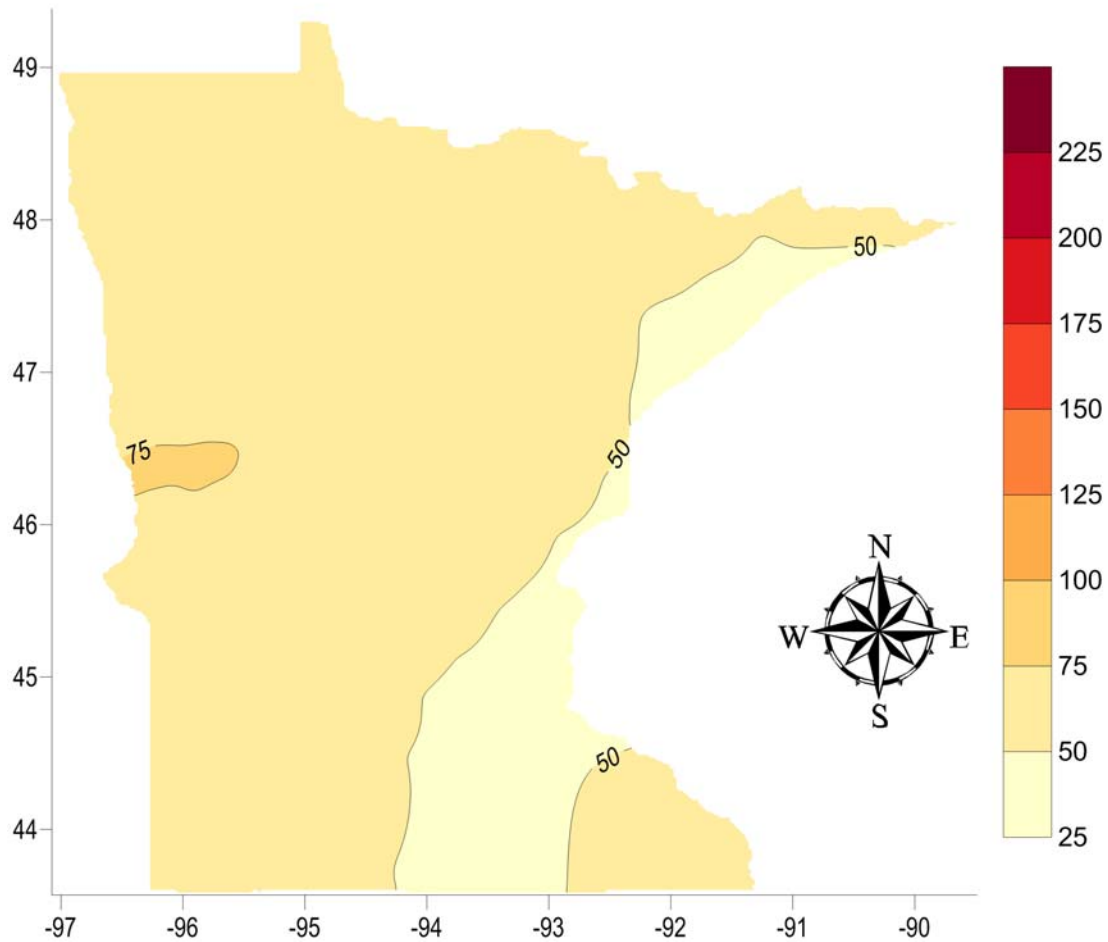


Figure 43. Temperature Map of Minnesota at a Depth of 4 Kilometers. The colored vertical scale is heat flow in mW m^{-2} . Horizontal and vertical axes on the map are in degrees latitude and longitude.

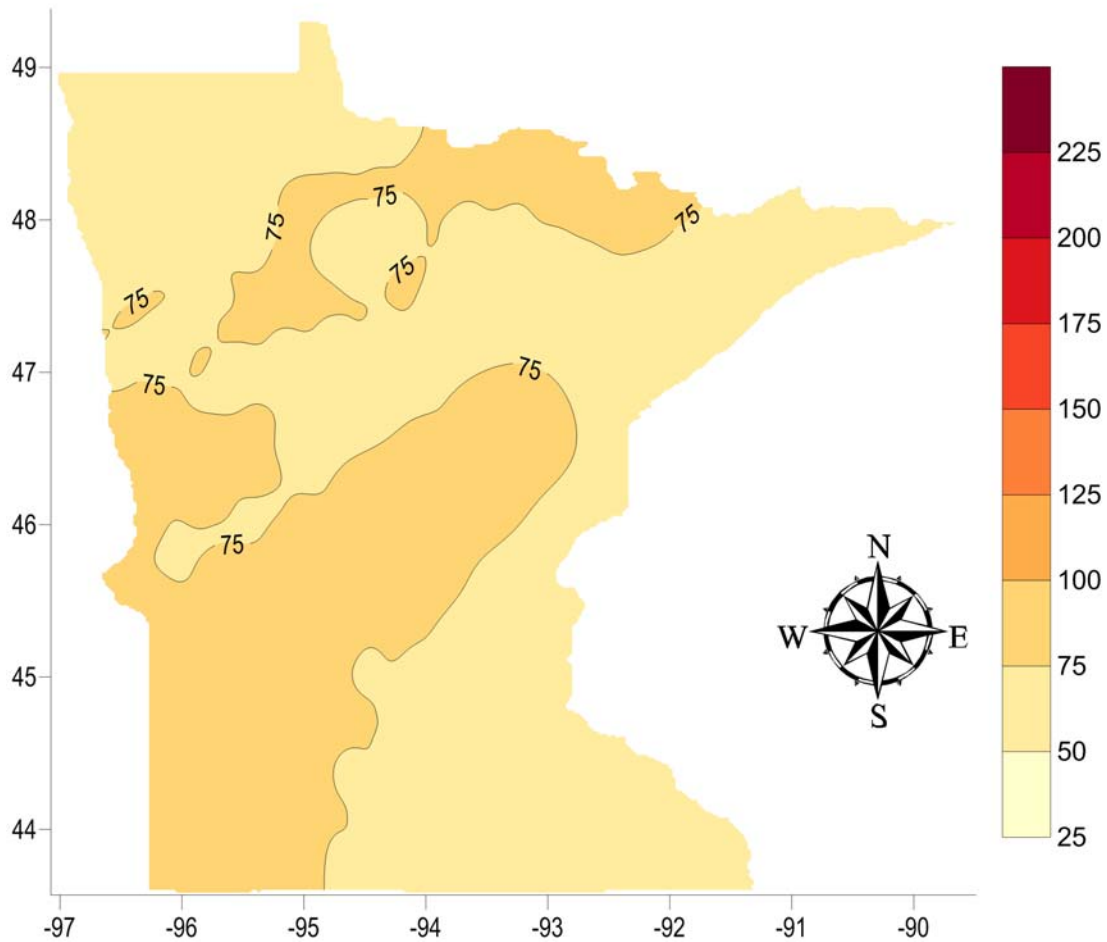


Figure 44. Temperature Map of Minnesota at a Depth of 5 Kilometers. The colored vertical scale is heat flow in mW m^{-2} . Horizontal and vertical axes on the map are in degrees latitude and longitude.

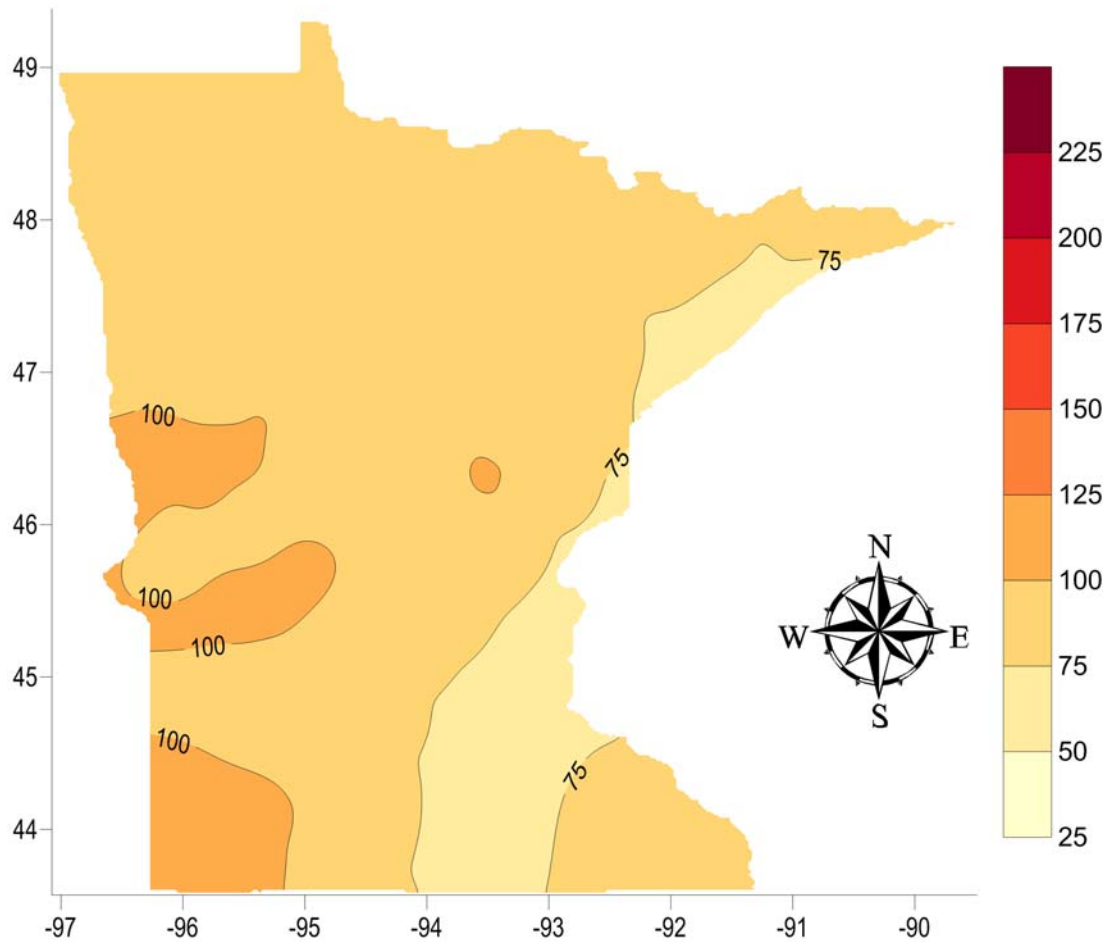


Figure 45. Temperature Map of Minnesota at a Depth of 6 Kilometers. The colored vertical scale is heat flow in mW m^{-2} . Horizontal and vertical axes on the map are in degrees latitude and longitude.

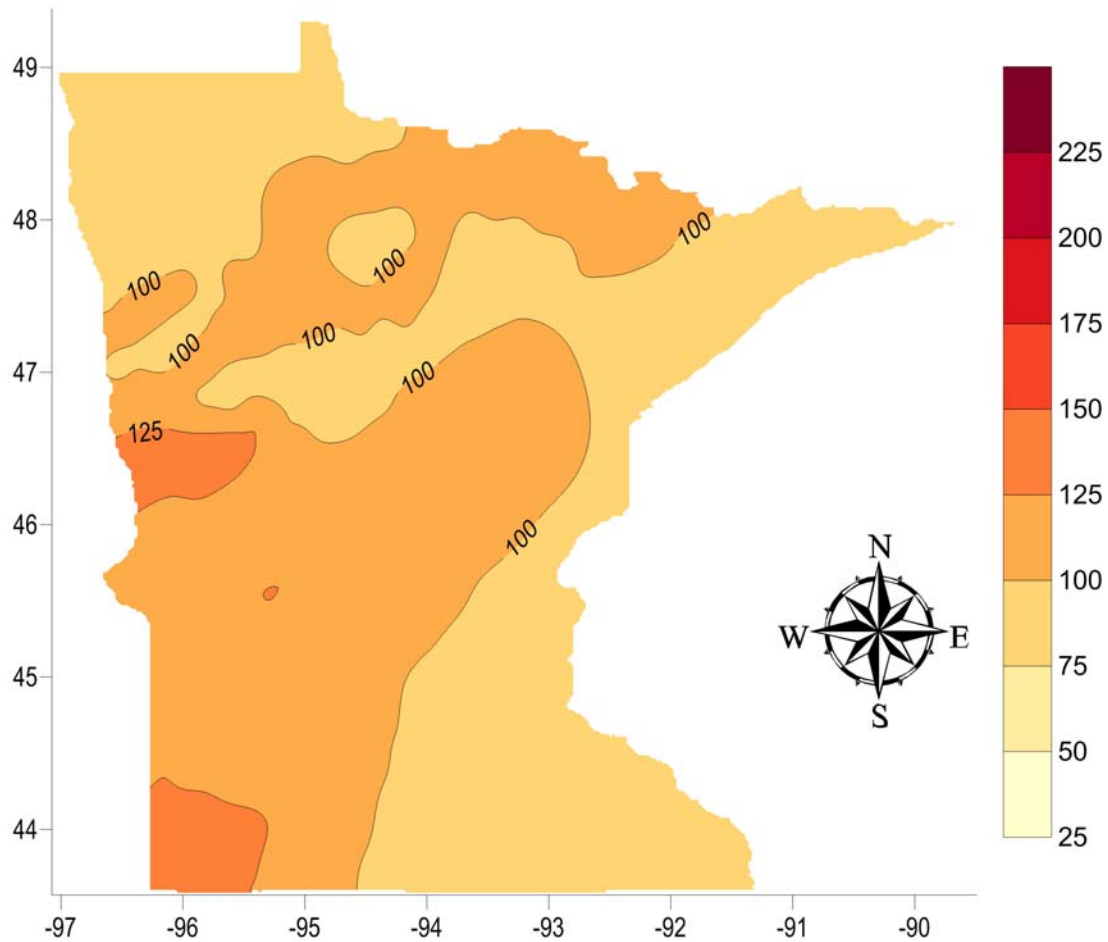


Figure 46. Temperature Map of Minnesota at a Depth of 7 Kilometers. The colored vertical scale is heat flow in mW m^{-2} . Horizontal and vertical axes on the map are in degrees latitude and longitude.

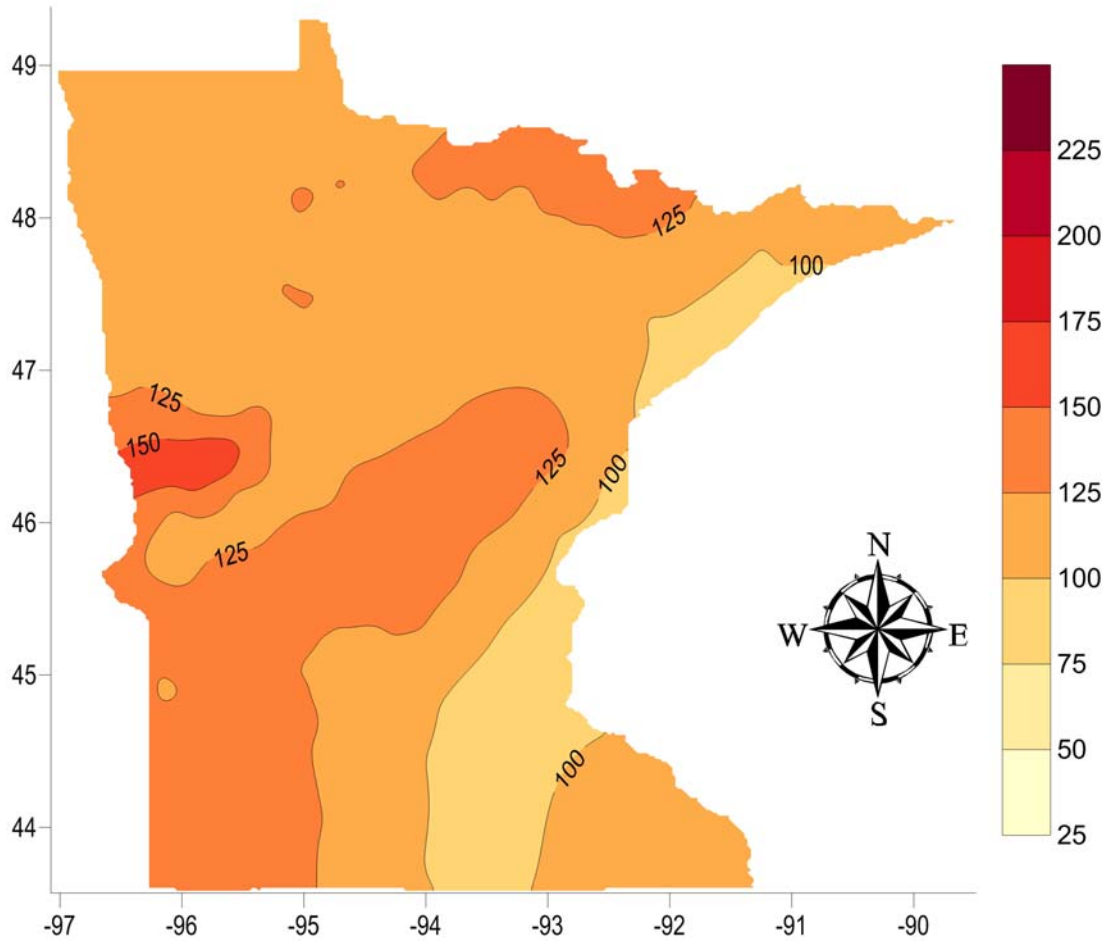


Figure 47. Temperature Map of Minnesota at a Depth of 8 Kilometers. The colored vertical scale is heat flow in mW m^{-2} . Horizontal and vertical axes on the map are in degrees latitude and longitude.

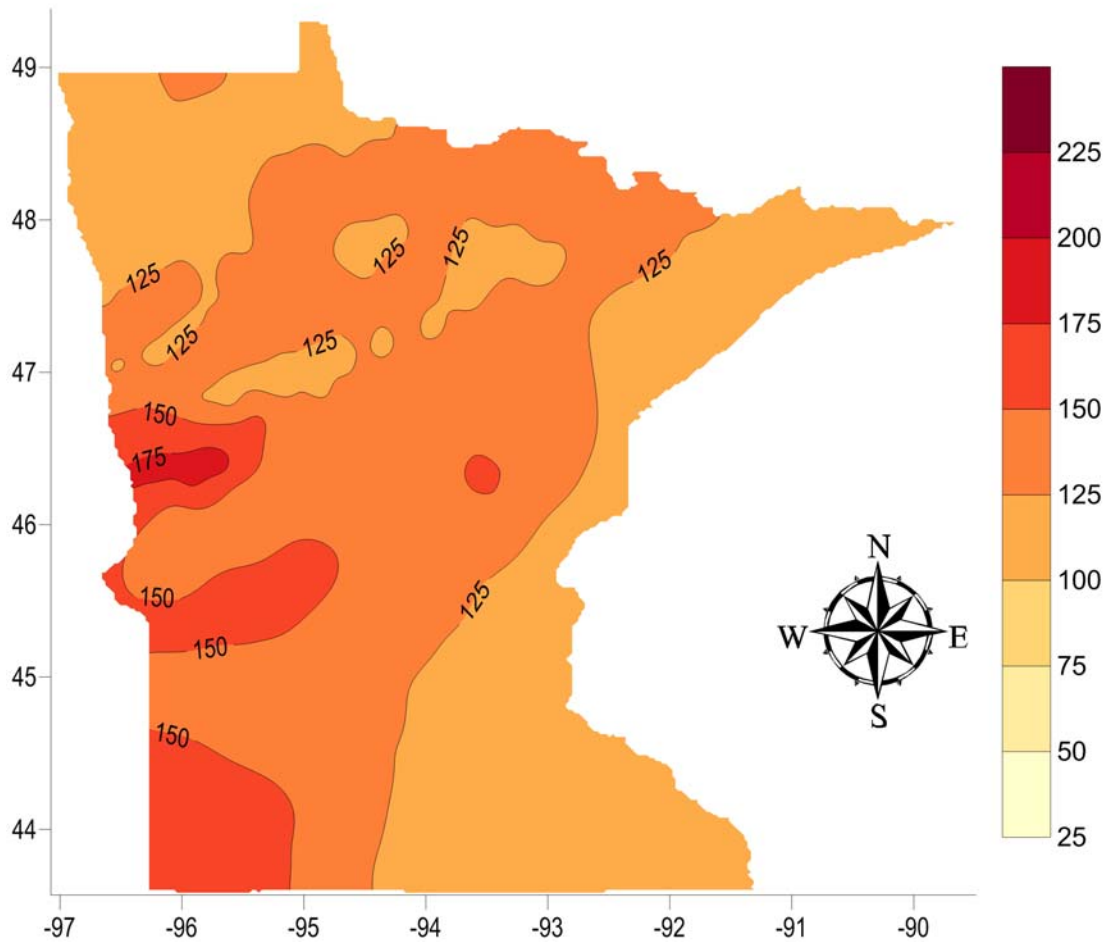


Figure 48. Temperature Map of Minnesota at a Depth of 9 Kilometers. The colored vertical scale is heat flow in mW m^{-2} . Horizontal and vertical axes on the map are in degrees latitude and longitude.

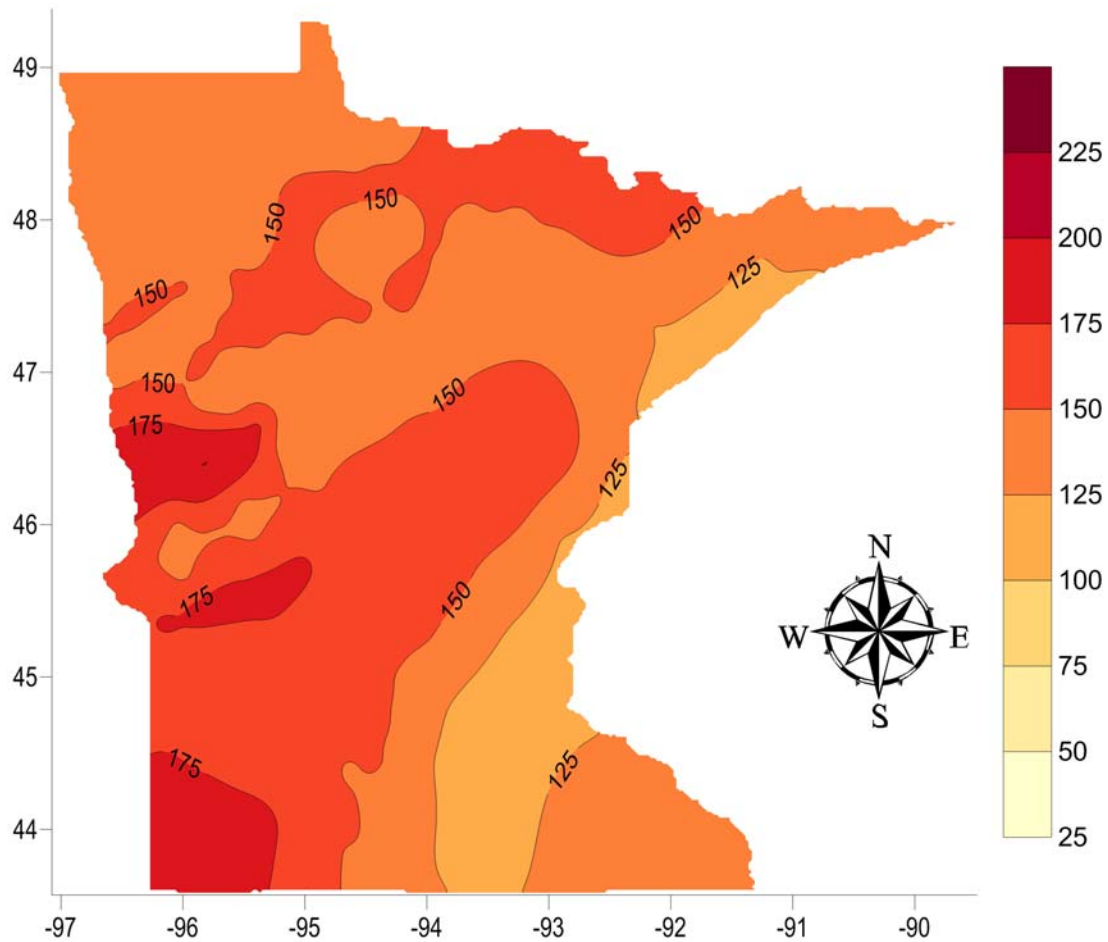


Figure 49. Temperature Map of Minnesota at a Depth of 10 Kilometers. The colored vertical scale is heat flow in mW m^{-2} . Horizontal and vertical axes on the map are in degrees latitude and longitude.

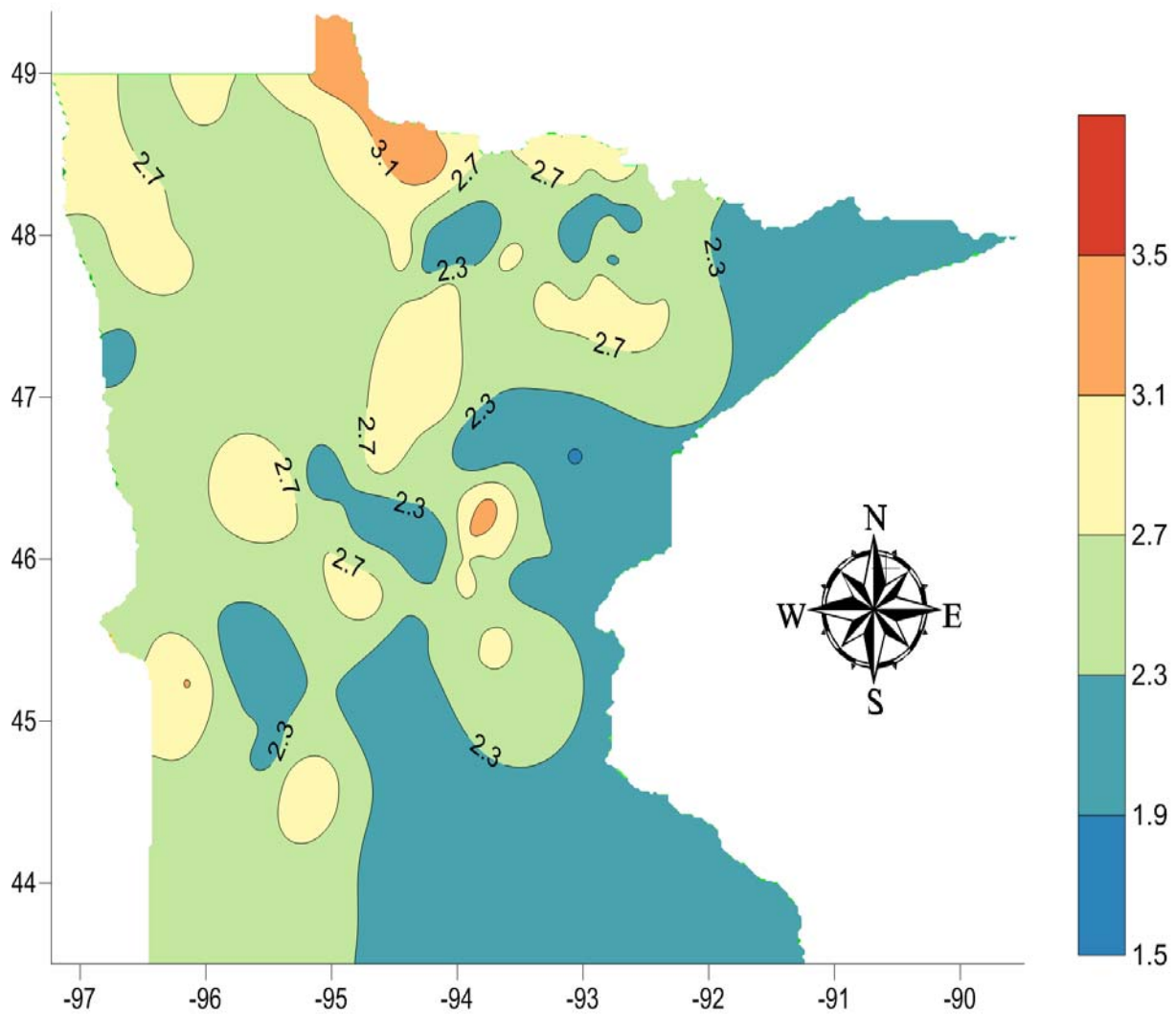


Figure 50. Thermal Conductivity Map of Precambrian Bedrock in Minnesota. The colored vertical scale is thermal conductivity in $W/(m \cdot K)$. Horizontal and vertical axes on the map are in degrees latitude and longitude.

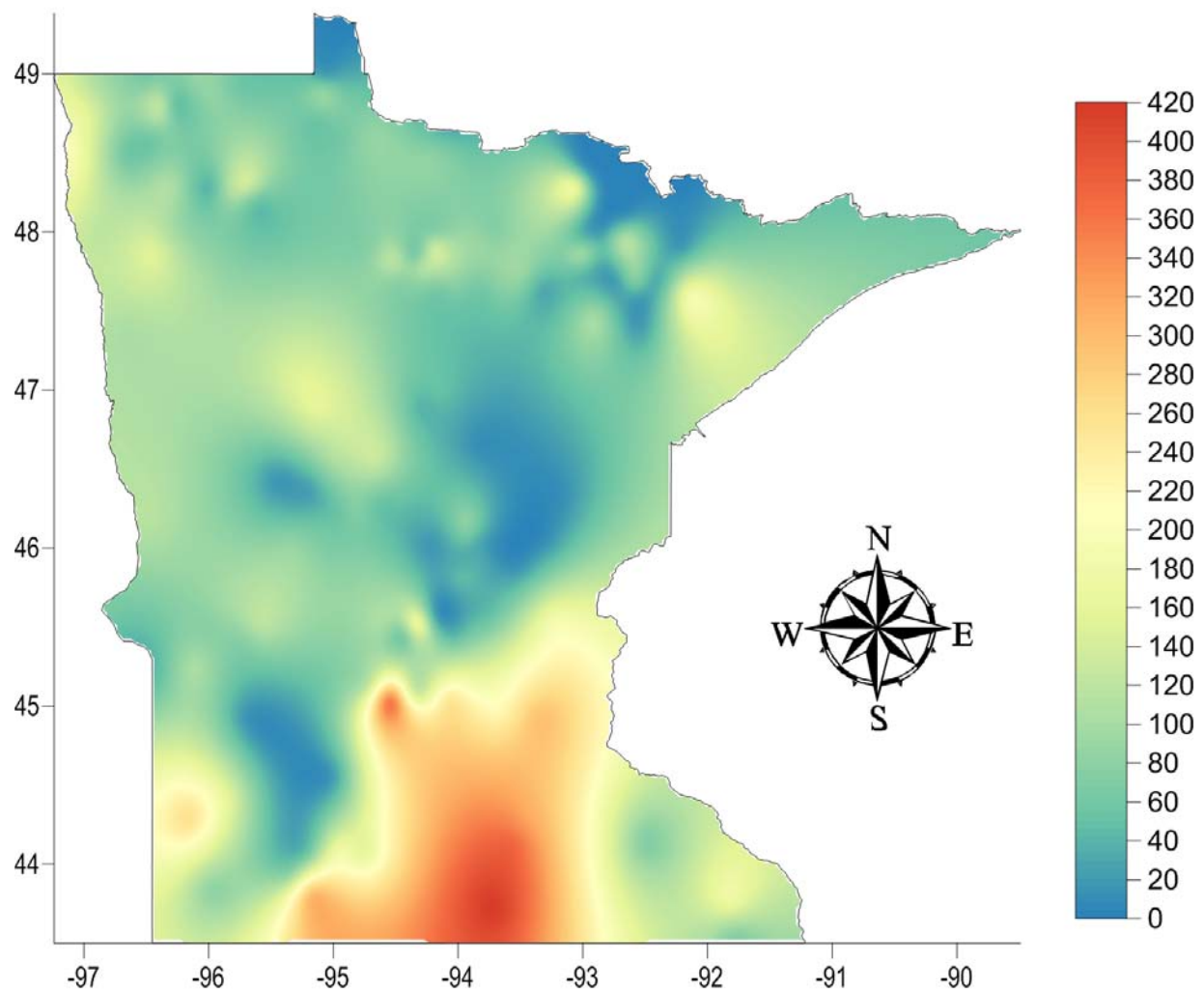


Figure 51. Depth to Precambrian bedrock. Overburden consists of glacial till and sedimentary rocks. The colored vertical scale is in meters. Horizontal and vertical axes on the map are in degrees latitude and longitude.

APPENDIX B:

Heat Flow Observation Data

See *Appendix B - Heat Flow Calculations for All of Minnesota.xls*
on CD in the Back Pocket of this Report

Site	Lat Degree	Long Degree	κ $Wm^{-1}k^{-1}$	Δh meters	Conductivity Statistics	Γ mKm^{-1}	Q $mW m^{-2}$	ΔQ $mW m^{-2}$	Q_c $mW m^{-2}$
Rio Tinto	46.609	-93.060					35.2	11.9	47.1
RT38	46.609	-93.060	2.4	236-482	n=12	16.17	38.8	13.1	51.9
RT39	46.622	-93.043	2.3	115-481	n=10	15.35	35.3	11.9	47.2
RT22	46.583	-93.039	2.4	194-327	n=10	13.17	31.6	10.6	42.2
Duluth Metals	47.809	-91.703				18.52	33.3	9.3	42.6
DM-003	47.809	-91.703	1.8	400-600	n=5	17.78	32	7	39.0
DM-34	47.809	-91.703	1.8	240-600	Estimated from DM-003	18.44	33.2	9.1	42.3
DM-105	47.801	-91.745	1.8	50-325	Estimated from DM-003	18.94	34.1	9.4	43.5
DM-109	47.800	-91.735	1.8	100-600	Estimated from DM-003	18.39	33.1	9.1	42.2
DM-111	47.802	-91.723	1.8	100-610	Estimated from DM-003	18.94	34.1	11.5	45.6
DM-116	47.793	-91.740	1.8	100-606	Estimated from DM-003	18.61	33.5	9.2	42.7
PolyMet	47.623	-91.953					29.4	10.4	39.8
00-457	47.623	-91.953	2.3	88-261	Estimated κ from PolyMet measurements	13.09	30.1	10.4	40.5
2	47.624	-91.958	2.3	100-180	Estimated κ from PolyMet measurements	12.48	28.7	10.4	39.1
Trimont East 2	43.804	-94.583	3.7	100-120	Estimated κ from sediment measurements	8.38	31	11.5	42.5
Courtland	44.295	-94.353	2.75	80-130	Estimated κ from sediment measurements	12.36	34	12.6	46.6
Tyler	44.284	-96.146	1.5	170-250	Estimated κ from sediment measurements	24.53	36.8	13.2	50.0
Glencoe	44.784	-94.152	2.5	110-155	Estimated κ from sediment measurements	11.80	29.5	10.9	40.4

Site	Lat Degree	Long Degree	κ $Wm^{-1}K^{-1}$	Δh meters	Conductivity Statistics	Γ mKm^{-1}	Q $mW m^{-2}$	ΔQ $mW m^{-2}$	Q_c $mW m^{-2}$
Eden Prairie	44.841	-93.458				14.18	27.7	6.925	34.6
769457/DNR 27055	44.841	-93.458	2	105-261	Estimated κ from sediment measurements	14.7	29.4	7.35	36.75
782117/DNR 27058	44.841	-93.458	2	100-180	Estimated κ from sediment measurements	13	26	6.5	32.5
Gaylord	44.544	-94.185	2.4	100-130	Estimated κ from sediment measurements	14.17	34	12.6	46.6
Manley 67007	43.599	-96.433	1.5	56-139	Estimated κ from sediment measurements	28	42	12.0	54.0
550052	44.706	-96.433	3	97-130	Estimated κ from sediment measurements	12.4	37.2	11.2	48.4
213503/DNR 66010	44.283	-93.409	3.5	150-180	Estimated κ from sediment measurements	11	38.5	10.9	49.4
BB-01	45.456	-95.167	2.5	70-88	Estimated κ from sediment measurements	13	32.5	9.4	41.9
DNR 29034	46.891	-95.150	3	100-122	Estimated κ from sediment measurements	10	30	10.5	40.5
769458/DNR 19081	44.660	-93.083	2.5	100-285	Estimated κ from sediment measurements	12.7	31.75	7.9	39.7
782101/DNR 27061	44.989	-93.487	2	150-288	Estimated κ from sediment measurements	14	28	8.4	36.4
773241/DNR 43005	44.906	-94.120	2.5	100-173	Estimated κ from sediment measurements	16	40	11.4	51.4
771161/DNR 46008	43.732	-94.655	2	100-135	Estimated κ from sediment measurements	16.4	32.8	9.4	42.2
768263/DNR 52001	44.272	-94.241	2.5	100-130	Estimated κ from sediment measurements	17	42.5	12.2	54.7

Site	Lat Degree	Long Degree	κ $Wm^{-1}K^{-1}$	Δh meters	Conductivity Statistics	Γ mKm^{-1}	Q $mW m^{-2}$	ΔQ $mW m^{-2}$	Q_c $mW m^{-2}$
770449/DNR 52005	44.346	-94.280	3	100-125	Estimated κ from sediment measurements	10.4	31.2	10.9	42.1
770444/DNR 52007	44.454	-94.186	3	100-160	Estimated κ from sediment measurements	10.2	30.6	9.2	39.8
Gaylord 2	44.544	-94.185					34.25	9.4	43.6
770441/DNR 72001	44.544	-94.185	2	100-130	Estimated κ from sediment measurements	18.5	37	9.3	46.3
770440/DNR 72000	44.544	-94.185	2.5	120-150	Estimated κ from sediment measurements	12.6	31.5	9.5	41.0
221523/DNR 56049	46.301	-96.082	3.5	100-127	Estimated κ from sediment measurements	12.1	42.35	12.1	54.5
770442/DNR 72002	44.674	-94.127	2.5	100-150	Estimated κ from sediment measurements	17	42.5	12.2	54.7
783609/DNR 82053	44.848	-92.791	3	200-160	Estimated κ from sediment measurements	9	27	8.1	35.1
760691/DNR 83021	44.094	-94.393	2.5	100-150	Estimated κ from sediment measurements	11.3	28.25	8.1	36.4
773244/DNR 86011	45.023	-94.055	2.5	100-135	Estimated κ from sediment measurements	16.5	41.25	11.4	52.6
777348/DNR 86013	45.124	-94.033	3.5	100-120	Estimated κ from sediment measurements	11.5	40.25	11.5	51.7
593579	44.760	-93.380	3	100-150	Estimated κ from sediment measurements	8.7	26.1	7.8	33.9
200660/DNR 19004	44.892	-93.095	2.5	180-200	Estimated κ from sediment measurements	11	27.5	8.3	35.8
Centerpoint	44.153	-93.497					31.68	5.3	37.0

Site	Lat Degree	Long Degree	κ $Wm^{-1}K^{-1}$	Δh meters	Conductivity Statistics	Γ mKm^{-1}	Q $mW m^{-2}$	ΔQ $mW m^{-2}$	Q_c $mW m^{-2}$
Gurbish Charles 7	44.208	-93.513	3.5	98-320	Estimated κ from sediment measurements	7.4	25.9	6.5	32.4
Hagen 1	44.178	-93.517	3.25	100-365	Estimated κ from sediment measurements	11.1	36.075	9.0	45.1
Steinhaus 1-Inner	44.184	-93.555	3.25	190-210	Estimated κ from sediment measurements	10.7	34.775	8.7	43.5
Fretham 1	44.142	-93.500	3.25	100-310	Estimated κ from sediment measurements	10.4	33.8	8.5	42.3
Frank Maas 1	44.153	-93.497	3.25	290-330	Estimated κ from sediment measurements	9.9	32.175	8.0	40.2
Schwartz 2	44.218	-93.526	3.25	150-330	Estimated κ from sediment measurements	8.3	26.975	6.7	33.7
Pratt Estate 3	44.167	-93.506	3.25	100-245	Estimated κ from sediment measurements	8	26	6.5	32.5
Gurbish 8	44.191	-93.522	3.25	110-220	Estimated κ from sediment measurements	8	26	6.5	32.5
Schwartz 1	44.217	-93.526	3.25	190-320	Estimated κ from sediment measurements	8	26	6.5	32.5
Mehl 1-Inner	44.230	-93.504	3.25	100-260	Estimated κ from sediment measurements	7.5	24.375	6.1	30.5
Jobe Norris	44.221	-93.515	3.25	200-230	Estimated κ from sediment measurements	7.4	24.05	6.0	30.1
Lee 3	44.172	-93.514	3.25	100-250	Estimated κ from sediment measurements	12	39	9.8	48.8
Melstrom 1	44.211	-93.479	3.25	200-306	Estimated κ from sediment measurements	9	29.25	7.3	36.6

APPENDIX C:

Thermal Conductivity and Radioactivity Data

See *Appendix C - Radioactivity and Conductivity.xls*
on CD in the Back Pocket of this Report

**Sample Location Data
(Columns 1-7)**

	Sample_Number	Type	Drill_Hole	Latitude Deg.	Longitude Deg.	Depth From Ft.	Depth To Ft.
1	1985-14 180.5-181.5	Drill Hole	1985-14	45.78	-94.70	180.5	181.5
2	1985-2 288.5-290	Drill Hole	1985-2	46.57	-94.63	288.5	290
3	1985-3 473-474	Drill Hole	1985-3	46.52	-95.00	473	474
4	1985-4 330-331.5	Drill Hole	1985-4	46.49	-95.07	330	331.5
5	1985-5 262.5-263.5	Drill Hole	1985-5	46.18	-95.07	262.5	263.5
6	1985-8 179.5-180.5	Drill Hole	1985-8	46.02	-95.28	179.5	180.5
7	1985-9 303.5-305	Drill Hole	1985-9	45.94	-95.21	303.5	305
8	1986-11 287-288	Drill Hole	1986-11	48.61	-94.65	287	288
9	1986-16 307.5-308.5	Drill Hole	1986-16	48.63	-94.95	307.5	308.5
10	1986-20 178-178.5	Drill Hole	1986-20	48.72	-95.13	178	178.5
11	1986-2A 144-144.6	Drill Hole	1986-2A	48.48	-94.23	144	144.6
12	27004 283-286	Drill Hole	27004	45.52	-95.99	283	286
13	27005 221-224	Drill Hole	27005	45.62	-95.91	221	224
14	27007 309-311.5	Drill Hole	27007	45.24	-96.12	309	311.5
15	27008 378-381	Drill Hole	27008	45.41	-95.72	378	381
16	27009 220-223	Drill Hole	27009	45.53	-95.58	220	223
17	27011 436-434	Drill Hole	27011	45.50	-94.57	436	434
18	97-3 365-367	Drill Hole	97-3	46.36	-93.75	365	367
19	AB-10 90-92	Drill Hole	AB-10	46.33	-93.14	90	92
20	BB-11 284-28	Drill Hole	BB-11	47.90	-94.37	284	28
21	BB-3 152-156	Drill Hole	BB-3	47.87	-94.25	152	156
22	BB-6 208-210	Drill Hole	BB-6	47.94	-94.18	208	210
23	BB-8 221-227	Drill Hole	BB-8	47.92	-94.19	221	227
24	BKU-81-1 800-803	Drill Hole	BKU-81-1	45.04	-94.54	800	803
25	BO-1 1550-1553	Drill Hole	BO-1	43.53	-91.78	1550	1553
26	BR-2 152-156.5	Drill Hole	BR-2	47.99	-93.75	152	156.5
27	BR-4 185-192	Drill Hole	BR-4	47.97	-93.77	185	192
28	CB-12 302-306	Drill Hole	CB-12	47.84	-94.32	302	306
29	CB-13 20-23	Drill Hole	CB-13	47.78	-94.31	20	23
30	CB-14 400-404	Drill Hole	CB-14	47.82	-94.30	400	404
31	CC-14 518-519	Drill Hole	CC-14	45.95	-95.02	518	519
32	CC-22 223-224.2	Drill Hole	CC-22	46.22	-95.00	223	224.2
33	CC-32 120.5-122.2	Drill Hole	CC-32	46.37	-95.18	120.5	122.2
34	CD-17 31-33	Drill Hole	CD-17	47.81	-92.80	31	33
35	CD-7 79-81	Drill Hole	CD-7	47.77	-93.02	79	81
36	CS-1 110-111	Drill Hole	CS-1	45.45	-94.50	110	111

	Sample_Number	Type	Drill_Hole	Latitude Deg.	Longitude Deg.	Depth From Ft.	Depth To Ft.
37	EC-1 158-159.2	Drill Hole	EC-1	45.75	-94.12	158	159.2
38	EC-13 60-61	Drill Hole	EC-13	45.71	-93.65	60	61
39	EC-2 131.5-132.5	Drill Hole	EC-2	45.75	-94.12	131.5	132.5
40	EC-25 130-131	Drill Hole	EC-25	45.60	-93.77	130	131
41	EC-26 124.5-125.5	Drill Hole	EC-26	45.56	-93.77	124.5	125.5
42	EC-27 145-146.5	Drill Hole	EC-27	45.53	-93.66	145	146.5
43	EC-3 229.5-230.5	Drill Hole	EC-3	45.82	-93.97	229.5	230.5
44	EC-31 204.5-206	Drill Hole	EC-31	45.48	-93.94	204.5	206
45	EC-34 144-145	Drill Hole	EC-34	45.44	-93.93	144	145
46	EC-35 205.5-206.5	Drill Hole	EC-35	45.45	-94.01	205.5	206.5
47	EC-4 78-79	Drill Hole	EC-4	45.96	-93.85	78	79
48	EC-5 161-162	Drill Hole	EC-5	45.92	-93.92	161	162
49	EC-6 50-52	Drill Hole	EC-6	46.00	-93.84	50	52
50	EC-8 34-35	Drill Hole	EC-8	45.88	-93.51	34	35
51	G10-001	Outcrop	Outcrop	44.92	-95.70	0	0
52	G10-002	Outcrop	Outcrop	44.80	-95.55	0	0
53	G10-003	Outcrop	Outcrop	44.69	-95.34	0	0
54	G10-004	Outcrop	Outcrop	44.69	-95.34	0	0
55	G10-005	Outcrop	Outcrop	44.66	-95.32	0	0
56	G10-006	Outcrop	Outcrop	44.66	-95.23	0	0
57	G10-007	Outcrop	Outcrop	44.58	-95.09	0	0
58	G10-008	Outcrop	Outcrop	44.55	-94.99	0	0
59	G10-009	Outcrop	Outcrop	45.55	-94.24	0	0
60	G10-010	Outcrop	Outcrop	45.54	-94.13	0	0
61	G10-011	Outcrop	Outcrop	45.45	-94.43	0	0
62	G10-012	Outcrop	Outcrop	45.66	-94.19	0	0
63	G10-013	Outcrop	Outcrop	46.01	-94.21	0	0
64	G10-014	Outcrop	Outcrop	46.01	-93.68	0	0
65	G10-015	Outcrop	Outcrop	46.05	-93.28	0	0
66	G10-016	Outcrop	Outcrop	46.23	-93.31	0	0
67	GRG-1	Outcrop	Outcrop	47.58	-92.54	0	0
68	GRG-2	Outcrop	Outcrop	47.70	-92.65	0	0
69	GRG-3	Outcrop	Outcrop	47.70	-92.65	0	0
70	GRG-LTV	Outcrop	Outcrop	47.60	-92.14	0	0
71	HB-87-4 723-727	Drill Hole	HB-87-4	47.10	-95.35	723	727
72	HS-1-88 492.3-493.5	Drill Hole	HS-1-88	46.44	-95.45	492.3	493.5
73	HS-1-88 494.5-495.5	Drill Hole	HS-1-88	46.44	-95.45	494.5	495.5
74	ID-1	Outcrop	Outcrop	47.70	-92.63	0	0

	Sample_Number	Type	Drill_Hole	Latitude Deg.	Longitude Deg.	Depth From Ft.	Depth To Ft.
75	J-1 470-472	Drill Hole	J-1	48.89	-95.76	470	472
76	KEX 05L022 1046.2-1048.2	Drill Hole	KEX 05L022	46.58	-93.04	1046.2	1048.2
77	KEX 05L022 1093.5-1095.5	Drill Hole	KEX 05L022	46.58	-93.04	1093.5	1095.5
78	KEX 05L022 1186.6-1188.6	Drill Hole	KEX 05L022	46.58	-93.04	1186.6	1188.6
79	KEX 05L022 1255.5-1257.5	Drill Hole	KEX 05L022	46.58	-93.04	1255.5	1257.5
80	KEX 05L022 1263-1265	Drill Hole	KEX 05L022	46.58	-93.04	1263	1265
81	KEX 05L022 263-265	Drill Hole	KEX 05L022	46.58	-93.04	263	265
82	KEX 05L022 305-307	Drill Hole	KEX 05L022	46.58	-93.04	305	307
83	KEX 05L022 355.5-357.5	Drill Hole	KEX 05L022	46.58	-93.04	355.5	357.5
84	KEX 05L022 563-565	Drill Hole	KEX 05L022	46.58	-93.04	563	565
85	KEX 05L022 635-637	Drill Hole	KEX 05L022	46.58	-93.04	635	637
86	KEX07L038 060	Drill Hole	KEX07L038	46.61	-93.06	196.85	196.85
87	KEX07L038 120	Drill Hole	KEX07L038	46.61	-93.06	393.7	393.7
88	KEX07L038 180	Drill Hole	KEX07L038	46.61	-93.06	590.55	590.55
89	KEX07L038 240	Drill Hole	KEX07L038	46.61	-93.06	787.4	787.4
90	KEX07L038 300	Drill Hole	KEX07L038	46.61	-93.06	984.25	984.25
91	KEX07L038 360	Drill Hole	KEX07L038	46.61	-93.06	1181.1	1181.1
92	KEX07L038 420	Drill Hole	KEX07L038	46.61	-93.06	1377.95	1377.95
93	KEX07L038 480	Drill Hole	KEX07L038	46.61	-93.06	1574.8	1574.8
94	KEX07L038 540	Drill Hole	KEX07L038	46.61	-93.06	295.28	295.28
95	KEX07L038 600	Drill Hole	KEX07L038	46.61	-93.06	1968.5	1968.5
96	KEX07L038 660	Drill Hole	KEX07L038	46.61	-93.06	2165.35	2165.35
97	KEX07L038 720	Drill Hole	KEX07L038	46.61	-93.06	2362.2	2362.2
98	KEX07L039 060	Drill Hole	KEX07L039	46.62	-93.04	196.85	196.85
99	KEX07L039 120	Drill Hole	KEX07L039	46.62	-93.04	393.7	393.7
100	KEX07L039 180	Drill Hole	KEX07L039	46.62	-93.04	590.55	590.55
101	KEX07L039 240	Drill Hole	KEX07L039	46.62	-93.04	787.4	787.4
102	KEX07L039 293	Drill Hole	KEX07L039	46.62	-93.04	961.29	961.29
103	KEX07L039 360	Drill Hole	KEX07L039	46.62	-93.04	1181.1	1181.1
104	KEX07L039 420	Drill Hole	KEX07L039	46.62	-93.04	1377.95	1377.95
105	KEX07L039 480	Drill Hole	KEX07L039	46.62	-93.04	1574.8	1574.8
106	KEX07L039 540	Drill Hole	KEX07L039	46.62	-93.04	295.28	295.28
107	KIB-12 169-170	Drill Hole	KIB-12	47.85	-93.60	169	170
108	KIB-40 300.5-301.5	Drill Hole	KIB-40	47.63	-93.84	300.5	301.5
109	KIB-45 163.5-164.5	Drill Hole	KIB-45	47.88	-93.87	163.5	164.5
110	KIB-50 297-298	Drill Hole	KIB-50	47.66	-93.60	297	298
111	KIB-51 279-280	Drill Hole	KIB-51	47.66	-94.07	279	280
112	KIB-52 256-257	Drill Hole	KIB-52	47.66	-94.17	256	257

	Sample_Number	Type	Drill_Hole	Latitude Deg.	Longitude Deg.	Depth From Ft.	Depth To Ft.
113	KIB-5B 154-155	Drill Hole	KIB-5B	47.64	-93.33	154	155
114	KIB-6 42-43.4	Drill Hole	KIB-6	47.73	-93.48	42	43.4
115	KIB-68 336.5-338	Drill Hole	KIB-68	47.90	-94.70	336.5	338
116	KIB-7 218.5-219.5	Drill Hole	KIB-7	47.67	-93.68	218.5	219.5
117	KIB-74 256.5-258	Drill Hole	KIB-74	47.82	-94.51	256.5	258
118	KIB-77 507-508.3	Drill Hole	KIB-77	47.71	-94.44	507	508.3
119	KIB-79 252-253.5	Drill Hole	KIB-79	47.70	-94.50	252	253.5
120	LF-2 226-229	Drill Hole	LF-2	47.92	-93.04	226	229
121	LF-5 128-131	Drill Hole	LF-5	47.87	-93.02	128	131
122	LL-1-81-8 586-588.5	Drill Hole	LL-81-8	45.11	-94.68	586	588.5
123	LV-1 365-367	Drill Hole	LV-1	46.89	-94.29	365	367
124	LV-12A 81-83	Drill Hole	LV-12A	46.28	-94.64	81	83
125	LV-13 135-136	Drill Hole	LV-13	46.24	-94.80	135	136
126	LV-14 264-265.5	Drill Hole	LV-14	45.97	-95.20	264	265.5
127	LV-4 251.5-253	Drill Hole	LV-4	46.98	-94.16	251.5	253
128	MEX-0003 186-187	Drill Hole	MEX-0003	47.81	-91.70	186	187
129	MEX-0003 2361.5-2363	Drill Hole	MEX-0003	47.81	-91.70	2361.5	2363
130	MEX-0003 2368.5-2369.5	Drill Hole	MEX-0003	47.81	-91.70	2368.5	2369.5
131	MEX-0003 284-285	Drill Hole	MEX-0003	47.81	-91.70	284	285
132	MEX-0003 750.5-752	Drill Hole	MEX-0003	47.81	-91.70	750.5	752
133	MEX-0102 3580-3580.8	Drill Hole	MEX-0102	47.80	-91.74	3580	3580.8
134	MEX-0116 2938-2939	Drill Hole	MEX-0116	47.81	-91.73	2938	2939
135	MEX-0137M 1450-1451	Drill Hole	MEX-0137M	47.81	-91.74	1450	1451
136	MEX-0153 2217-2217.8	Drill Hole	MEX-0153	47.81	-91.73	2217	2217.8
137	MG887 278-279.5	Drill Hole	MG887	48.49	-97.14	278	279.5
138	MN MORT 1	Outcrop	Outcrop	44.55	-94.98	0	0
139	mnely1	Outcrop	Outcrop	47.70	-92.41	0	0
140	MNGF1	Outcrop	Outcrop	44.81	-95.54	0	0
141	MNKBL1	Outcrop	Outcrop	48.40	-93.02	0	0
142	MNLO1	Outcrop	Outcrop	48.63	-94.11	0	0
143	MNLOTW2	Outcrop	Outcrop	48.96	-95.07	0	0
144	MNMV1A	Outcrop	Outcrop	44.92	-95.70	0	0
145	MNMV1B	Outcrop	Outcrop	44.92	-95.70	0	0
146	MNVA2	Outcrop	Outcrop	47.39	-92.54	0	0
147	MNVA3	Outcrop	Outcrop	47.59	-92.54	0	0
148	NB-81-1 724-726	Drill Hole	NB-81-1	45.09	-94.35	724	726
149	NCB-2 220.5-224	Drill Hole	NCB-2	48.59	-94.11	220.5	224
150	NM-3 4364-4367	Drill Hole	NM-3	47.80	-91.70	4364	4367

	Sample_Number	Type	Drill_Hole	Latitude Deg.	Longitude Deg.	Depth From Ft.	Depth To Ft.
151	NM-5 5178-5186	Drill Hole	NM-5	47.79	-91.70	5178	5186
152	NW-1 201-202	Drill Hole	NW-1	48.86	-95.92	201	202
153	NW-10 287-288.8	Drill Hole	NW-10	48.27	-95.90	287	288.8
154	NW-11 320.321.5	Drill Hole	NW-11	48.30	-96.30	320	321.5
155	NW-19 396.5-398	Drill Hole	NW-19	48.00	-96.29	396.5	398
156	NW-2 302-304	Drill Hole	NW-2	48.95	-96.11	302	304
157	NW-2 304.5-306	Drill Hole	NW-2	48.95	-96.11	304.5	306
158	NW-23 531-532.5	Drill Hole	NW-23	47.87	-96.42	531	532.5
159	NW-3 542-543	Drill Hole	NW-3	48.92	-96.91	542	543
160	NW-4B 344-345	Drill Hole	NW-4B	48.78	-96.49	344	345
161	NW-6 356-357.5	Drill Hole	NW-6	48.72	-96.38	356	357.5
162	NW-7 397.5-399	Drill Hole	NW-7	48.59	-96.47	397.5	399
163	NW-7 400.5-401.25	Drill Hole	NW-7	48.59	-96.47	400.5	401.25
164	P-11 138-139	Drill Hole	P-11	46.14	-93.98	138	139
165	P-12 231-232	Drill Hole	P-12	46.14	-93.96	231	232
166	PL-1 389-400	Drill Hole	PL-1	48.96	-96.48	389	400
167	PL-3 171-173	Drill Hole	PL-3	48.21	-95.64	171	173
168	PL-3 173.5-175	Drill Hole	PL-3	48.21	-95.64	173.5	175
169	PLC-1 93-95	Drill Hole	PLC-1	48.30	-93.04	93	95
170	RL-1 833.5-835	Drill Hole	RL-1	46.65	-93.84	833.5	835
171	RP-1	Outcrop	Outcrop	48.90	-95.08	0	0
172	RRVD-23 415-418	Drill Hole	RRVD-23	46.19	-96.50	415	418
173	RRVD-26 391-394	Drill Hole	RRVD-26	47.38	-96.64	391	394
174	RRVD-27 218-321	Drill Hole	RRVD-27	48.00	-96.90	218	321
175	RRVD-30 374-377	Drill Hole	RRVD-30	48.49	-96.69	374	377
176	SC1A	Outcrop	Outcrop	45.54	-94.25	0	0
177	SC1B	Outcrop	Outcrop	45.54	-94.25	0	0
178	SDMIL-A	Outcrop	Outcrop	45.21	-96.52	0	0
179	SDMIL-B	Outcrop	Outcrop	45.21	-96.52	0	0
180	SJ-1 155-156	Drill Hole	SJ-1	45.53	-94.28	155	156
181	SK-1 1098-1101	Drill Hole	SK-1	43.79	-95.84	1098	1101
182	SQ-1 283-288	Drill Hole	SQ-1	44.24	-94.61	283	288
183	SQ-11 677-681	Drill Hole	SQ-11	43.92	-95.34	677	681
184	SQ-13 220-225	Drill Hole	SQ-13	44.06	-94.77	220	225
185	SQ-3A 434-439	Drill Hole	SQ-3A	44.11	-94.94	434	439
186	SQ-4 653-658	Drill Hole	SQ-4	43.82	-95.19	653	658
187	SQ-7 1097-1102	Drill Hole	SQ-7	43.85	-95.99	1097	1102
188	STAR 2 222-225	Drill Hole	STAR 2	48.28	-95.68	222	225

	Sample_Number	Type	Drill_Hole	Latitude Deg.	Longitude Deg.	Depth From Ft.	Depth To Ft.
189	Star-1 567-570.5	Drill Hole	Star-1	48.28	-95.95	567	570.5
190	STG-1	Outcrop	Outcrop	47.78	-92.83	0	0
191	VM-1	Outcrop	Outcrop	47.89	-92.19	0	0
192	VM-10	Outcrop	Outcrop	48.39	-92.92	0	0
193	VM-11	Outcrop	Outcrop	48.44	-93.05	0	0
194	VM-2	Outcrop	Outcrop	48.00	-92.83	0	0
195	VM-3	Outcrop	Outcrop	48.04	-92.97	0	0
196	VM-4a	Outcrop	Outcrop	48.24	-92.48	0	0
197	VM-4b	Outcrop	Outcrop	48.24	-92.48	0	0
198	VM-5	Outcrop	Outcrop	48.17	-92.52	0	0
199	VM-6a	Outcrop	Outcrop	48.07	-92.67	0	0
200	VM-6b	Outcrop	Outcrop	48.07	-92.67	0	0
201	VM-7a	Outcrop	Outcrop	48.19	-92.89	0	0
202	VM-7b	Outcrop	Outcrop	48.19	-92.89	0	0
203	VM-8	Outcrop	Outcrop	48.34	-92.96	0	0
204	VM-9	Outcrop	Outcrop	48.40	-92.82	0	0
205	WMP-1	Outcrop	Outcrop	47.95	-92.66	0	0
206	YGH-1 540-542	Drill Hole	YGH-1	48.81	-96.34	540	542
207	YGH-2 591.5-593.5	Drill Hole	YGH-2	48.81	-96.31	591.5	593.5

**Radioactivity and Conductivity Data
(Columns 8-15)**

	County	Intrusion	Rock_Type	U ppm	Th ppm	K %	Q est. mW m⁻²	Conductivity W/(m*K)
1	Todd	Unnamed	Granite	0.00	42.45	3.14	69.03	3.01
2	Cass	Unnamed	Diorite	0.69	0.57	0.90	35.70	2.93
3	Wadena	Unnamed	Granite	0.49	8.72	2.04	42.77	2.12
4	Wadena	Unnamed	Brecciated Leucotonalite	0.94	6.78	2.31	42.59	1.79
5	Todd	Unnamed	Metamorphosed Hornblende Tonalite/Diorite	0.35	1.55	0.95	35.71	2.65
6	Douglas	Unnamed	Biotite Hornblende Granodiorite	0.82	3.91	1.13	38.82	2.57
7	Douglas	Unnamed	Gneissic Biotite Hornblende Tonalite	0.25	2.65	0.97	36.36	2.51
8	Lake of the Woods	Baudette Intrusion	Porphyritic Syenite	0.39	1.93	4.55	39.88	1.60
9	Lake of the Woods	Baudette Intrusion	Gneissic Tonalite	0.22	2.37	0.87	35.96	2.88
10	Roseau	Unnamed	Granodiorite	0.60	0.85	0.84	35.64	2.68
11	Koochiching	Unnamed	Granodiorite	0.39	1.18	3.08	37.76	3.57
12	Stevens	Unnamed	Biotite Gneiss	0.08	6.70	1.88	40.08	
13	Stevens	Unnamed	Foliated Biotite Granite	2.09	5.52	1.80	43.73	2.27
14	Big Stone	Ortonville Granite	Granite	4.71	16.31	3.23	59.71	3.26
15	Pope	Unnamed	Tonalitic Gneiss	0.40	25.36	3.04	56.56	1.89
16	Pope	Unnamed	Tonalitic Gneiss	0.76	13.46	1.67	46.70	2.15
17	Sterns	Unnamed	Biotite Hornblende Granite	0.94	5.97	1.50	41.12	2.35
18	Aitkin	Mille Lacs Lake Granite	Granite	3.90	21.09	3.20	61.52	3.32
19	Aitkin	McGrath Gneiss	Granitic Augen Gneiss	0.28	9.62	2.95	43.95	1.67
20	Koochiching	Unnamed	Chloritized Diorite	0.49	0.48	0.36	34.59	2.93
21	Koochiching	Unnamed	Granodiorite	0.08	0.84	0.58	32.70	1.47
22	Koochiching	Unnamed	Granodiorite	0.14	1.47	0.74	34.94	1.89
23	Koochiching	Unnamed	Foliated Monzonite	0.37	1.54	0.78	35.57	
24	Meeker	Rockville Granite	Diorite	0.19	0.03	0.01	33.19	1.98
25	Fillmore	Unnamed	Amphibolitic Gneiss	0.86	1.36	1.16	36.97	1.94
26	Koochiching	Unnamed	Monzodiorite	0.73	0.56	0.79	35.66	1.85
27	Koochiching	Unnamed	Quartz Diorite	0.43	2.60	0.66	36.41	1.76
28	Itasca	Unnamed	Monzodiorite	0.36	1.07	0.88	35.30	2.71
29	Itasca	Unnamed	Granite	0.31	1.17	1.49	35.90	2.36
30	Itasca	Unnamed	Quartz Monzodiorite	0.13	2.01	1.05	35.68	1.79
31	Todd	Unnamed	Biotitic Gneissic Tonalite	1.32	10.52	1.67	45.70	2.78
32	Todd	Unnamed	Diorite	0.76	2.64	1.27	37.84	2.78
33	Otter Tail	Unnamed	Hornblende Diorite	0.28	0.00	0.41	33.77	2.45
34	St. Louis	Rice River Pluton	Hornblende Diorite	2.38	8.82	2.83	48.06	1.71

	County	Intrusion	Rock_Type	U ppm	Th ppm	K %	Q est. mW m ⁻²	Conductivity W/(m*K)
35	St. Louis	Morcom Pluton	Monzonite	0.55	1.96	2.47	38.10	2.26
36	Stearns	Richmond Charnokitic Granite	Charnokitic Granite (weathered)	0.38	4.42	3.08	40.25	1.82
37	Benton	Watab Quartz Diorite	Biotite Hornblende Diorite	0.60	2.10	0.80	36.56	2.15
38	Mille Lacs	Pease Pluton	Granite	3.15	5.87	2.18	46.86	2.57
39	Benton	Foley Granite	Porphyritic Granite	3.64	14.63	3.43	56.13	3.06
40	Benton	Glendorado Pluton	Biotite Hornblende Granodiorite	1.43	7.58	2.76	44.82	2.44
41	Benton	Glendorado Pluton	Granite	2.32	3.15	3.10	43.78	2.87
42	Sherburne	Tonalitic Orthogneiss	Tonalitic Orthogneiss	0.21	0.88	1.59	35.55	2.85
43	Morrison	Foley Granite	Biotite Granite	2.03	10.18	2.32	47.78	2.94
44	Sherburne	Reformatory Granite	Granite	0.86	4.64	1.42	39.81	2.28
45	Sherburne	Granite (in Archean Gneiss)	Granite	0.80	3.29	2.22	39.46	2.65
46	Sherburne	Reformatory Granite	Granodiorite	2.41	3.53	1.22	42.33	2.44
47	Morrison	Pease Pluton	Granite	1.16	10.58	3.35	47.14	2.40
48	Morrison	Pease Pluton	Porphyritic Granite	0.74	0.97	2.54	37.85	3.00
49	Morrison	Hillman Migmatite	Granite Migmatite Mixture	1.89	4.54	1.49	42.18	2.49
50	Kanabec	Foley Granite	Granite	1.16	4.47	1.67	40.62	1.98
51	Chippewa	Montevideo Gneiss	Tonalitic Gneiss	0.56	7.68	1.63	41.70	2.75
52	Yellow Medicine	Montevideo Gneiss	Hornblende-Biotite Gneiss with Amphibolite pods	0.07	0.00	0.03	32.89	1.68
53	Redwood	Sacred Heart Granite	Weakly Foliated Biotite Granite	0.22	8.70	2.69	42.81	2.80
54	Renville	Sacred Heart Granite	Weakly Foliated Biotite Granite	0.13	5.84	1.99	39.64	2.72
55	Redwood	Morton Gneiss	Hornblende-Biotite Gneiss with Amphibolite pods	0.72	1.97	0.56	36.48	
56	Redwood	Morton Gneiss	Pegmatitic Phase of Morton Gneiss	0.78	2.03	0.79	36.91	2.90
57	Renville	Morton Gneiss	Granitic Phase of Morton Gneiss	3.09	8.55	2.46	49.11	3.13
58	Renville	Morton Gneiss	Hornblende-Biotite Gneiss	1.20	2.05	0.88	38.00	2.84
59	Stearns	St. Cloud Granite	Hornblende-Biotite Granite "Old Gray"	1.31	2.42	2.01	39.75	1.88
60	Sherburne	Rockville Granite	Hornblende Granite	2.45	5.04	4.28	46.80	2.80
61	Stearns	Richmond Charnokitic Granite	Charnokitic Granite (orthopyroxene-bearing)	0.24	3.63	3.01	39.24	2.32
62	Benton	St. Cloud Granite	Porphyritic Hornblende Granite	3.06	23.61	3.07	61.40	3.04
63	Morrison	Freedham Granodiorite	Granodiorite	1.53	6.54	1.57	42.98	2.04
64	Mille Lacs	Bradbury Creek Granodiorite	Granodiorite	2.07	6.98	1.32	44.32	2.83
65	Pine	Warman Granite	Biotite Granite	2.17	4.28	1.59	42.74	2.35
66	Aitkin	McGrath Gneiss	Biotite Gneiss	0.35	2.75	3.15	38.95	2.27

	County	Intrusion	Rock_Type	U ppm	Th ppm	K %	Q est. mW m ⁻²	Conductivity W/(m*K)
67	St. Louis	Giants Range Batholith	Foliated Granite	0.14	2.19	0.79	35.55	2.86
68	St. Louis	Shannon Lake Granite of GRB	Medium to Coarse Grained Pink Granite	6.21	3.81	0.43	50.51	2.57
69	St. Louis	Shannon Lake Granite of GRB	Weakly Foliated Granodiorite	0.82	2.57	2.05	38.75	
70	St. Louis	Giants Range Batholith	Hornblende Granite	0.69	6.20	2.45	41.69	2.61
71	Becker	Unnamed	Monzodiorite	1.87	5.84	1.75	43.42	2.35
72	Otter Tail	Unnamed	Potassium Metasomatized Granite	3.04	15.90	3.42	55.73	3.19
73	Otter Tail	Unnamed	Pegmatitic Granite	2.27	2.31	3.31	43.24	3.19
74	St. Louis	Iddington Pluton	Monzodiorite	1.14	1.62	2.76	39.50	2.63
75	Roseau	Roseau River Batholith	Gneissic Tonalite	1.22	2.23	1.23	38.55	2.54
76	Carlton	Tamarack Intrusion	Tamarack int = biotitic norite	0.01	0.10	0.00	32.79	2.19
77	Carlton	Tamarack Intrusion	Tamarack int = gabbro	0.52	1.95	0.60	36.06	2.50
78	Carlton	Tamarack Intrusion	Tamarack int = Monzogabbro	0.22	3.75	0.71	36.87	2.37
79	Carlton	Tamarack Intrusion	Tamarack int = Monzogabbro	0.05	0.75	0.28	33.70	3.18
80	Carlton	Tamarack Intrusion	Tamarack int = Monzogabbro w/20% granophyre	1.16	4.84	1.37	40.59	2.14
81	Carlton	Tamarack Intrusion	Thomson Fm = well-cleaved argillite	3.13	5.67	2.07	46.55	2.21
82	Carlton	Tamarack Intrusion	Thomson Fm = graywacke and siltstone	1.69	4.27	2.00	42.04	2.49
83	Carlton	Tamarack Intrusion	Thomson Fm = massive flow/sill??	0.42	1.26	0.00	34.67	2.53
84	Carlton	Tamarack Intrusion	Thomson Fm = graywacke w/mudstone	0.96	3.20	0.41	37.85	1.92
85	Carlton	Tamarack Intrusion	Thomson Fm = well-cleaved mixed sediments	1.33	5.57	1.95	42.18	2.37
86	Carlton	Tamarack Intrusion	Feldspathic Peridotite					2.45
87	Carlton	Tamarack Intrusion	Granophyre					2.46
88	Carlton	Tamarack Intrusion	Epidote Altered Granophyre					1.97
89	Carlton	Tamarack Intrusion	Melatroctolite - Serpentinized					1.83
90	Carlton	Tamarack Intrusion	Epidote Altered Melatroctolite					1.79
91	Carlton	Tamarack Intrusion	Melatroctolite - Weakly Serpentinized					1.78
92	Carlton	Tamarack Intrusion	Troctolite					2.22
93	Carlton	Tamarack Intrusion	Peridotite					1.92
94	Carlton	Tamarack Intrusion	Peridotite - Serpentinized					2.81
95	Carlton	Tamarack Intrusion	Peridotite - Weakly Serpentinized					3.09
96	Carlton	Tamarack Intrusion	Peridotite					
97	Carlton	Tamarack Intrusion	Peridotite					3.77
98	Carlton	Tamarack Intrusion	Thomson Fm = graywacke and siltstone					2.72
99	Carlton	Tamarack Intrusion	Thomson Fm = massive flow/sill??					3.15
100	Carlton	Tamarack Intrusion	Granophyre					1.98

	County	Intrusion	Rock_Type	U ppm	Th ppm	K %	Q est. mW m ⁻²	Conductivity W/(m*K)
101	Carlton	Tamarack Intrusion	Granophyre					1.81
102	Carlton	Tamarack Intrusion	Fine Grained Melatroctolite					1.51
103	Carlton	Tamarack Intrusion	Oxide-Bearing Melatroctolite					2.11
104	Carlton	Tamarack Intrusion	Melatroctolite					2.22
105	Carlton	Tamarack Intrusion	Feldspathic Peridotite					2.66
106	Carlton	Tamarack Intrusion	Feldspathic Peridotite					2.59
107	Itasca	Effie Pluton	Leucogranodiorite	0.01	0.83	1.24	34.67	3.26
108	Itasca	Bello Lake Pluton	Monzonite					2.17
109	Koochiching	Unnamed	Granodiorite	0.16	0.80	1.02	34.76	2.20
110	Itasca	Unnamed	Granite	7.99	63.79	2.86	103.87	2.36
111	Itasca	Unnamed	Hornblende Quartz Diorite	0.47	1.65	0.41	35.50	3.08
112	Itasca	Unnamed	Hornblende Quartz Diorite	0.38	0.94	0.84	35.19	2.74
113	Itasca	Unnamed	Quartz Diorite	0.00	0.04	0.48	33.24	3.01
114	Itasca	Coon Lake Pluton	Syenite	0.35	4.10	3.49	40.38	2.12
115	Beltrami	Unnamed	Quartz Diorite	0.74	5.26	1.59	40.17	2.38
116	Itasca	Bello Lake Pluton	Monzonite	1.75	6.00	2.11	43.64	2.55
117	Beltrami	Unnamed	Granodiorite	1.19	0.52	1.30	37.22	1.66
118	Beltrami	Decker Lake Pluton	Hornblende Granite	0.51	1.09	1.17	35.95	2.66
119	Beltrami	Decker Lake Pluton	Hornblende Monzodiorite	0.24	3.81	2.94	39.30	
120	St. Louis	Linden Pluton	Foliated Quartz Monzonite	1.52	8.31	8.44	51.55	2.18
121	St. Louis	Linden Pluton	Chloritized Granodiorite	0.52	4.00	3.65	40.85	2.20
122	Meeker	Rockville Granite	Diorite	0.59	3.90	0.53	37.67	2.05
123	Cass	Unnamed	Granitic Gneiss	0.14	0.85	0.77	34.51	2.79
124	Morrison	Unnamed	Granite	0.99	22.62	3.53	56.30	1.98
125	Todd	Unnamed	Epidotized Gneissic Leucotonalite	0.68	1.10	0.97	36.15	2.04
126	Douglas	Unnamed	Biotite Hornblende Tonalite	0.82	3.19	1.52	38.67	2.44
127	Cass	Unnamed	Biotitic Leucogranite	1.33	19.19	4.29	55.22	3.05
128	Lake	Duluth Complex	ATA Series	0.00	0.00	0.00	32.70	1.92
129	Lake	Duluth Complex	AN Series = Anorthosite	0.40	0.69	0.40	34.59	1.40
130	Lake	Duluth Complex	AN Series = Gabbro	0.42	1.29	0.51	35.21	1.86
131	Lake	Duluth Complex	Upper Basalt	0.14	0.08	0.00	33.08	2.12
132	Lake	Duluth Complex	Upper Gabbro	0.14	0.00	0.00	33.03	1.73
133	Lake	Giants Range Batholith	Giants Range Batholith	0.20	1.60	1.56	36.05	2.07
134	Lake	Giants Range Batholith	Giants Range Batholith	0.67	15.11	2.29	48.42	2.63
135	Lake	Duluth Complex	BMZ = Melatroctolite	0.32	0.00	0.09	33.53	1.38
136	Lake	Giants Range Batholith	Giants Range Batholith	0.23	2.06	2.26	37.20	1.96
137	Marshall	Unnamed	Granite	0.00	0.00	0.00	32.70	2.88
138	Marshall	Unnamed	Gneissic	1.78	2.83	3.72	42.94	2.75

	County	Intrusion	Rock_Type	U ppm	Th ppm	K %	Q est. mW m ⁻²	Conductivity W/(m*K)
139	Marshall	Unnamed	Mafic	0.03	0.75	0.83	34.22	2.74
140	Marshall	Unnamed	Granitic	0.10	0.05	0.04	33.02	1.92
141	Marshall	Unnamed	Granitic	0.64	14.04	1.89	47.09	2.90
142	Marshall	Unnamed	Granitic	1.22	8.50	2.41	44.67	2.80
143	Marshall	Unnamed	Granitic	0.15	0.36	0.61	33.97	3.33
144	Marshall	Unnamed	Gneiss	1.90	8.90	1.85	45.98	2.26
145	Marshall	Unnamed	Gneiss	1.34	6.89	1.80	43.08	2.26
146	Marshall	Unnamed	Mafic	0.07	1.06	0.84	34.58	2.80
147	Marshall	Unnamed	Mafic	0.03	0.13	0.31	33.20	2.44
148	Meeker	Rockville Granite	Granodiorite	0.45	1.54	0.26	35.22	1.99
149	Koochiching	Birchdale Intrusion	Granite	1.01	5.11	3.00	42.18	3.09
150	Lake	Giants Range Batholith	Hornblende Granite	0.38	1.15	1.61	36.16	
151	Lake	Giants Range Batholith	Granodiorite					1.44
152	Roseau	Roseau River Batholith	Gneissic Tonalite	0.75	2.83	2.32	39.09	2.95
153	Marshall	Unnamed	Monzodiorite	1.39	6.30	1.59	42.51	2.70
154	Marshall	Unnamed	Tonalite	0.54	2.21	1.30	37.03	2.71
155	Pennington	Unnamed	Granodiorite	0.73	2.12	1.77	37.92	2.71
156	Roseau	Unnamed	Granite	0.25	3.30	3.47	39.50	3.15
157	Roseau	Unnamed	Hornblende Biotite Gneiss	0.30	10.81	2.07	43.98	3.41
158	Red Lake	Red Lake Falls Pluton	Granodiorite	0.11	2.70	0.79	35.88	3.07
159	Kittson	Roseau River Batholith	Gneissic Tonalite	0.00	141.40	3.14	146.03	3.06
160	Kittson	Unnamed	Granodiorite	0.56	2.10	1.82	37.54	2.51
161	Roseau	Unnamed	Hornblende Diorite	0.11	0.00	0.00	32.96	2.56
162	Kittson	Unnamed	Granodiorite	1.88	20.48	2.87	56.02	2.64
163	Kittson	Unnamed	Pegmatite in Granodiorite	2.38	1.37	1.70	41.07	2.56
164	Morrison	Unnamed	Hornblende Biotite Gneiss	0.33	3.52	1.21	37.46	2.35
165	Morrison	Unnamed	Biotite Gneiss	0.19	4.84	0.67	37.61	3.39
166	Kittson	Roseau River Batholith	Monzodiorite	0.48	2.25	1.26	36.89	2.31
167	Marshall	Grygla Pluton	Coarse Grained Hornblende Granite	0.67	2.21	1.37	37.42	2.68
168	Marshall	Grygla Pluton	Medium Grained Hornblende Granite	0.79	1.31	1.63	37.27	2.76
169	St. Louis	Vermillion Massif	Weakly Foliated Granite	3.76	2.06	2.89	46.06	2.74
170	Crow Wing	Unnamed	Tonalite	1.15	5.52	1.20	40.91	1.75
171	Lake of the Woods	WG Unit (Day)	Granodiorite	0.32	3.18	0.82	36.79	3.09
172	Wilkin	Unnamed	Granodiorite	0.24	0.23	0.76	34.22	2.47
173	Norman	Unnamed	Biotite Granite	0.21	1.02	0.85	34.87	2.22
174	Polk	Snake River Batholith	Tonalite-Granodiorite	0.30	0.30	0.68	34.34	2.62
175	Marshall	Florlian Batholith	Foliated Granodiorite	0.07	0.42	0.52	33.75	2.82
176	Marshall	Unnamed	Granitic	2.29	5.97	1.19	43.91	2.65

	County	Intrusion	Rock_Type	U ppm	Th ppm	K %	Q est. mW m ⁻²	Conductivity W/(m*K)
177	Marshall	Unnamed	Granitic	3.01	9.54	3.94	51.26	2.65
178	Marshall	Unnamed	Granitic	0.00	14.75	2.96	47.28	2.60
179	Marshall	Unnamed	Granitic	0.23	18.25	3.13	50.73	2.60
180	Stearns	Rockville Granite	Granite (weathered)	1.25	5.45	2.84	42.83	1.79
181	Nobles	Unnamed	Diorite	0.25	2.24	0.55	35.61	2.47
182	Brown	Unnamed	Weakly Foliated Hornblende Granite	0.61	5.66	2.05	40.68	2.12
183	Cottonwood	Jeffers Block	Granitic Gneiss	0.38	2.12	2.86	38.24	2.53
184	Watowan	Unnamed	Foliated Hornblende Granite	0.60	3.97	2.95	40.29	1.69
185	Cottonwood	Unnamed	Granitic Gneiss	0.01	26.59	3.02	56.58	2.42
186	Jackson	Jeffers Block	Granitic Gneiss	0.00	3.33	0.94	36.28	2.51
187	Murray	Unnamed	Granitic Gneiss	5.17	18.81	0.26	59.61	
188	Marshall	Grygla Pluton	Tonalite-Granodiorite	0.38	0.96	0.19	34.53	2.37
189	Marshall		Foliated Hornblende Monzonite	0.86	2.73	0.80	37.68	3.11
190	St. Louis	Sturgeon Granite	Biotite Granite	1.01	12.73	2.70	47.79	2.42
191	St. Louis	Vermillion Massif	Fine Grained Diorite	1.37	5.01	1.28	41.13	2.39
192	St. Louis	Vermillion Massif	Pink Granite	0.69	2.37	2.96	39.25	2.87
193	St. Louis	Kenora-Kabatogama Dike Swarm	Gabbro	0.31	1.02	0.32	34.54	3.13
194	St. Louis	Vermillion Massif	Granitic Migmatite	0.27	2.34	2.92	38.22	1.84
195	St. Louis	Vermillion Massif	Lac La Croix Granite	1.12	5.78	1.74	41.63	2.41
196	St. Louis	Vermillion Massif	Amphibolite	1.71	3.54	1.25	40.73	3.23
197	St. Louis	Vermillion Massif	Granite	1.38	11.17	4.36	49.16	2.41
198	St. Louis	Vermillion Massif	Granite	0.17	8.91	1.85	41.98	3.19
199	St. Louis	Vermillion Massif	Granite					1.97
200	St. Louis	Vermillion Massif	Schist					2.95
201	St. Louis	Vermillion Massif	Granite	3.20	14.64	4.10	55.83	1.97
202	St. Louis	Vermillion Massif	Schist	2.07	9.67	3.21	48.40	2.48
203	St. Louis	Vermillion Massif	Granite	1.44	4.35	1.01	40.48	3.14
204	St. Louis	Vermillion Massif	Pink Gneissic Granite	0.29	8.82	3.07	43.46	2.50
205	St. Louis	Wakem Up Pluton	Schistose Diorite	1.28	4.00	1.09	39.94	2.63
206	Roseau	Unnamed	Diorite	0.43	3.24	0.91	37.18	2.45
207	Roseau	Unnamed	Diorite	0.08	1.21	0.79	34.66	

APPENDIX D:

Equations Used for Zones 1-9 in Minnesota to correct for recent warming

Zone #	Equation
Zone 1	$y = 1.01694E-09x^4 - 8.03399E-07x^3 + 0.000228828x^2 - 0.027688169x + 1.195375288$
Zone 2	$y = 4.43774E-10x^4 - 3.69464E-07x^3 + 0.000109604x^2 - 0.013488432x + 0.563397016$
Zone 3	$y = -7.35742E-13x^5 + 8.29126E-10x^4 - 3.46185E-07x^3 + 6.56417E-05x^2 - 0.005386531x + 0.131371412$
Zone 4	$y = -2.28163E-12x^5 + 2.45133E-09x^4 - 1.03306E-06x^3 + 0.000214001x^2 - 0.021933609x + 0.901361562$
Zone 5	$y = 5.6389E-10x^4 - 4.61136E-07x^3 + 0.00013658x^2 - 0.017271376x + 0.783039788$
Zone 6	$y = -1.16316E-14x^6 + 2.67177E-12x^5 + 3.94798E-09x^4 - 2.23296E-06x^3 + 0.000460452x^2 - 0.041907223x + 1.397574474$
Zone 7	$y = -2.97592E-12x^5 + 2.85859E-09x^4 - 1.07582E-06x^3 + 0.000200267x^2 - 0.018836049x + 0.741946133$
Zone 8	$y = -3.41438E-15x^6 + 1.28968E-12x^5 + 7.29459E-10x^4 - 5.37263E-07x^3 + 0.000128551x^2 - 0.014205038x + 0.636266045$
Zone 9	$y = -2.15347E-14x^6 + 1.73558E-11x^5 - 4.38505E-09x^4 + 9.73554E-08x^3 + 0.000124327x^2 - 0.018870458x + 0.862949375$

APPENDIX E:
Petrography and Geochemistry of Collected Granite Samples

Granite Geochemistry

In order to get a better idea of what the heat flow is in Minnesota, it was decided to investigate the geochemistry of 99 granitoid samples within Minnesota (see *Appendix E - Geothermal Granite Samples.xls*). The term “granitoid” is used loosely in this study to include rocks ranging from diorite to granite. Rocks have been classified based on the major elements SiO₂, K₂O, and Na₂O (LeBas et al., 1986). Whole rock major element and trace element compositions of the samples are included in the accompanying spreadsheet (*Appendix E - Geothermal_Lithochemisrty Classification Data.xls*). Included in these analyses was the determination of the radioactivity (radionuclides – ²³⁸U, ²³²Th, and ⁴⁰K) for better determination of the heat production of each sample.

Granitic samples were collected from outcrops and mineral exploration drill holes at the Minnesota Department of Natural Resources, Hibbing Drill Core Library and from active drilling programs operated by Rio Tinto/Kennecott Exploration’s Tamarack nickel deposit in Carlton and Aitkin counties, and in St. Louis County from Duluth Metals’ Nokomis Cu-Ni-PGE-Au deposit and PolyMet Mining Company’s NorthMet Cu-Ni-PGE deposit. Samples from these deposits included some mafic rocks, but mainly granitic rocks.

For the outcrop samples, all effects of weathering were physically removed prior to submittal for geochemistry. A thin section billet was also cut to size and then sent to San Diego Petrographics in Emmett, Idaho for polished thin sections. Polished thin sections were made to be able to identify the opaque metallic minerals, e.g., pyrite, magnetite, etc. These samples were studied for the mineralogy of any phenocryst phases and the mineralogy of the groundmass (*Appendix E - Granitic Thin Sections - Estimated Modal Percentages of Minerals.xls*).

The samples were sent to Activation Laboratories (Actlabs) in Ontario, Canada for whole rock and trace element (including uranium and thorium) analyses. Upon receipt of the analyses, the data set was checked, including standards, blanks run by Actlabs (certificate and data in spreadsheet). The 99 analyses were analyzed using standard statistical methods, i.e., mean, average, minimum value, max value, etc. The maximum value was highlighted in red and one sigma standard deviation above the average (highlighted in blue) was considered anomalous to the complete dataset in determining which samples had anomalous values compared to the dataset.

The most interesting data were the rare earth elements, which were primarily associated in or near alkalic intrusive rocks in northern Minnesota (Boerboom, 1994), e.g., Bello Lake, Coon Lake, Linden Pluton. For example, the second highest radionuclide analysis in this study for thorium also has anomalous > 1 standard deviation barium, strontium, lanthanum, cerium, praseodymium, uranium, thorium, and lead and the second highest heat flow value. This value and the Roseau Batholith sample were removed from the heat flow analyses (see Fig. 32 – The two yellow points, e.g., one point in west-central MN (WC) and the other point in north-central MN (NC), have the highest radionuclide thorium analyses) because the analyses were “point source” anomalies, and not necessarily representative of the heat flow of the geology in their respective areas. These areas obviously need additional research to understand these “point source” anomalies.

The figures below (Figs. 52-57) illustrate the distribution of granitic samples throughout the State. To generally evaluate the chemistry, these samples were examined by region, e.g., northwest = NW, EC = east-central, etc. The diagrams following this regional distribution map (Fig. 52) are plotted to graphically illustrate the different types of rocks in each region and to begin to understand their different origins. Figures 53 and 54 provide a geochemically-derived rock name based upon immobile element ratios that are not affected by metamorphic or metasomatic processes (Winchester and Floyd, 1977). Figure 54 plots CIPW normative calculated end member plagioclase feldspar, i.e., Ab-Albite and An-Anorthite, Na-Ca-rich feldspars versus Or (Orthoclase) for the potassium-rich feldspars (Barker, 1979). A granite rich in potassium would plot toward the Or corner of the triangle along the Ab-Or join.

Figure 55 gives a measure of the alkalinity of the igneous rocks. Alkaline rocks can have higher rare earth element contents, and therefore, more potassium feldspar, uranium, and thorium. Additional analysis and collection of these particular rock samples in the field might further define the heat flow in their particular areas.

Figure 56 illustrates whether the rocks originated in tectonically active, e.g., subduction zones (I- & S-type) or formed in stable or anorogenic areas away from active plate tectonics. A-type granites, i.e., Wausau Batholith in northern Wisconsin, are considered to have formed by partial melting away from active tectonism. It has also been prospected for uranium and rare earth elements. Although additional research is required to determine if the A-type granitoids indicated on these diagrams have an anorogenic origin, the rocks contain elevated values of uranium, thorium, and rare earth elements that would produce higher heat flow.

Figure 57 is a plot of U+Th (ppm) versus K (wt. %) and was constructed from the data from this study. The plots illustrate the linear relationship between these elements. The East Central exhibits two linear relationships that need to be investigated further to see if there is a local or more regional relationship between these trends and how they relate to regional heat flow.

It is clear from the rock and radionuclide chemistry that additional research is required to better define the heat flow in specific areas. Concentrating additional sampling around alkalic plutons in north-central Minnesota may further increase areas of higher heat flow seen in Figures 2 and 3.

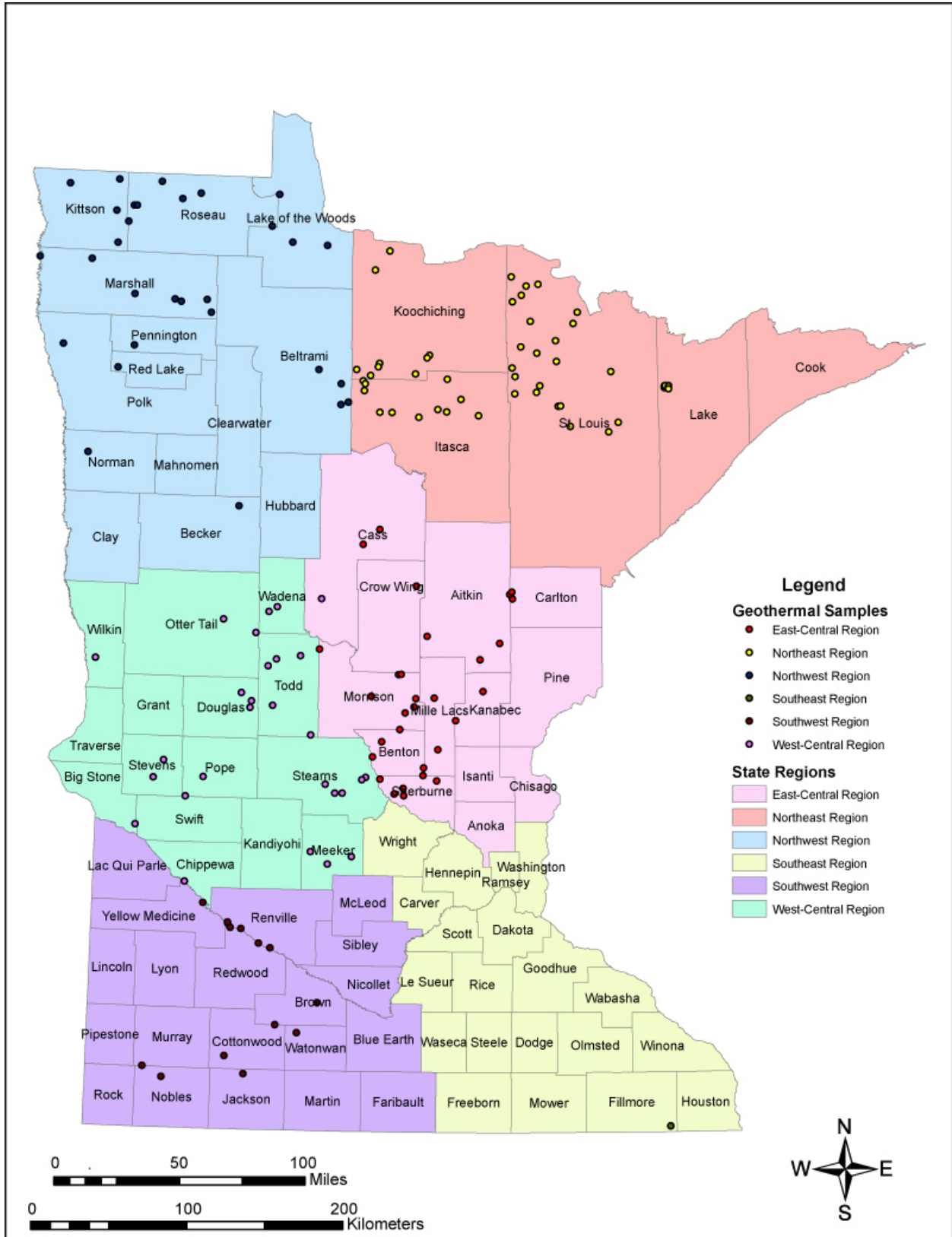


Figure 52. This map is arbitrarily divided into regions of the State to better illustrate graphically the various plots of the chemistry in the diagrams to follow. The circles are the granitic rock sample locations.

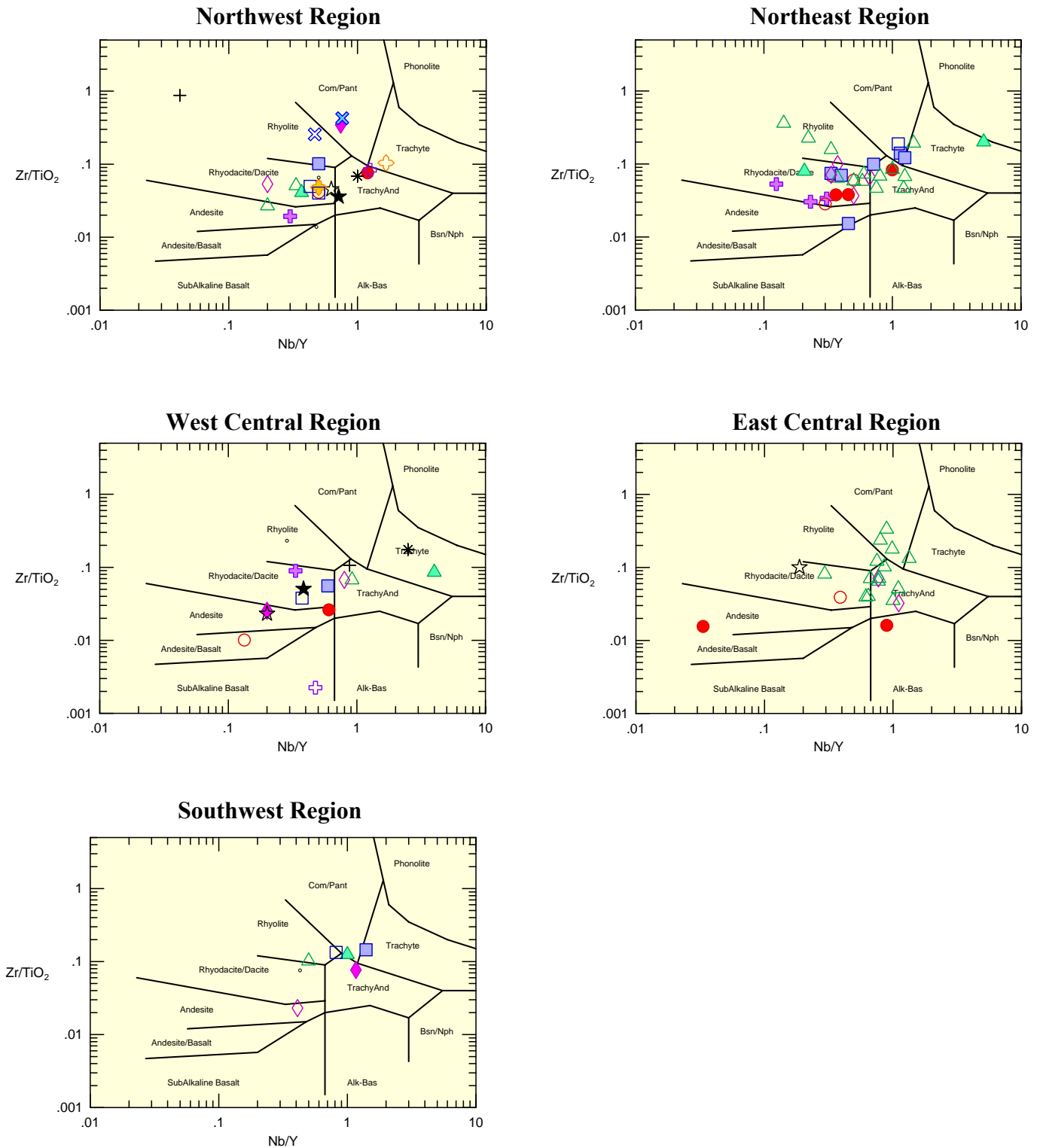


Figure 53. A Floyd-Winchester plot of Zr/TiO_2 versus Nb/Y (ppm) illustrating the types of granitic and other rocks in each region (Floyd and Winchester, 1975).

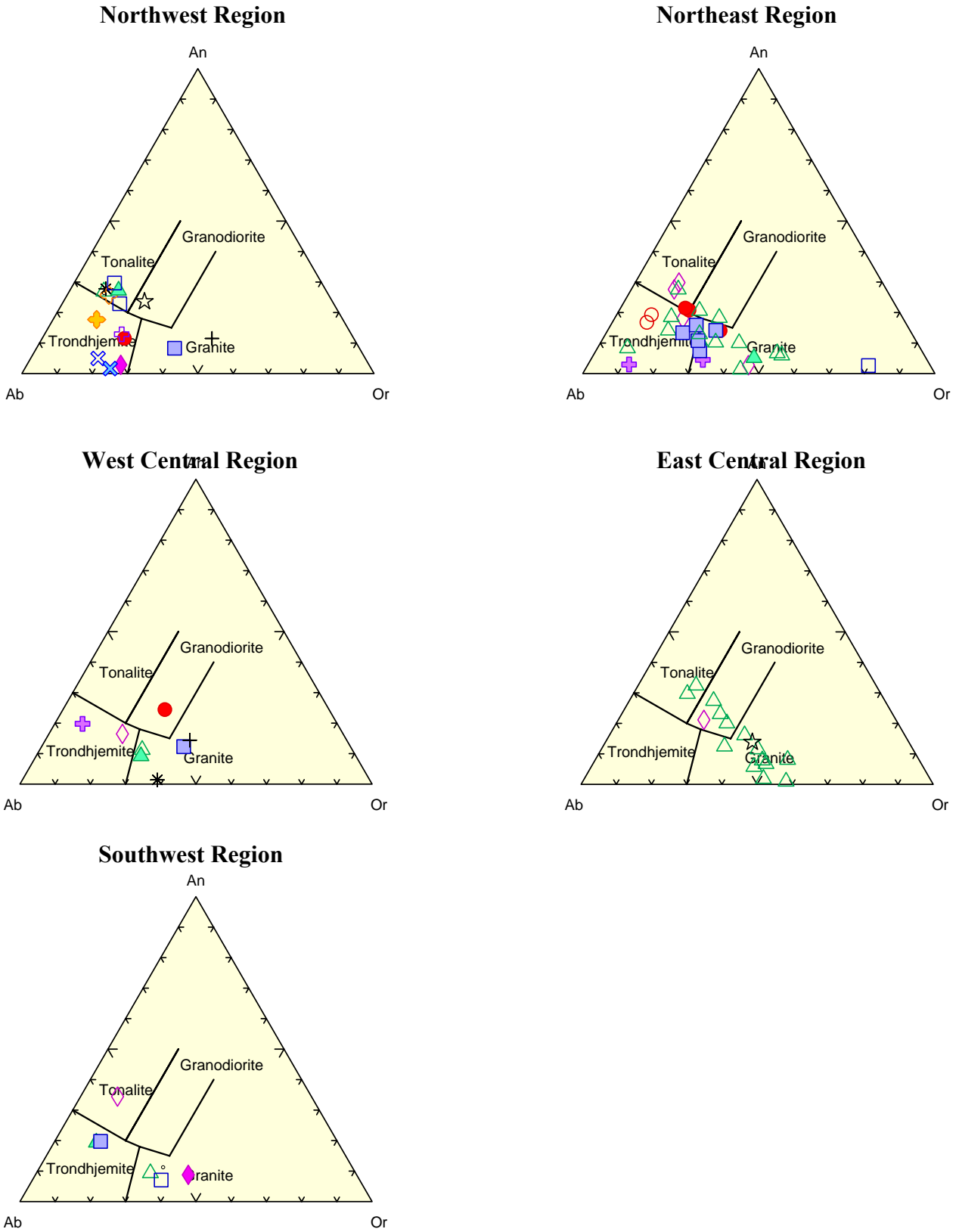


Figure 54. Ab-An-Or plot illustrating the type of granitic rock the samples in each region (Barker, 1979). Calculated from a CIPW norm (Terra Softa, Inc., 2002). Sample IDs represent individual samples only, due to a limited pool of sample symbols available in Iqpet.

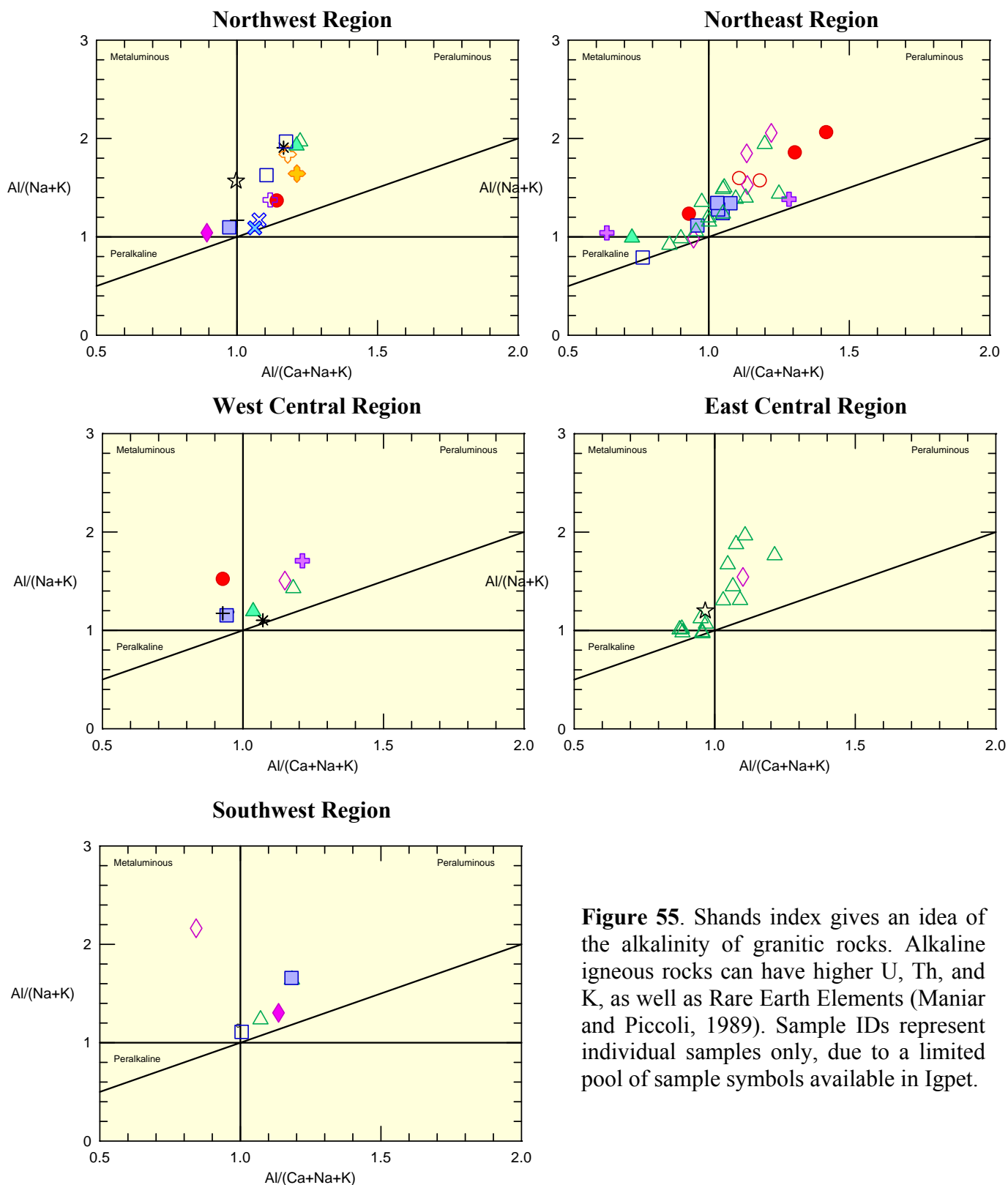


Figure 55. Shands index gives an idea of the alkalinity of granitic rocks. Alkaline igneous rocks can have higher U, Th, and K, as well as Rare Earth Elements (Maniar and Piccoli, 1989). Sample IDs represent individual samples only, due to a limited pool of sample symbols available in Igppt.

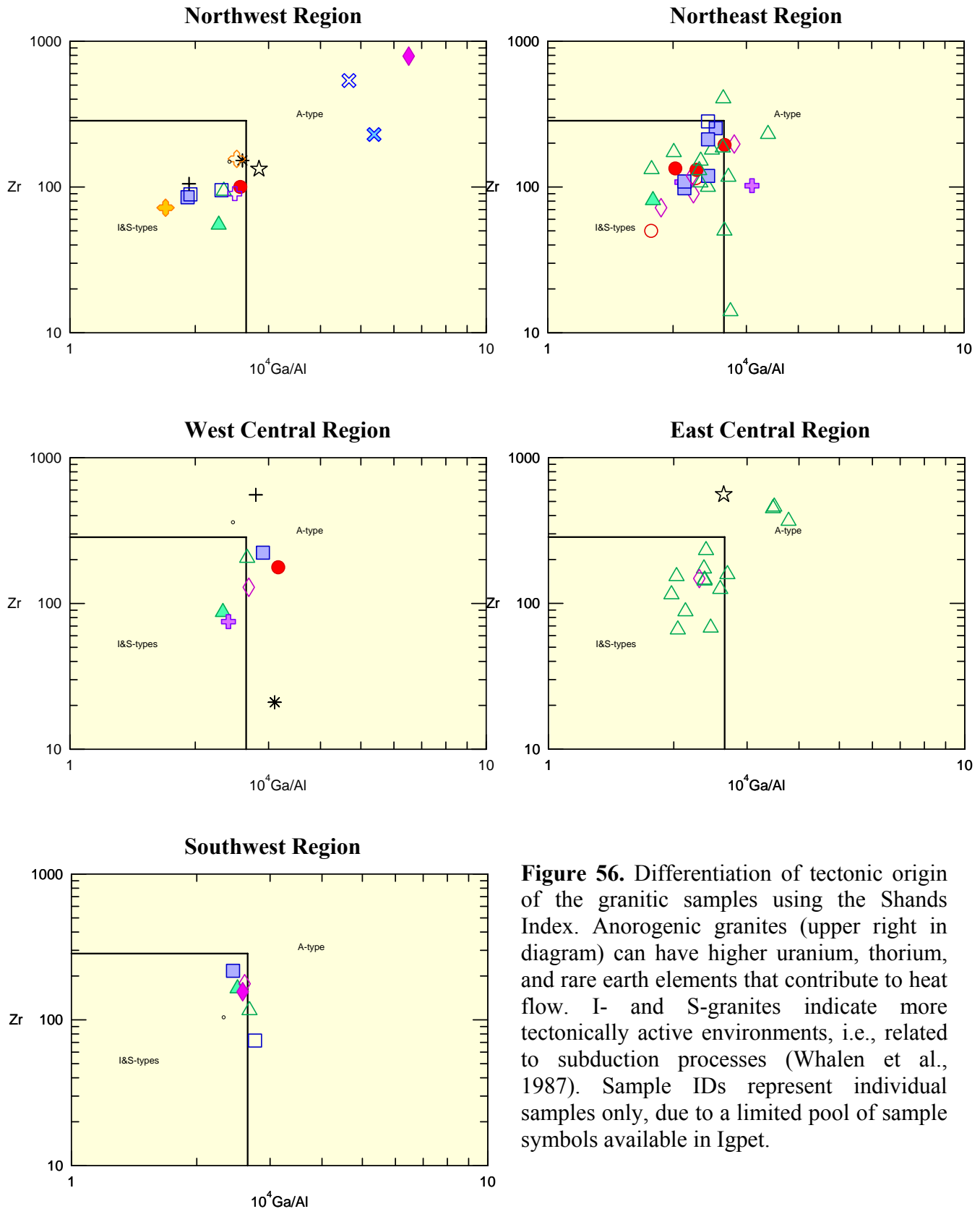


Figure 56. Differentiation of tectonic origin of the granitic samples using the Shands Index. Anorogenic granites (upper right in diagram) can have higher uranium, thorium, and rare earth elements that contribute to heat flow. I- and S-granites indicate more tectonically active environments, i.e., related to subduction processes (Whalen et al., 1987). Sample IDs represent individual samples only, due to a limited pool of sample symbols available in Igpet.

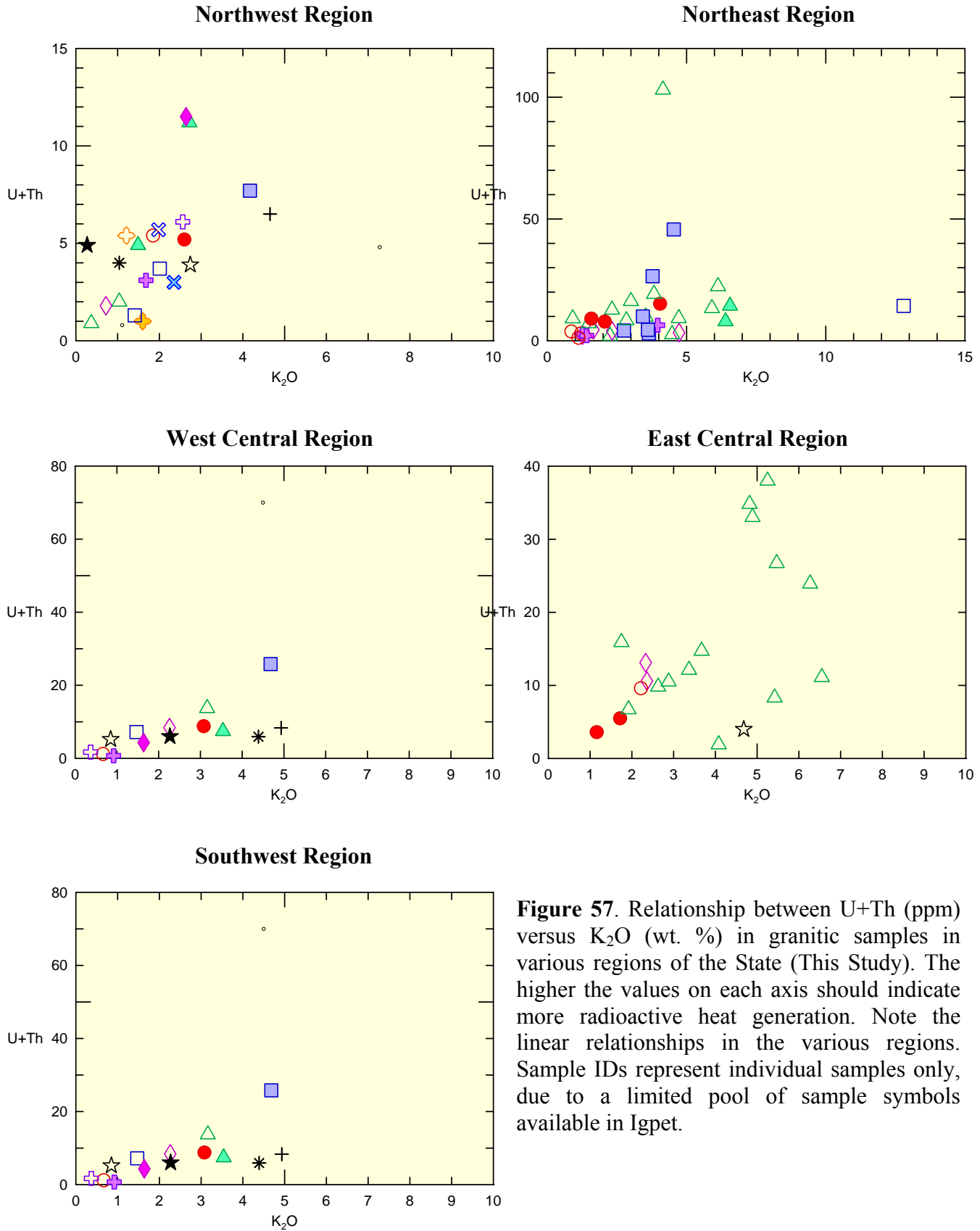


Figure 57. Relationship between U+Th (ppm) versus K₂O (wt. %) in granitic samples in various regions of the State (This Study). The higher the values on each axis should indicate more radioactive heat generation. Note the linear relationships in the various regions. Sample IDs represent individual samples only, due to a limited pool of sample symbols available in Iqpet.

REFERENCES – APPENDIX E

- Barker, F., 1979, Trondhjemite: definition, environment and hypotheses of origin, *in* Barker, F. (ed.), Trondhjemites, dacites, and related rocks, p. 1-12.
- Boerboom, T.J., 1994, Alkalic Rocks in Northeastern Minnesota, *in* Southwick, D. (ed.), Short Contributions to Minnesota Geology: Minnesota Geological Survey, RI-43, p. 20-38.
- Floyd, P.A., and Winchester, J.A., 1977, Geochemical discrimination of different magmas series and their differentiation products using immobile elements: *Chemical Geology*, v. 20, p. 325-343.
- LeBas, M.J., LeMaitre, R.W., Streckeisen, A., and Zanettin, B., 1986, A chemical classification of volcanic rocks based on the total alkali silica diagram: *Journal of Petrology*, v. 27, p. 745-750.
- Maniar, P.D., and Piccoli, P.M., 1989, Tectonic discrimination of granitoids: *Geological Society of America Bulletin*, v. 101, p. 635-643.
- Terra Softa Inc., 2002, Igpert for Windows, Manual, 36 p.
- Whalen, J.B., Currie, K.L., and Chappell, B.W., 1987, A-type granites: geochemical characteristics, discrimination and petrogenesis: *Contributions to Mineralogy and Petrology*, v. 95, p. 407-419.
- Winchester, J.A., and Floyd, P.A., 1977, Geochemical discrimination of different magma series and their differentiation products using immobile elements: *Chemical Geology*, v. 20, no. 4, p. 325-343.

APPENDIX F:
NRRI Field Collection Data

Well Temperature Data Collection

The wells used for temperature measurements were located from three sources:

- 1) the MnDNR Water Division Observation Well Database;
- 2) the County Well Index (maintained by the MGS); and
- 3) the listing of drill holes supplied by the MnDNR Lands and Minerals Division.

Wells over 300 ft. in depth were selected from each database with additional criteria used to narrow the search depending on the database. The Observation Well Database was the most useful, with most of the wells still active and available for use in the project.

The County Well Index provided additional well locations used for the project. In addition to the greater than 300 ft. depth restriction, the following well types were initially used to narrow the search:

- 1) exploratory boring;
- 2) exploration;
- 3) irrigation;
- 4) monitoring well;
- 5) observation well;
- 6) other;
- 7) piezometer;
- 8) recovery well;
- 9) scientific investigation;
- 10) test well; and
- 11) unknown.

These were further reduced over time to irrigation, monitoring, observation, test wells, and unknown, as experience showed that the other types were either reclaimed or currently in use and unsuitable for the study.

The listing of drill holes provided by the MnDNR was used to try to locate potential drill holes drilled prior to 1981 when the abandonment rules were changed. It was hoped that some of these holes would still be available in Northern and Western Minnesota where there was a limited number of available wells. None of these wells were located during the project.

All of the wells and drill holes, 667 total, that were used, located, or not located are listed in the spreadsheet *Geothermal Wells Progress01092012.xls* included with this report (Fig. 58). The total number of wells measured for the project by all participants was 112 (Fig. 59) and are listed in Table 2.

Wells and Drill Holes Investigated During Project

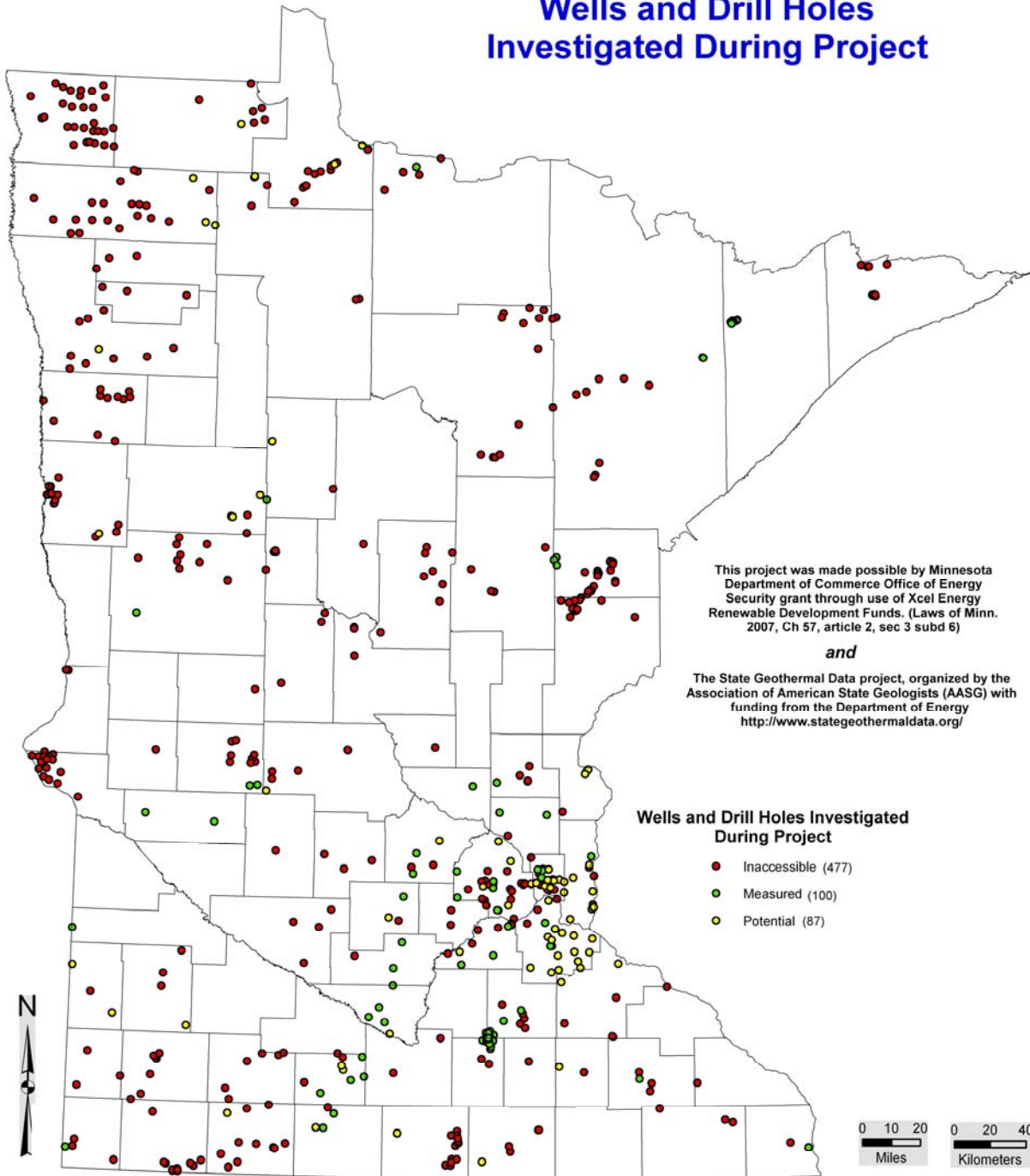


Figure 58. Wells and drill holes investigated during project.

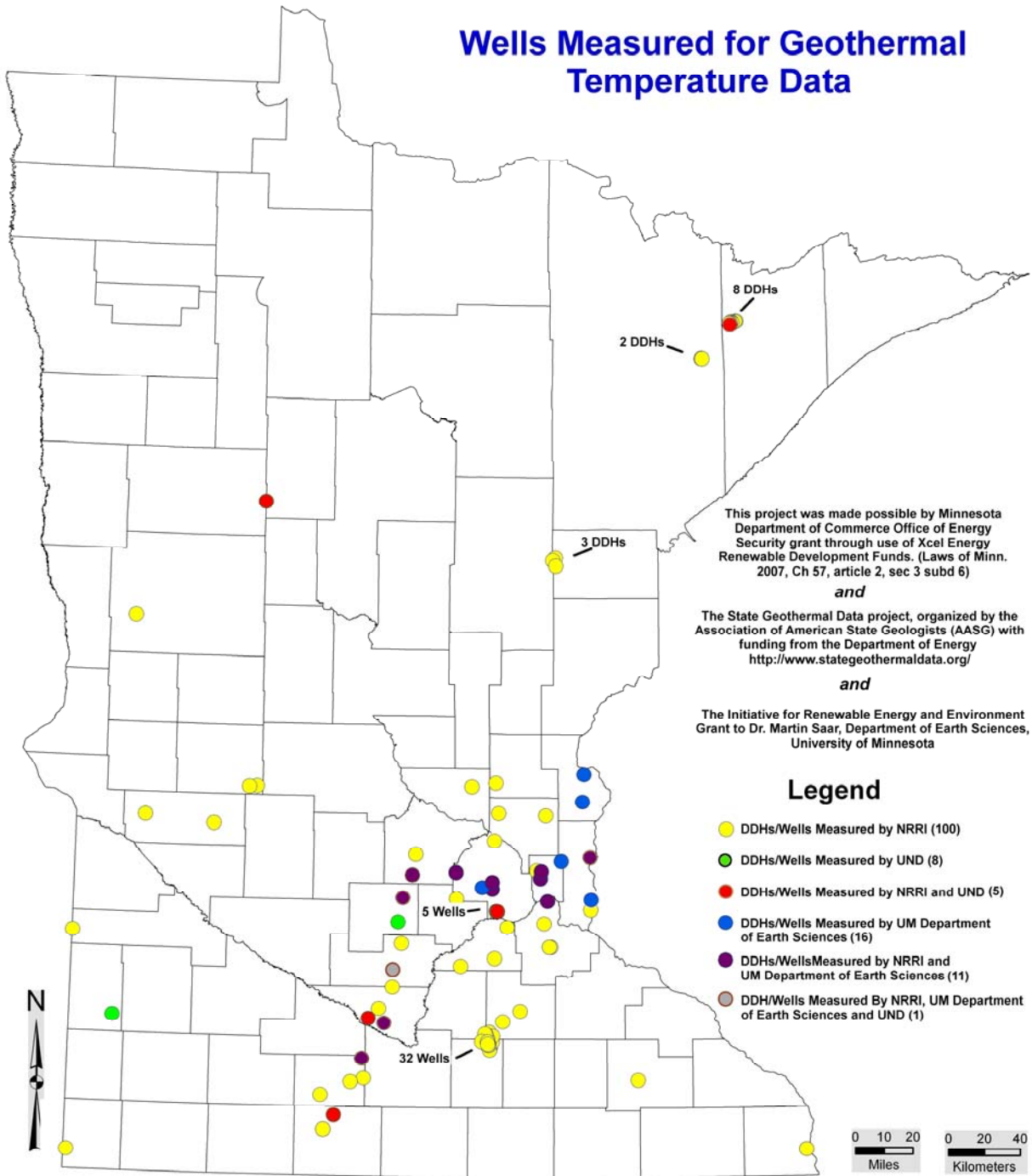


Figure 59. Wells measured for geothermal temperature data.

Table 2. List of wells and drill holes run by the groups for the project showing which wells were run as duplicates as checks for the data from the different equipment used on the project.

NAME	COUNTY	UM Geology	UND	NRRI	NRRI Redux
DNR OB 2031	Anoka			1	
C. Avery Old Shop	Anoka			1	
Tamarack	Carlton			1	
Tamarack	Carlton			1	
Tamarack	Carlton			1	
Waters Edge Condos	Chisago	1			
Stolp N	Chisago	2			
DNR OB 19086	Dakota			1	
West St. Paul- USGS2N	Dakota	1			
USGS 1N	Dakota			1	
DNR OB 19085	Dakota			1	
Vermillion River	Dakota			1	
DNR OB 19084	Dakota			1	
DNR OB 27062	Hennepin			1	
Robina	Hennepin	2		1	
St. Bonifacius	Hennepin			1	
Mnnetonka Boat Works	Hennepin	1			
Gray's Bay Pilot Well 2	Hennepin	1		1	
Luce Line MTS	Hennepin	1			
Luce Line Vicksburg	Hennepin			1	
Staring Lake 27055	Hennepin			1	
DNR OB 27058	Hennepin			1	
EDEN PRAIRIE	Hennepin		1		
EDEN PRAIRIE	Hennepin		1		
Staring Lake 27047	Hennepin			1	
DNR 28004	Houston			1	
DNR 28005	Houston			1	
DNR 28003	Houston			1	
Becker County Line	Hubbard		1	1	1
DNR OB Well 30015	Isanti			1	
Humble Oil	Koochiching			1	
Duluth Metals	Lake			1	
Duluth Metals	Lake			1	
Duluth Metals	Lake			1	
Duluth Metals	Lake			1	
Duluth Metals	Lake			1	
Duluth Metals	Lake			1	
Duluth Metals	Lake		1	1	
Duluth Metals	Lake			1	
State Park 1	Le Sueur			1	
Hering 2	Le Sueur			1	
Schwartz 1	Le Sueur			1	
Schwartz 2	Le Sueur			1	
TYLER	Lincoln		1		

NAME	COUNTY	UM Geology	UND	NRRI	NRRI Redux
DNR OB Well 46009	Martin			1	
DNR OB Well 46008	Martin			1	
DNR OB Well 46006	Martin		1	1	
DNR OB Well 46007	Martin			1	
GLENCOE	McLeod		1		
Cloustier, WMA	McLeod	1		1	
DNR OB Well 52003	Nicollet		1	1	
DNR OB Well 52005	Nicollet	1		1	
DNR OB Well 52001	Nicollet			1	
DNR OB Well 52007	Nicollet			1	
Golden Hill School	Olmstead			1	
Fergus Falls RTC	Otter Tail			1	
USGS BB07	Pope			1	1
USGS BB01	Pope			1	
Elm Creek Park Horse Trail ObWell	Ramsey			1	
Lake Johanna #19	Ramsey			1	
Lexington Court Apts	Ramsey	1		1	
City of Shoreview	Ramsey	1		1	
White Bear Lake #3	Ramsey	1			
Jobe Norris 1	Rice			1	
Grubish Charles 7	Rice			1	
Gregor Roland 1	Rice			1	1
Meehl 2	Rice			1	
Meehl 1	Rice			1	
Hand Vern 1	Rice			1	
Hand Vern 2	Rice			1	
Melstrom 1	Rice			1	
Lillevang Mary 1	Rice			1	
MN Municipal Power Agency	Rice			1	
MNDOT Gravel Pit 2	Rock			1	1
Michelle Wildlife	Scott			1	
ObWell	Scott			1	
Savage OB-8	Scott			1	
DNR OB Well 71029	Sherburne			1	
DNR OB Well 72000	Sibley			1	
DNR OB Well 72001	Sibley	1	1	1	
DNR OB Well 72002	Sibley			1	
PolyMet	St. Louis			1	
PolyMet	St. Louis			1	
DNR OBWell 76-032	Swift			1	
Steinhaus 1	Waseca			1	
Earl Davison 1	Waseca			1	
S Hagen 1	Waseca			1	
Grubish 8	Waseca			1	
Grubish 6	Waseca			1	
Clarence Prehn 3	Waseca			1	
Sydney Dahle 1	Waseca			1	1

NAME	COUNTY	UM Geology	UND	NRRI	NRRI Redux
Schuette 2	Waseca			1	
Schuette 3	Waseca			1	
Schuette 1	Waseca			1	
Sydney Lee 3	Waseca			1	
BG-30	Waseca			1	
Pratt Estate 1	Waseca			1	
Pratt Estate 3	Waseca			1	
Pratt Estate 2	Waseca			1	
Fretham 1	Waseca			1	
Frank Mass 1	Waseca			1	
Kanne 1	Waseca			1	
DNR-Lake Carnelian #6	Washington	1		1	
Afton SP	Washington			1	
USGS AFTON NORTH	Washington	1			
DNR OB Well 83023	Watonwan			1	
DNR OB Well 83019	Watonwan			1	
DNR OB Well 83021	Watonwan	1		1	
DNR OB Well 83017	Watonwan			1	
Lake Ann WA	Wright	1		1	
Anderson County Park	Wright			1	
Lincoln Pipstone B4	Yellow Medicine			1	

Temperature measurements in the wells and drill holes were completed using two instruments: 1) the UND probe; and 2) in the latter half of 2011, the NRRI Mount Sopris 2WQA-100 probe with winch and data acquisition system. For both systems, once a candidate well was located and opened, the hole was probed immediately. An exception was made for the MnDNR Observation Well that had depth logging probes installed. These logging probes were carefully removed and the water depth was measured with a chalked steel tape prior to the temperature measurements at the request of the MnDNR. After the downhole measurements were made, the probes were replaced where necessary and closed to their original condition. All data collected by NRRI was entered into an Excel Spreadsheet for each of the logged holes, with location and operator data, and are included with this report (*Well Temperature And Location Data.zip*). All Excel spreadsheets were delivered to UND to produce the revised map, along with air photo and topographic maps showing the location of the hole. An example of the header information and data is found in Figure 60.

The UND probe is described as a “specialty instrument built to measure temperature with a resolution of 0.01 degrees C and depth resolution of 0.01 m” by Dr. Will Gosnold of UND. The following process summarizes the data collection procedure:

- 1) after assembly of the unit on site, the units multimeter is tuned using a cutout circuit with a known resistance;
- 2) the depth counter is set to zero at ground level in the hole;
- 3) once the probe is in tune, the probe is lowered down the hole, using a hand on the cable drum as a brake; and
- 4) the probe is stopped at the required depth and the resistance is measured on the multimeter.

One person would operate the equipment (Fig. 61) and another person would record the data on log sheets (Fig. 62). This procedure is completed for every meter from the top of the hole to 100 m and every 10 m thereafter. The tuning of the unit was checked every 10th reading and adjusted as needed. At the bottom of the hole the unit was hand cranked back up the hole using the attachable handle, with one person drying the cable and guiding cable on the drum and the other person cranking. The data are manually converted from resistivity to temperature data using a conversion table supplied with the probe and entered in an Excel Spreadsheet for each hole with the associated resistivity reading from the instrument. NRRI probed fifty wells and drill holes using the UND probe. Additionally, eight holes were probed for the study by the UND group and two holes were duplicated by NRRI as checks by different instruments.

There were problems with the UND equipment that required repairs, and NRRI decided to buy a newer model probe and winch system to be able to complete the project. The NRRI Mount Sopris 2WQA-100 probe with winch and data acquisition system was delivered in mid-June 2011. After setup on site and zeroing the probe depth to the ground surface:

- 1) the winch was set to lower the probe at 8-9 meters per minute; and
- 2) data acquisition was set to record every 20 cm for the length of the hole.

A	B	C	D	E	F	G	H	I	J
1		Location	Nokomis Property		TRS	62 11 35	Hole Number	MEX 3	
2		Latitude	47 48 32.01924	Longitude	91 42 09.57501	Elevation	469.213	Angle	89.5
3		Map 1:250K	Two Harbors		Quad Map	Bogberry Lake			
4		Probe/Cable/Bridge				Operator	MJS/JJH	Date	12/17/2009
5	Apparent	Hole	Corrected						
6	Depth (m)	Angle	Depth (m)	Resistance	Temp (°C)	ΔT/ΔK	Comments	Surface Readings	
7				(ohms)		(°C/km)		Time	Resistance
8	1	89.51	-0.1300	183.07	-0.13			None - Ground Frozen	Solid
9	2	89.52	1.9999	182.74	-0.07	28.17			
10	3	89.53	2.9999	182.54	-0.03	40.00			
11	4	89.54	3.9999	144.41	7.43	7460.21			
12	5	89.55	4.9998	141.28	8.09	660.02			
13	6	89.56	5.9998	142.15	7.90	-190.00			
14	7	89.57	6.9998	143.68	7.58	-320.01			
15	8	89.58	7.9998	145.46	7.21	-370.01			
16	9	89.59	8.9998	146.90	7.08	-130.00			
17	10	89.60	9.9998	148.11	6.66	-420.01			
18	11	89.61	10.9997	148.98	6.48	-180.00			
19	12	89.62	11.9997	149.54	6.37	-110.00			
20	13	89.63	12.9997	149.96	5.28	-1090.01			
21	14	89.64	13.9997	150.24	6.23	950.01			
22	15	89.65	14.9997	150.37	6.20	-30.00			
23	16	89.66	15.9997	150.51	6.17	-30.00			

Figure 60. The header information supplied for each hole measured includes name and location data for each hole, operators for the measurement and on what date. For angled drill hole, which are common in exploration drilling, the depth is corrected to true vertical depth from the cable measurement using deviation data supplied by the exploration company.



Figure 61. Set up and operation of downhole temperature collection equipment, winter 2010, Duluth Metals Nokomis Cu-Ni-PGE deposit, drill hole MEX-3.



Figure 62. Recording of downhole temperature data, winter 2010, Duluth Metals Nokomis Cu-Ni-PGE deposit, drill hole MEX-3.

The operator adjusted the winch to keep the speed in the desired range. Once the bottom of the hole was reached one person dried the cable while the other individual operated the winch. Two people were needed to operate the equipment due to the weight and logistics of controlling the winch and retrieving the probe. The data were stored on a laptop that controls the electronics package in a proprietary format. The Scintrex software converted the format of the data into one applicable for inserting into an Excel Spreadsheet along with the conductivity data that the probe also measured.

Granite and Thermal Conductivity Sample Collection

Two sets of rock samples were collected from drill holes and outcrops for the project. The first set was a group of 156 granites and related rocks, of which 99 thin sections were made and run for geochemistry. Forty-three other rock types were collected for thermal conductivity measurements by UND. Locations for all of these samples are shown in Figures 63 and 64. The results for the UND work are presented in Appendix E and the associated spreadsheets.

Forty-two samples from drill holes were provided by Kennecott Exploration (31), Duluth Metals (9) and PolyMet Mining (2) from their project areas. The remainder of the 120 drill hole samples were collected from MnDNR Lands and Minerals Drill Core Repository in Hibbing, MN. Where possible, an 800-1000g sample was collected for all samples for radionuclide testing by UND and flat slab or cross-section of the core for thermal conductivity measurements by UND. The remaining thirty-nine samples were collected in the field from outcrops across the state. Enough sample was collected to produce an 800-1000g sample for radionuclide analyses by UND and a flat slab or cross-section of the core was made to conduct thermal conductivity measurements at UND from all outcrops. Prior to shipment to UND, the 800-1000g sample was crushed to -1/4" size at NRRI and a flattened slab was produced, where possible, from the sample for final dimensioning at UND. A listing of all the samples collected by NRRI for this project is in Appendix B and Excel Spreadsheet *Geothermal_samples_01_09_12.xls* on the disk accompanying this report.

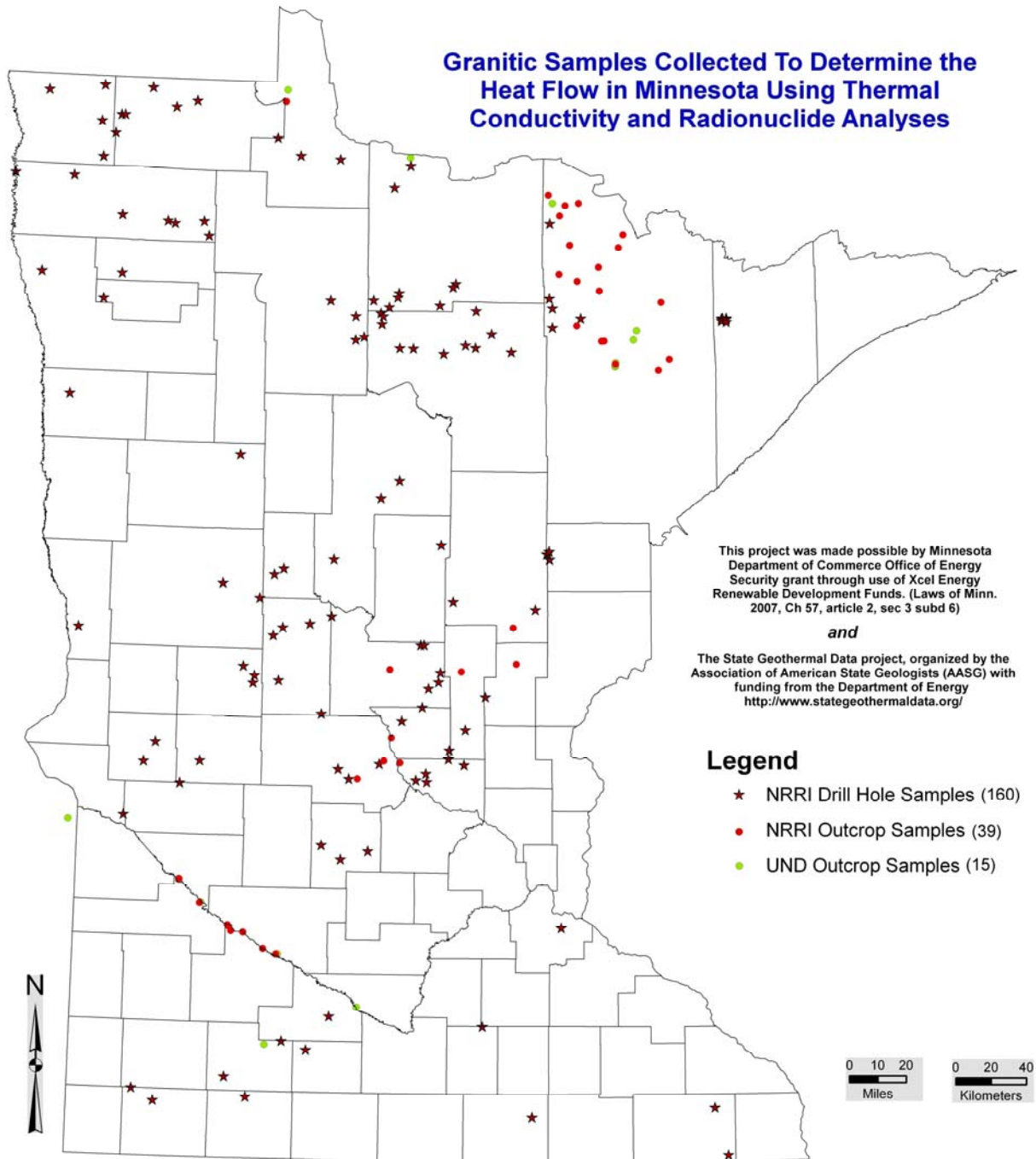


Figure 63. Granitic samples collected to determine the heat flow in Minnesota using thermal conductivity and radionuclide analyses.

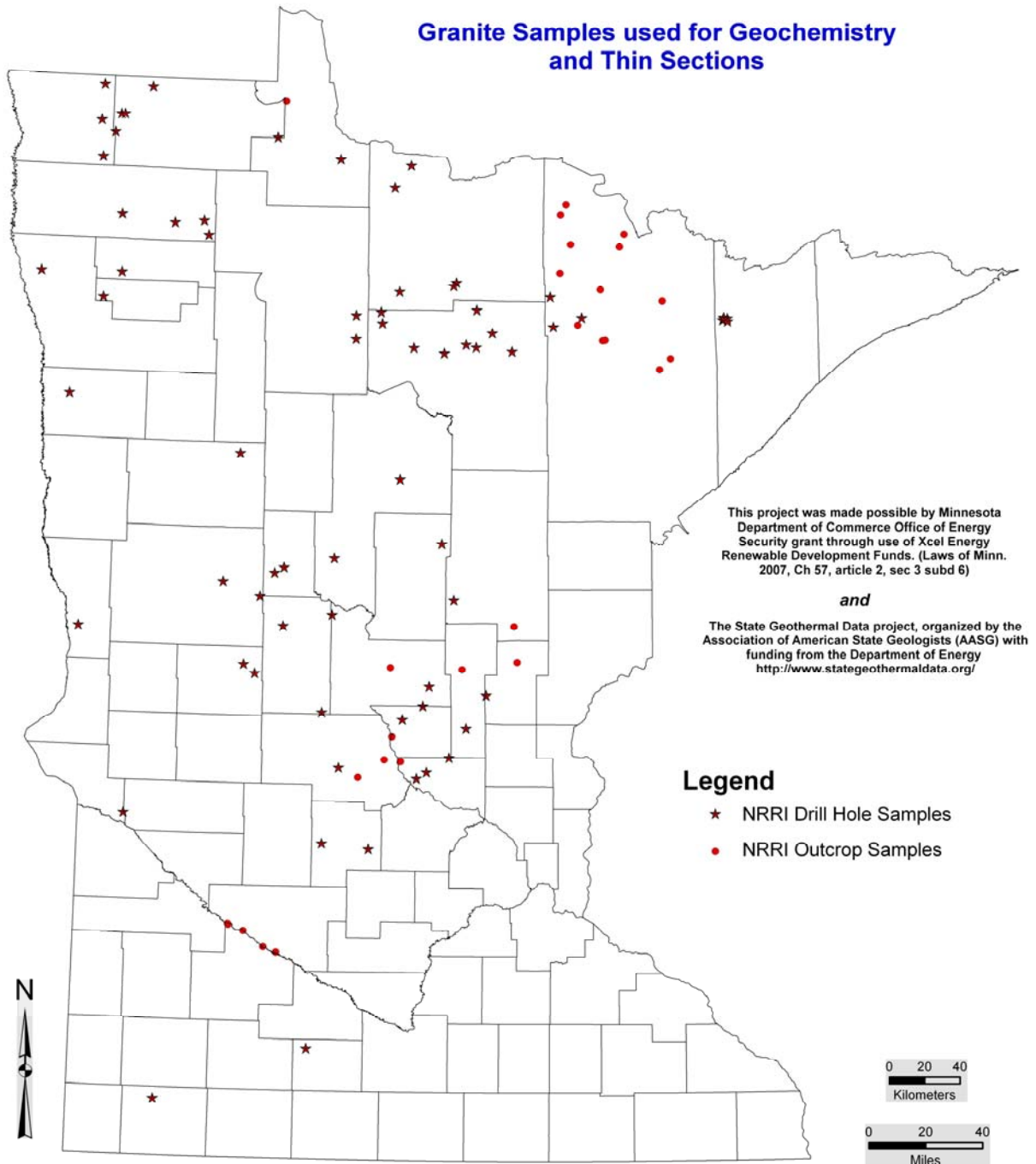


Figure 64. Granite samples used for geochemistry and thin sections.